



NATIONAL AND KAPODISTRIAN UNIVERSITY OF ATHENS

SCHOOL OF SCIENCES

DEPARTMENT OF INFORMATICS AND TELECOMMUNICATIONS

PROGRAM OF POSTGRADUATE STUDIES

PhD THESIS

**Rate-optimum Beamforming Transmission in MIMO
Rician Fading Channels**

DIMITRIOS E. KONTAXIS

ATHENS

FEBRUARY 2014



ΕΘΝΙΚΟ ΚΑΙ ΚΑΠΟΔΙΣΤΡΙΑΚΟ ΠΑΝΕΠΙΣΤΗΜΙΟ ΑΘΗΝΩΝ

**ΣΧΟΛΗ ΘΕΤΙΚΩΝ ΕΠΙΣΤΗΜΩΝ
ΤΜΗΜΑ ΠΛΗΡΟΦΟΡΙΚΗΣ ΚΑΙ ΤΗΛΕΠΙΚΟΙΝΩΝΙΩΝ**

ΠΡΟΓΡΑΜΜΑ ΜΕΤΑΠΤΥΧΙΑΚΩΝ ΣΠΟΥΔΩΝ

ΔΙΔΑΚΤΟΡΙΚΗ ΔΙΑΤΡΙΒΗ

**Βέλτιστη Εκπομπή Beamforming σε Κανάλια MIMO με
Κατανομή Rice**

ΔΗΜΗΤΡΙΟΣ Ε. ΚΟΝΤΑΞΗΣ

ΑΘΗΝΑ

ΦΕΒΡΟΥΑΡΙΟΣ 2014

PhD THESIS

Rate-Optimum Beamforming Transmission in MIMO Rician Fading Channels

Dimitrios E. Kontaxis

SUPERVISOR: Serafeim Karaboyas, Assistant Professor UoA

THREE-MEMBER ADVISORY COMMITTEE:

Lazaros Merakos, Professor UoA

George Tsoulos, Associate Professor UoP

Serafeim Karaboyas, Assistant Professor UoA

SEVEN-MEMBER EXAMINATION COMMITTEE

(Signature)

(Signature)

**Lazaros Merakos,
Professor Univ. of Athens**

**Georgios Tsoulos,
Associate Professor Univ. of
Peloponnese**

(Signature)

(Signature)

**Serafeim Karaboyas,
Assistant Professor Univ. of Athens**

**Panagiotis Mathiopoulos,
Professor Univ. of Athens**

(Signature)

(Signature)

**Georgios Stefanou,
Assistant Professor Univ. of Athens**

**Athanasios Kanatas,
Professor Univ. of Piraeus**

(Signature)

**Eleftherios Kofidis,
Assistant Professor Univ. of Piraeus**

Examination Date 14/02/2014

ΔΙΔΑΚΤΟΡΙΚΗ ΔΙΑΤΡΙΒΗ

Βέλτιστη Εκπομπή Beamforming σε Κανάλια MIMO με Κατανομή Rice

Δημήτριος Ε. Κονταξής

ΕΠΙΒΛΕΠΩΝ ΚΑΘΗΓΗΤΗΣ: Σεραφεύμ Καραμπογιάς, Επίκουρος Καθηγητής ΕΚΠΑ

ΤΡΙΜΕΛΗΣ ΕΠΙΤΡΟΠΗ ΠΑΡΑΚΟΛΟΥΘΗΣΗΣ:

Λάζαρος Μεράκος, Καθηγητής ΕΚΠΑ

Γεώργιος Τσούλος, Αναπληρωτής Καθηγητής ΠΑΠΕΛ

Σεραφεύμ Καραμπογιάς, Επίκουρος Καθηγητής ΕΚΠΑ

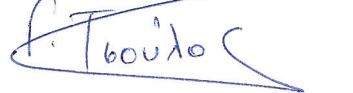
ΕΠΤΑΜΕΛΗΣ ΕΞΕΤΑΣΤΙΚΗ ΕΠΙΤΡΟΠΗ

(Υπογραφή)



Λάζαρος Μεράκος,
Καθηγητής ΕΚΠΑ

(Υπογραφή)



Γεώργιος Τσούλος,
Αναπληρωτής Καθηγητής ΠΑΠΕΛ

(Υπογραφή)



Σεραφεύμ Καραμπογιάς,
Επίκουρος Καθηγητής ΕΚΠΑ

(Υπογραφή)



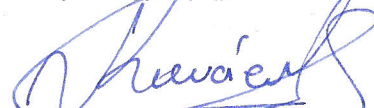
Παναγιώτης Μαθιόπουλος,
Καθηγητής ΕΚΠΑ

(Υπογραφή)



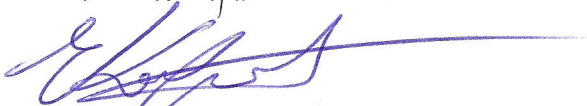
Γεώργιος Στεφάνου,
Επίκουρος Καθηγητής ΕΚΠΑ

(Υπογραφή)



Αθανάσιος Κανάτας,
Καθηγητής ΠΑΠΕΙ

(Υπογραφή)



Ελευθέριος Κοφίδης,
Επίκουρος Καθηγητής ΠΑΠΕΙ

Ημερομηνία εξέτασης 14.12.2014

ABSTRACT

In this doctoral thesis, the focus is on the capability of MIMO systems to increase channel capacity: A MIMO system can achieve much higher capacity than a conventional SISO system, and it can be proven that the achieved capacity increases linearly with the number of transmit or receive antenna elements. However, the capacity achieved by MIMO systems is closely related to the “channel knowledge” model which is assumed at both ends of the MIMO link. Considering the case of MIMO complex Gaussian ergodic channels, where the receiver has perfect Channel State Information (CSI) whereas the transmitter has Channel Distribution Information (CDIT), the mutual information between transmitter and receiver must be maximized statistically: maximization is achieved by an optimum transmission strategy (spatial precoding) and the maximum value is referred to as “ergodic capacity”. For the case of beamforming transmission, the maximum average mutual information is achieved by the “optimum beamformer” and is referred to as “ergodic beamforming capacity”. In this work the calculation of the optimum beamformer is studied and the related problem is referred to as “optimum beamforming problem”.

The solution of the optimum beamforming problem has been addressed extensively in the open literature for Gaussian CDIT models: for MIMO Rayleigh fading channels (CCI model) and for spatially uncorrelated (with unit covariance matrix) MIMO Rician fading channels (CMI model). For these two cases, closed-form solutions have been derived. However, the corresponding solution for spatially correlated or uncorrelated with non-unit covariance matrix MIMO Rician fading channels (combined CMI-CCI model) has received less attention: for this channel distribution model, there is no closed-form expression for the optimum beamformer and hence, the solution of the related optimization problem remains very complex for real time applications.

In this work, first it is proven that the aforementioned complex, multi-dimensional, convex constrained, (beamforming) optimization problem for the combined CMI-CCI model

can be reduced/transformed to an 1-D optimization problem, which can be solved very fast using standard 1-D algorithms. The solution of the problem was based on geometrical properties, basis transformations and the Karush-Kuhn-Tucker (KKT) conditions. Then, simulations demonstrate that:

a. The proposed 1-D method has significantly lower computational complexity, compared to multi-dimensional algorithms.

b. In some operational environments the ergodic beamforming capacity is very close or equal to the ergodic capacity. The equality holds when a certain necessary and sufficient condition is satisfied.

Additionally the 3GPP MIMO channel model was employed in order to study further the performance of the optimum beamformer in practical operational scenarios. The 3GPP MIMO channel model was implemented in Matlab and is able to produce independent channel realizations/samples that simulate different operational environments. In this context, simulations were performed in order to:

a. Study the performance of the optimum beamformer in urban micro environments with LOS for the combined CMI-CCI model. The analysis showed that the optimum beamformer achieves ergodic capacity (with probability > 0.9) for a wide SNR range.

b. Study and compare the ergodic capacity and the performance of the optimum beamformer in different operational environments (suburban and urban macro/micro-cellular without LOS) for different channel information models. The analysis showed that in the context of the CMI and CCI models the optimum beamformer achieves ergodic capacity with probability ≥ 0.5 , in all operational environments and for a wide SNR range.

The aforementioned analysis, along with the fact that the optimum beamforming transmission is characterized by lower cost, compared to higher rank transmission schemes, justify the significance of the proposed solutions and the contribution of this work.

SUBJECT AREA: MIMO systems

KEYWORDS: MIMO channel, Capacity, Beamforming, Rician fading

ΠΕΡΙΛΗΨΗ

Η παρούσα διδακτορική διατριβή επικεντρώνεται στη δυνατότητα που έχουν τα συστήματα Πολλάπλών Εισόδων Πολλάπλών Εξόδων (MIMO) να αυξάνουν τη χωρητικότητα του καναλιού: Ένα σύστημα MIMO μπορεί να επιτύχει υψηλότερη χωρητικότητα από ένα συμβατικό σύστημα Μονής Εισόδου Μονής Εξόδου (SISO) και υπό ορισμένες συνθήκες αποδεικνύεται ότι η χωρητικότητα των συστημάτων MIMO αυξάνεται γραμμικά με το πλήθος των στοιχείων της κεραίας εκπομπής ή λήψης. Όμως η χωρητικότητα που επιτυγχάνουν τα συστήματα MIMO σχετίζεται στενά με τη γνώση/πληροφορία την οποία έχουν ο πομπός και ο δέκτης για το κανάλι. Θεωρώντας ένα εργοδικό κανάλι MIMO με μιγαδική κανονική (Gaussian) κατανομή, στο οποίο ο δέκτης έχει πλήρη γνώση του καναλιού και ο πομπός γνωρίζει μόνο την κατανομή αυτού, η αμοιβαία πληροφορία μεταξύ πομπού-δέκτη πρέπει να μεγιστοποιηθεί στατιστικά (δηλ. επιδιώκεται η μεγιστοποίηση της μέσης αμοιβαία πληροφορίας): τη μεγιστοποίηση επιτυγχάνει μια βέλτιστη πολιτική εκπομπής και η επιτυγχανόμενη μέγιστη τιμή αναφέρεται ως «εργοδική χωρητικότητα». Στην περίπτωση εκπομπής beamforming, τη μέγιστη μέση αμοιβαία πληροφορία μεταξύ πομπού-δέκτη επιτυγχάνει ο «βέλτιστος beamformer» και η επιτυγχανόμενη μέγιστη τιμή αναφέρεται ως «εργοδική beamforming χωρητικότητα». Στα πλαίσια της παρούσας διατριβής μελετάται ο τρόπος υπολογισμού του «βέλτιστου beamformer» και το πρόβλημα βελτιστοποίησης που σχετίζεται με τον εν λόγω υπολογισμό αναφέρεται ως πρόβλημα υπολογισμού της «βέλτιστης εκπομπής beamforming».

Η επίλυση του προβλήματος υπολογισμού της «βέλτιστης εκπομπής beamforming» έχει μελετηθεί στην βιβλιογραφία για μοντέλα καναλιού με κατανομή Gauss: για κανάλια MIMO με κατανομή Rayleigh (μοντέλο CCI) και χωρικώς ασυσχέιστα κανάλια MIMO με μοναδιαίο πίνακα συμμεταβολής και κατανομή Rice (μοντέλο CMI). Για τις δύο αυτές περιπτώσεις καναλιού υφίστανται μαθηματικές εκφράσεις κλειστού τύπου για τον «βέλτιστο beamformer». Δεν συμβαίνει όμως το ίδιο και για την περίπτωση χωρικώς συσχετισμένων ή ασυσχέιστων με μη-μοναδιαίο πίνακα συμμεταβολής καναλιών MIMO με κατανομή Rice (μοντέλο combined CMI-CCI): για αυτό το μοντέλο δεν

επίλυση ενός τέτοιου προβλήματος βελτιστοποίησης είναι αρκετά πολύπλοκη και χρονοβόρα και δεν ενδείκνυται για εφαρμογές πραγματικού χρόνου.

Στην παρούσα διατριβή αρχικά αποδεικνύεται ότι το προαναφερθέν πολύπλοκο και πολυδιάστατο πρόβλημα υπολογισμού της «βέλτιστης εκπομπής beamforming» για το εν λόγω μοντέλο κατανομής καναλιού (combined CMI-CCI) μπορεί να μετασχηματιστεί σε ένα μονοδιάστατο (1-Δ) πρόβλημα βελτιστοποίησης, το οποίο μπορεί να επιλυθεί πολύ γρήγορα κάνοντας χρήση κοινών μονοδιάστατων αλγορίθμων. Η απόδειξη του ανωτέρω μετασχηματισμού βασίστηκε σε γεωμετρικές ιδιότητες, σε κατάλληλους μετασχηματισμούς βάσης και στις συνθήκες Karush-Kuhn-Tucker (KKT). Στη συνέχεια υλοποιήθηκαν προσομοιώσεις οι οποίες ανέδειξαν τα ακόλουθα:

α. Η προτεινόμενη μονοδιάστατη μέθοδος υπολογισμού έχει πολύ χαμηλότερη πολυπλοκότητα συγκριτικά με αντίστοιχες πολυδιάστατες μεθόδους.

β. Σε ορισμένα κανάλια η «εργοδική beamforming χωρητικότητα» προσεγγίζει ή ισούται με την εργοδική χωρητικότητα του καναλιού. Η ισότητα ισχύει όταν ικανοποιείται μια αναγκαία και ικανή συνθήκη, η οποία εκφράζεται μέσω μιας μαθηματικής ανισότητας που περιλαμβάνει τις παραμέτρους της κατανομής του καναλιού.

Επιπρόσθετα, στα πλαίσια της διατριβής, εφαρμόστηκε το μοντέλο προσομοίωσης καναλιού MIMO της 3GPP, με σκοπό την περαιτέρω μελέτη της απόδοσης του «βέλτιστου beamformer» σε πρακτικά λειτουργικά σενάρια. Το μοντέλο της 3GPP υλοποιήθηκε σε κώδικα Matlab και δύναται να παράγει ανεξάρτητα δείγματα καναλιού με επιθυμητά χαρακτηριστικά, (προσομοίωση ενός ημιαστικού μακρο-κυψελωτού ή αστικού μικρο/μάκρο-κυψελωτού περιβάλλοντος). Σε αυτά τα πλαίσια υλοποιήθηκαν προσομοιώσεις:

α. Για τη μελέτη της απόδοσης του «βέλτιστου beamformer» σε ένα αστικό μικρο-κυψελωτό περιβάλλον με συνιστώσα οπτικής επαφής (κάνάλι MIMO με κατανομή Rice) και για το μοντέλο combined CMI-CCI. Η μελέτη έδειξε ότι, ο «βέλτιστος beamformer» μπορεί να επιτυγχάνει την εργοδική χωρητικότητα με υψηλή πιθανότητα (>0.9) και σε μεγάλο εύρος του λόγου Σήματος-Προς-Θόρυβο.

β. Για τη μελέτη της εργοδικής χωρητικότητας και της απόδοσης του «βέλτιστου beamformer» σε διάφορα λειτουργικά σενάρια (ημιαστικό ή αστικό μακρο/μικρο-

κυψελωτό κανάλι χωρίς συνιστώσα οπτικής επαφής) και διαφορετικά μοντέλα γνώσεως του καναλιού στον πομπό, (πλήρως γνωστό κανάλι, άγνωστο κανάλι, μοντέλα CMI και CCI). Η μελέτη έδειξε ότι, στα πλαίσια των μοντέλων CMI και CCI ο «βέλτιστος beamformer» μπορεί να επιτυγχάνει την εργοδική χωρητικότητα με πιθανότητα >0.5 , σε όλα τα λειτουργικά σενάρια και σε μεγάλο εύρος του λόγου Σήματος-Προς-Θόρυβο.

Η ανωτέρω ανάλυση σε συνδυασμό με το γεγονός ότι ο «βέλτιστος beamformer» αποτελεί μια πολιτική εκπομπής χαμηλότερου κόστους σε σχέση με οποιοδήποτε σχήμα εκπομπής υψηλότερης τάξης, δικαιολογούν τη σημαντικότητα της προτεινόμενης λύσης και τη συνεισφορά της παρούσας διατριβής.

ΘΕΜΑΤΙΚΗ ΠΕΡΙΟΧΗ: Συστήματα MIMO

ΛΕΞΕΙΣ ΚΛΕΙΔΙΑ: Κανάλι MIMO, Beamforming, Χωρητικότητα, Διαλείψεις Rice

I dedicate this dissertation to my precious wife Aria and my two lovely daughters, Nefeli and Eirini. I also wish to dedicate it to my parents and my father-in-law, who are and was so proud of me...

ACKNOWLEDGEMENTS

This dissertation would have never been possible without my advisors, Assistant Professor Serafim Karaboyas and Associate Professor George Tsoulos. I am deeply grateful for their support and patience to hear all the problems related to my research and try to find solutions with me. They encouraged me to further improve my results and their advice changed my way of thinking about research. I really thank you both.

I would like to thank Assistant Professors Georgia Athanasiadou and Kostantino Slavaki, from the University of Peloponnese (Informatics and Telecommunications Department), for reading part of my work and providing me with very useful comments and suggestions, that helped me improve its quality.

I would also like to mention that this work has been supported in part by the National and Kapodistrian University of Athens, in terms of conferences/funding publications.

Last but not least, I would like to thank my family - my wife and my two daughters - for the great patience that showed all these years, until the completion of this work, and their unreserved support to all my problems and concerns. They really helped me to feel better and think positive when I felt disappointed and encouraged me to continue my work.

LIST OF PUBLICATIONS

Journals Papers

1. D. E. Kontaxis, G. V. Tsoulos, G. E. Athanasiadou, and S. Karaboyas, "Optimality of transmit beamforming for spatially correlated MIMO Rician fading channels", *submitted*.
2. D. E. Kontaxis, G. V. Tsoulos, and S. Karaboyas, "Ergodic capacity optimization for single-stream beamforming transmission in MISO Rician fading channels", *IEEE Trans. Veh. Technol.*, vol. 62, no. 2, pp. 628-641, Feb. 2013.
3. D. E. Kontaxis, G. V. Tsoulos, and S. Karaboyas, "Beamforming capacity optimization for Rician MIMO wireless channels", *IEEE Wireless Commun. Lett.*, vol. 1, no. 3, pp. 257-260, June 2012.

Conference Papers

1. D. E. Kontaxis, G. V. Tsoulos, and S. Karaboyas, "Optimum ergodic beamforming capacity in urban microcellular operational environments", in *Proc. 2012 IEEE IWCMC (8th Wireless Communications and Mobile Computing Conference)*.
2. D. E. Kontaxis, G. V. Tsoulos, and S. Karaboyas, "Optimum beamforming for correlated Rician MISO channels", in *Proc. 2011 IEEE VTC - Spring (73rd Vehicular Technology Conference)*.
3. D. E. Kontaxis, G. V. Tsoulos, and S. Karaboyas, "Performance of multiple antenna systems in different operational environments", in *Proc. 2007 IEEE PIMRC (18th Personal, Indoor and Mobile Radio Communications)*.

ΣΥΝΟΠΤΙΚΗ ΠΑΡΟΥΣΙΑΣΗ ΤΗΣ ΔΙΔΑΚΤΟΡΙΚΗΣ ΔΙΑΤΡΙΒΗΣ

Τα συστήματα Πολλαπλών-Εισόδων Πολλαπλών-Εξόδων (Multiple-Input Multiple-Output ή MIMO) αποτελούν μία από τις σημαντικότερες τεχνολογικές εξελίξεις στον τομέα των τηλεπικοινωνιών και χαρακτηρίζονται από ένα ευρύ φάσμα εφαρμογών, για τις οποίες τα τελευταία χρόνια έχει αναπτυχθεί σημαντική ερευνητική δραστηριότητα και υφίσταται μεγάλο πλήθος δημοσιεύσεων στη βιβλιογραφία.

Ένα σύστημα MIMO με N κεραιές εκπομπής και M κεραιές λήψης μπορεί να επιτυγχάνει - εκμεταλλευόμενο το «πολυοδικό φαινόμενο» (multipath effect) το οποίο αναπτύσσεται στο (ραδιο)κανάλι μετάδοσης δεδομένων - υψηλότερη «αμοιβαία πληροφορία» (mutual information) καναλιού από αυτή που επιτυγχάνει ένα συμβατικό σύστημα Μονής-Εισόδου Μονής-Εξόδου (Single-Input Single-Output ή SISO), εντός του ίδιου καναλιού και για την ίδια ισχύ εκπομπής. Υπό συγκεκριμένες συνθήκες αποδεικνύεται ότι η αμοιβαία πληροφορία των συστημάτων MIMO αυξάνεται γραμμικά με το $\min\{N, M\}$.

Η αμοιβαία πληροφορία που επιτυγχάνουν τα συστήματα MIMO σχετίζεται στενά με τη γνώση/πληροφορία την οποία έχουν ο πομπός και ο δέκτης για το κανάλι. Θεωρώντας ότι ο δέκτης έχει πλήρη γνώση του καναλιού (το οποίο επιτυγχάνεται με χρήση ακολουθιών δεδομένων «εκπαίδευσης» (training data) και αλγορίθμων «εκτίμησης καναλιού») ο πομπός δύναται να έχει:

α. **Πλήρη γνώση του καναλιού**, κατόπιν ανατροφοδότησεως της πληροφορίας του καναλιού από τον δέκτη. Στην περίπτωση αυτή ο πομπός μπορεί να υπολογίζει τον τρόπο εκπομπής ο οποίος μεγιστοποιεί την αμοιβαία πληροφορία μεταξύ πομπού-δέκτη, επιτυγχάνοντας με τον τρόπο αυτό τη «χωρητικότητα» του καναλιού (channel capacity) κατά Shannon. Ο βέλτιστος τρόπος εκπομπής έγκειται στην εκπομπή ανεξάρτητων ακολουθιών δεδομένων (data streams) «κατά μήκος» κατάλληλων, ορθογώνιων μεταξύ τους διανυσμάτων (πιο συγκεκριμένα, των “right singular vectors” του πίνακα καναλιού) και με κατάλληλη κατανομή της διαθέσιμης ισχύος του πομπού μεταξύ αυτών, βάσει του αλγορίθμου “water-filling” (ο εν λόγω αλγόριθμος αποδίδει

υψηλότερο τμήμα της διαθέσιμης ισχύος στα right singular vectors που αντιστοιχούν σε υψηλότερες “singular values” του πίνακα καναλιού).

β. Καμία γνώση για το κανάλι. Στην περίπτωση αυτή ο πομπός εκπέμπει ανεξάρτητες ακολουθίες δεδομένων από κάθε στοιχείο της κεραίας και με ίση ισχύ. Η επιτυγχάνομενη αμοιβαία πληροφορία αναφέρεται ως «χωρητικότητα αγνώστου καναλιού».

γ. Γνώση της κατανομής του καναλιού. Στην πράξη η τέλεια/πλήρης γνώση του καναλιού στον πομπό (περίπτωση α. ανωτέρω) θεωρείται μη ρεαλιστική, εξαιτίας της μεγάλης καθυστέρησης (μεγαλύτερης από τον χρόνο συσχέτισης - coherence time - του καναλιού) που μπορεί να υπεισέρχεται στο κανάλι ανατροφοδότησης, με αποτέλεσμα τη μη έγκαιρη γνώση του καναλιού από τον πομπό και ως εκ τούτου την αδυναμία/αποτυχία επίτευξης της χωρητικότητας καναλιού. Κατά συνέπεια, η «μερική γνώση» του καναλιού και πιο συγκεκριμένα η γνώση της κατανομής του από τον πομπό θεωρείται ως ένα πιο ρεαλιστικό μοντέλο, (παράμετροι της κατανομής ανατροφοδοτούνται από τον δέκτη), καθόσον η κατανομή του καναλιού έχει την ιδιότητα να παραμένει σταθερή για χρόνο δεκάδες ή εκατοντάδες φορές πολλαπλάσιο του χρόνου συσχέτισης του καναλιού. Στα πλαίσια αυτού του μοντέλου ο πομπός δύναται να εκπέμπει με τρόπο (δηλ. κατά μήκος καταλλήλων ορθογώνιων διανυσμάτων, με κατάλληλη κατανομή ισχύος μεταξύ αυτών) ο οποίος μεγιστοποιεί τη μέση αμοιβαία πληροφορία (average mutual information), βασιζόμενος στην υπόθεση της εργοδικότητας του καναλιού. Η μέγιστη μέση αμοιβαία πληροφορία που επιτυγχάνεται αναφέρεται στη βιβλιογραφία ως «εργοδική χωρητικότητα» (ergodic capacity). Η εκπομπή που επιτυγχάνει την «εργοδική χωρητικότητα» σχετίζεται άμεσα με τον τύπο κατανομής του καναλιού και διαφοροποιείται βάσει αυτού.

Στη βιβλιογραφία, οι κατανομές που έχουν μελετηθεί στα πλαίσια του μοντέλου «μερικής γνώσης» του καναλιού (περίπτωση γ. ανωτέρω) είναι οι ακόλουθες:

1. Κανάλια MIMO με Rayleigh κατανομή πλάτους και χωρική συσχέτιση μεταξύ των στοιχείων της κεραίας του πομπού ή/και του δέκτη, (MIMO Rayleigh fading channels).

Η χωρική συσχέτιση εκφράζεται μέσω του πίνακα χωρικής συμμεταβολής (channel covariance matrix). Το εν λόγω μοντέλο κατανομής είναι Γκαουσιανό (Gaussian) με μηδενική μέση τιμή. Ως εκ τούτου, ο δέκτης ανατροφοδοτεί στον πομπό μόνο την

πληροφορία της χωρικής συσχέτισης και γι' αυτόν το λόγο το υπόψη μοντέλο «μερικής γνώσης» αναφέρεται στη βιβλιογραφία και ως μοντέλο «γνώσης της χωρικής μεταβολής του καναλιού» (Channel Covariance Information ή CCI model). Ο πίνακας χωρικής μεταβολής υπολογίζεται από τον δέκτη στα πλαίσια μιας μακροπρόθεσμης στατιστικής (long-term statistic) χρησιμοποιώντας πλήθος δειγμάτων του καναλιού. Ο πομπός επιτυγχάνει την «εργοδική χωρητικότητα» εκπέμποντας κατά μήκος των ιδιοδιανυσμάτων του πίνακα χωρικής μεταβολής και κατανέμοντας με αριθμητικές (μη-γραμμικές) μεθόδους τη διαθέσιμη ισχύ του μεταξύ αυτών με βέλτιστο τρόπο. Η ανωτέρω πολιτική εκπομπής εφαρμόζεται σταθερά από τον πομπό για χρονικό διάστημα (πολλαπλάσιο του χρόνου συσχέτισης του καναλιού) που εκτιμάται ότι η στατιστική/κατανομή του καναλιού που ανατροφοδοτήθηκε από τον δέκτη (δηλ. ο πίνακας χωρικής μεταβολής) παραμένει σταθερή και ως εκ τούτου χαρακτηρίζει το κανάλι. Η πολιτική εκπομπής θα αναπροσαρμόζεται όταν η κατανομή του καναλιού τροποποιηθεί και ο δέκτης ανατροφοδοτεί στον πομπό έναν νέο πίνακα χωρικής μεταβολής.

2. Κανάλια MIMO με Rician κατανομή πλάτους και χωρίς χωρική συσχέτιση μεταξύ των στοιχείων της κεραίας τόσο του πομπού όσο και του δέκτη, (uncorrelated MIMO Rician fading channels).

Το εν λόγω μοντέλο κατανομής είναι Γκαουσιανό (Gaussian) με μη-μηδενική μέση τιμή ενώ η απουσία χωρικής συσχέτισης εκφράζεται μέσω ενός μοναδιαίου πίνακα χωρικής μεταβολής. Ως εκ τούτου, ο δέκτης ανατροφοδοτεί στον πομπό μόνο τη μέση τιμή του καναλιού και γι' αυτόν το λόγο το υπόψη μοντέλο «μερικής γνώσης» αναφέρεται στη βιβλιογραφία και ως μοντέλο «γνώσης της μέσης τιμής του καναλιού» (Channel Mean Information ή CMI model). Στα πλαίσια του μοντέλου αυτού η μέση τιμή του καναλιού είναι πρακτικά η μέση τιμή του καναλιού που υπολογίζει ο δέκτη στα πλαίσια μιας μακροπρόθεσμης στατιστικής (long-term statistic) χρησιμοποιώντας πλήθος δειγμάτων του καναλιού. Θεωρητικά, η μη-μηδενική μέση τιμή θα αποτελεί τη συνιστώσα οπτικής επαφής του καναλιού - Line of Sight (LOS) multipath component. Στην περίπτωση αυτή έχουμε ένα «μακροπρόθεσμο» μοντέλο (long-term CMI model).

Το ίδιο ακριβώς μοντέλο μπορεί να προκύπτει και στην ακόλουθη περίπτωση: όταν ο δέκτης ανατροφοδοτεί δείγματα καναλιού στον πομπό και ο πομπός, εξαιτίας της

καθυστέρησης του καναλιού ανατροφοδότησης, επιχειρεί να εκτιμήσει (για κάθε λαμβανόμενο δείγμα) το πραγματικό κανάλι (πχ. με εκτίμηση τύπου MMSE) και στη συνέχεια να εφαρμόσει τη βέλτιστη πολιτική εκπομπής η οποία επιτυγχάνει τη χωρητικότητα του καναλιού. Η εκτίμηση όμως περιλαμβάνει σφάλμα και ως εκ τούτου η βέλτιστη πολιτική εκπομπή μετασχηματίζεται σε ένα πρόβλημα μεγιστοποίησης της μέσης αμοιβαίας πληροφορίας (δηλ. επίτευξης της «εργοδικής χωρητικότητας») θεωρώντας ένα εργοδικό κανάλι κατανομής Rice, με μέση τιμή το «εκτιμώμενο» κανάλι και μοναδιαίο πίνακα χωρικής μεταβολής, ο οποίος αντιπροσωπεύει τη διασπορά του σφάλματος εκτίμησης (error covariance matrix). Στην περίπτωση αυτή έχουμε ένα «βραχυπρόθεσμο» μοντέλο (short-term CMI model).

Σε κάθε περίπτωση, είτε στο «μακροπρόθεσμο» είτε στο «βραχυπρόθεσμο» μοντέλο, ο πομπός καλείται να επιλύσει ακριβώς το ίδιο πρόβλημα βελτιστοποίησης με την ακόλουθη διαφορά: Στην περίπτωση του «μακροπρόθεσμου» μοντέλου, η βέλτιστη πολιτική εκπομπής εφαρμόζεται για όλο το χρονικό διάστημα που η συνιστώσα οπτικής επαφής (LOS component) του καναλιού παραμένει σταθερή (χρονικό διάστημα δεκάδες ή εκατοντάδες φορές πολλαπλάσιο του χρόνου συσχέτισης του καναλιού) και αναπροσαρμόζεται κάθε φορά που ο δέκτης ανιχνεύει και ανατροφοδοτεί στον πομπό μια νέα/διαφορετική συνιστώσα οπτικής επαφής. Στο «βραχυπρόθεσμο» μοντέλο η βέλτιστη πολιτική εκπομπής υπολογίζεται και εφαρμόζεται μετά τη λήψη κάθε δείγματος καναλιού που ανατροφοδοτεί ο δέκτης και παραμένει σε ισχύ μόνο μέχρι τη λήψη του επόμενου δείγματος (δηλ. για χρονικό διάστημα συγκρίσιμο του χρόνου συσχέτισης του καναλιού). Το γεγονός αυτό καθιστά το «βραχυπρόθεσμο» μοντέλο πιο πολύπλοκο από το «μακροπρόθεσμο» μοντέλο.

Τόσο στο «μακροπρόθεσμο» όσο και στο «βραχυπρόθεσμο» μοντέλο, ο πομπός επιτυγχάνει την «εργοδική χωρητικότητα» εκπέμποντας κατά μήκος του κύριου (dominant) “right singular vector” (του πίνακα) της μέσης τιμής του καναλιού, καθώς και κατά μήκος $N-1$ τυχαίων διανυσμάτων, που όμως στο σύνολο τους τα N διανύσματα θα πρέπει να αποτελούν μια ορθοκανονική βάση. Επίσης η διαθέσιμη ισχύς του πομπού κατανέμεται μεταξύ των (N) διανυσμάτων εκπομπής με βέλτιστο τρόπο ο οποίος υπολογίζεται αριθμητικά.

3. Κανάλια MIMO με Rician κατανομή πλάτους και με χωρική συσχέτιση μεταξύ των στοιχείων της κεραίας του πομπού ή/και του δέκτη, (correlated MIMO Rician fading channels).

Στο μοντέλο αυτό η κατανομή του καναλιού είναι κανονική (Gaussian) με μη-μηδενική μέση τιμή, η οποία αντιπροσωπεύει τη συνιστώσα οπτικής επαφής, ενώ η χωρική συσχέτιση εκφράζεται μέσω ενός μη-μοναδιαίου πίνακα χωρικής συμεταβολής. Ο δέκτης ανατροφοδοτεί στον πομπό τόσο τη μέση τιμή του καναλιού όσο και τον πίνακα χωρικής συμεταβολής και για λόγο αυτό το υπόψη μοντέλο «μερικής γνώσης» αναφέρεται και ως μοντέλο «συνδυασμένης γνώσης της μέσης τιμής και της συσχέτισης του καναλιού» (combined CMI-CCI model). Επίσης το μοντέλο αυτό δύναται να είναι «βραχυπρόθεσμο», κατά τον τρόπο που αναλύθηκε ανωτέρω για τα MIMO Rician κανάλια χωρίς χωρική συσχέτιση, με τη διαφορά ότι ο πίνακας συμεταβολής του σφάλματος εκτίμησης (error covariance matrix) είναι πλέον μη-μοναδιαίος. Στο συνδυαστικό αυτό μοντέλο, η πολιτική εκπομπής που επιτυγχάνει την «εργοδική χωρητικότητα» δεν εκφράζεται μέσω εξισώσεων «κλειστού τύπου» και ως εκ τούτου, τόσο οι βέλτιστες κατευθύνσεις-διανύσματα εκπομπής όσο και ο βέλτιστος τρόπος κατανομής ισχύος σε αυτές θα πρέπει να υπολογιστούν αριθμητικά.

Στην περίπτωση εκπομπής beamforming όλη η διαθέσιμη ισχύς του πομπού εκπέμπεται κατά μήκος μιας και μοναδικής κατεύθυνσης/διανύσματος, το οποίο στη βιβλιογραφία αναφέρεται ως «διάνυσμα beamforming» (beamforming vector). Θεωρώντας ένα σύστημα MIMO υπό το μοντέλο «μερικής γνώσης» του καναλιού στον πομπό και στο οποίο ο πομπός εφαρμόζει αποκλειστικά εκπομπή beamforming, το διάνυσμα beamforming το οποίο μεγιστοποιεί τη μέση αμοιβαία πληροφορία μεταξύ πομπού και δέκτη αναφέρεται ως «βέλτιστο διάνυσμα beamforming» ή «βέλτιστος beamformer» (optimum beamformer), ενώ η επιτυγχανόμενη μέγιστη τιμή της μέσης αμοιβαίας πληροφορίας αναφέρεται ως «εργοδική χωρητικότητα beamforming» (ergodic beamforming capacity).

Μια εκπομπή η οποία εκμεταλλεύεται τον «βέλτιστο beamformer» θεωρείται σημαντική για τους ακόλουθους τρεις βασικούς λόγους:

α. Αποτελεί μια απλή τεχνική εκπομπής η οποία απλουστεύει στον μικρότερο δυνατό βαθμό τις απαιτήσεις υλικού (hardware) ενός συστήματος MIMO και κατά συνέπεια το κόστος αυτού.

β. Αν και η εργοδική χωρητικότητα επιτυγχάνεται εν γένει με εκπομπή υψηλότερης τάξης (δηλ. εκπέμποντας προς περισσότερες από μια κατευθύνσεις) και είναι υψηλότερη από την «εργοδική χωρητικότητα beamforming», αποδεικνύεται ότι υπάρχουν λειτουργικά περιβάλλοντα όπου ο «βέλτιστος beamformer» επιτυγχάνει την «εργοδική χωρητικότητα» (δηλ. η «εργοδική χωρητικότητα beamforming» ταυτίζεται με την «εργοδική χωρητικότητα» του καναλιού). Αυτό ισχύει όταν η κατανομή ενός καναλιού ικανοποιεί μια αναγκαία και ικανή μαθηματική συνθήκη, γνωστή στη βιβλιογραφία ως «συνθήκη βελτιστότητας του beamforming» (optimality of beamforming condition).

γ. Υφίσταται πλήθος καναλιών εντός των οποίων ο «βέλτιστος beamformer» παρουσιάζει πολύ υψηλή απόδοση και η «εργοδική χωρητικότητα beamforming» προσεγγίζει ικανοποιητικά την «εργοδική χωρητικότητα» του καναλιού. Η εν λόγω απόδοση πιστοποιήθηκε κατόπιν πλήθους προσομοιώσεων που υλοποιήθηκαν για το μοντέλο combined CMI-CCI στα πλαίσια της παρούσας διατριβής.

Στα μοντέλα CMI και CCI ο «βέλτιστος beamformer» ταυτίζεται με το κύριο ιδιοδιάνυσμα του πίνακα αυτοσυσχέτισης του καναλιού (channel correlation matrix) και πρακτικά ταυτίζεται με το διάνυσμα που μεγιστοποιεί το μέσο λαμβανόμενο SNR, το οποίο αναφέρεται ως “max SNR beamformer”. Όμως για το combined CMI-CCI μοντέλο δεν υφίσταται απλή μαθηματική έκφραση για τον «βέλτιστο beamformer». Στο μοντέλο αυτό ο «βέλτιστος beamformer» υπολογίζεται αριθμητικά και αποτελεί τη λύση ενός πολυδιάστατου, μη γραμμικού, convex προβλήματος βελτιστοποίησης: πιο συγκεκριμένα πρέπει να υπολογιστούν τα N μιγαδικά στοιχεία του «βέλτιστου beamformer», δηλ. $2N$ πραγματικές παράμετροι. Ως εκ τούτου, η επίλυση του συγκεκριμένου προβλήματος (με χρήση ευρέως διαδεδομένων πολυδιάστατων αλγορίθμων, πχ. μεθόδων «εσωτερικού σημείου» (interior-point methods)) χαρακτηρίζεται από υψηλή πολυπλοκότητα, η οποία είναι απαγορευτική για εφαρμογές με απαιτήσεις πραγματικού χρόνου. Στην πράξη, ο πομπός πρέπει να μπορεί να υπολογίζει τον «βέλτιστο beamformer» πολύ γρηγορότερα από τον χρόνο μεταβολής

της στατιστικής του καναλιού, ο οποίος εν γένει μπορεί να είναι μικρός, ιδιαίτερα σε κανάλια με μικρό χρόνο συσχέτισης.

Όλα τα ανωτέρω αναλύονται και περιγράφονται στο 1^ο και 2^ο Κεφάλαιο της διατριβής.

Στο 3^ο και 4^ο Κεφάλαιο της διατριβής αποδεικνύεται ότι το πρόβλημα υπολογισμού του «βέλτιστου beamformer» στα πλαίσια του μοντέλου combined CMI-CCI μπορεί να μετασχηματιστεί σε ένα μονοδιάστατο (1-Δ) πρόβλημα βελτιστοποίησης και στη συνέχεια να επιλυθεί πολύ γρήγορα με χρήση απλών αλγορίθμων (πχ. με τη μέθοδο της “χρυσής τομής”). Αρχικά η εν λόγω απόδειξη παρουσιάζεται για συστήματα Πολλαπλών-Εισόδων Μονής-Εξόδου (Multiple-Input Single-Output ή MISO) και στη συνέχεια γενικεύεται για συστήματα MIMO, για το «μακροπρόθεσμο» μοντέλο combined CMI-CCI. Επιπρόσθετα, αποδείχθηκαν και τα ακόλουθα:

- Το υπόψη μονοδιάστατο πρόβλημα βελτιστοποίησης απλοποιείται ακόμη περισσότερο για τις περιπτώσεις συστημάτων MISO 2×1 , MISO 3×1 και MIMO $2 \times M$.
- Στα συστήματα MISO η μέση αμοιβαία πληροφορία στην περίπτωση εκπομπής beamforming μπορεί να υπολογιστεί μέσω μια άπειρης σειράς (infinite-series representation), η οποία να συγκλίνει πολύ γρήγορα (δηλ. με μικρό πλήθος όρων) στην αντίστοιχη τιμή που προκύπτει μέσω ολοκλήρωσης Monte Carlo. Η χρήση της σειράς αυτής (αντί της μεθόδου Monte Carlo) επιταχύνει ακόμη περισσότερο τον υπολογισμό του «βέλτιστου beamformer».

Την ανωτέρω απόδειξη ακολούθησε πλήθος προσομοιώσεων (για το μοντέλο combined CMI-CCI και ομοιόμορφες γραμμικές στοιχειοκεραίες), στα πλαίσια των οποίων:

- α. Πραγματοποιήθηκε σύγκριση της μονοδιάστατης μεθόδου με πολυδιάστατους αλγόριθμους: αρχικά με αλγόριθμο «εσωτερικού σημείου» (interior-point) με λογαριθμική συνάρτηση φράγματος (logarithmic barrier function) και εν συνεχεία με μια αναδρομική ασυμπτωτική (και κατά συνέπεια υπο-βέλτιστη) μέθοδο υπολογισμού, η οποία χαρακτηρίζεται από υψηλή ταχύτητα σύγκλισης στη βέλτιστη λύση (δηλ. στον «βέλτιστο beamformer»), καθώς δεν απαιτείται ολοκλήρωση Monte Carlo. Σε κάθε

περίπτωση τα αποτελέσματα έδειξαν ότι η μονοδιάστατη μέθοδος είναι περίπου μια τάξη μεγέθους ταχύτερη από τις αντίστοιχες πολυδιάστατες μεθόδους.

β. Έγινε σύγκριση της «εργοδικής χωρητικότητας beamforming» που επιτυγχάνει ο «βέλτιστος beamformer», με τη μέση αμοιβαία πληροφορία που επιτυγχάνει ο “max SNR beamformer”. Η σύγκριση έδειξε ότι το κέρδος του ρυθμού μετάδοσης που επιτυγχάνει ο «βέλτιστος beamformer» έναντι του “max SNR beamformer” δύναται να είναι σημαντικό.

γ. Πραγματοποιήθηκε σύγκριση της «εργοδικής χωρητικότητας beamforming» που επιτυγχάνει ο «βέλτιστος beamformer», με την «εργοδική χωρητικότητα» και:

- Επιβεβαιώθηκε ότι σε περιβάλλοντα/κανάλια που ικανοποιείται η συνθήκη “optimality of beamforming”, η «εργοδική χωρητικότητα beamforming» ισούται με την «εργοδική χωρητικότητα».

- Πιστοποιήθηκε ότι υφίστανται περιβάλλοντα/κανάλια που δεν ικανοποιείται η συνθήκη “optimality of beamforming”, όμως ο «βέλτιστος beamformer» μπορεί να επιτυγχάνει «εργοδική χωρητικότητα beamforming» πολύ κοντά στην «εργοδική χωρητικότητα» (την οποία επιτυγχάνει μία εκπομπή υψηλότερης τάξης, γενικά).

δ. Πραγματοποιήθηκε στατιστική μελέτη της συνθήκης “optimality of beamforming” και προσδιορίστηκαν οι παράμετροι καθώς και ο τρόπος που αυτές επηρεάζουν την εν λόγω συνθήκη.

Στο 5^ο Κεφάλαιο της διατριβής έγινε ανάπτυξη λογισμικού (σε κώδικα Matlab), με το οποίο υλοποιήθηκε το μοντέλο προσομοίωσης καναλιών MIMO του 3GPP (3rd Generation Partnership Project). Το μοντέλο δύναται να προσομοιώνει διαφορετικά λειτουργικά περιβάλλοντα (αστικά ή ημιαστικά) στα πλαίσια ενός κυψελωτού συστήματος κινητών επικοινωνιών και να παράγει επιθυμητό πλήθος (ανεξάρτητων μεταξύ τους) δειγμάτων του πίνακα καναλιού. Επιπλέον, το μοντέλο μπορεί να προσομοιώνει και επιπρόσθετα χαρακτηριστικά που δύναται να ενσωματώνει ένα κανάλι, όπως είναι η συνιστώσα οπτικής επαφής (LOS component), οι μακρινοί σκεδαστές (far scatterer clusters), το αστικό «φαράγγι» (urban canyon) και κεραίες εκπομπής ή/και λήψης με πόλωση (polarized antennas).

Δείγματα του πίνακα καναλιού που παρήχθησαν με το ανωτέρω μοντέλο χρησιμοποιήθηκαν στη συνέχεια σε προσομοιώσεις ως ακολούθως:

α. Για τη σύγκριση των μοντέλων «γνωστό κανάλι στον πομπό», «άγνωστο κανάλι στον πομπό», CCI και «βραχυπρόθεσμο» CMI, ως προς την «εργοδική χωρητικότητα» που αυτά επιτυγχάνουν (ως συνάρτηση του SNR) για τα ακόλουθα κανάλια:

- αστικά μακροκυψελωτά (urban macrocellular) με 8° ή 15° μέση γωνιακή διασπορά (angular spread) στον σταθμό βάσης,
- αστικά μικροκυψελωτά (urban microcellular) ,
- ημιαστικά μακροκυψελωτά (suburban macrocellular).

Τα αποτελέσματα της σύγκρισης έδειξαν ότι σε όλα τα κανάλια ισχύει η ακόλουθη σειρά φθίνουσας απόδοσης για τα υπό μελέτη μοντέλα: «γνωστό κανάλι στον πομπό», CCI, «βραχυπρόθεσμο» CMI, «άγνωστο κανάλι στον πομπό». Επιπρόσθετα, φαίνεται ότι στα ημιαστικά μακροκυψελωτά και αστικά μακροκυψελωτά με μέσο “angular spread” 8° η απόδοση του μοντέλου CCI προσεγγίζει σε μεγάλο βαθμό την απόδοση του μοντέλου «γνωστό κανάλι στον πομπό».

β. Για τη στατιστική μελέτη της συνθήκης “optimality of beamforming”, για το «βραχυπρόθεσμο» μοντέλο CMI και τα ακόλουθα κανάλια:

- αστικά μακροκυψελωτά (urban macrocellular) με μέσο “angular spread” στον σταθμό βάσης 8° ή 15° ,
- αστικά μικροκυψελωτά (urban microcellular) ,
- ημιαστικά μακροκυψελωτά (suburban macrocellular).

Τα αποτελέσματα έδειξαν ότι η πιθανότητα να ικανοποιείται η υπόψη συνθήκη φθίνει με το SNR και το περιβάλλον ως ακολούθως: αστικό μακροκυψελωτό μέσου “angular spread” 15° , αστικό μακροκυψελωτό μέσου “angular spread” 8° , ημιαστικό μακροκυψελωτό (με πιθανότητα που προσεγγίζει σημαντικά αυτή του αστικού μακροκυψελωτού μέσου “angular spread” 8°) και αστικό μικροκυψελωτό.

γ. Για τη στατιστική μελέτη της συνθήκης “optimality of beamforming”, για το μοντέλο CCI και τα ακόλουθα κανάλια:

- αστικά μακροκυψελωτά (urban macrocellular) με μέσο “angular spread” στον σταθμό βάσης 8° ή 15° ,
- αστικά μικροκυψελωτά (urban microcellular) ,
- ημιαστικά μακροκυψελωτά (suburban macrocellular).

Τα αποτελέσματα έδειξαν ότι η πιθανότητα να ικανοποιείται η υπόψη συνθήκη φθίνει με το SNR και το περιβάλλον ως ακολούθως: ημιαστικό μακροκυψελωτό, αστικό μακροκυψελωτό μέσου “angular spread” 8° , αστικό μακροκυψελωτό μέσου “angular spread” 15° και αστικό μικροκυψελωτό.

δ. Για τη συγκριτική μελέτη της απόδοσης του «βέλτιστου beamformer» ως προς τον “max SNR beamformer”, (εκπομπή beamforming μικρότερης πολυπλοκότητας σε σχέση με τον υπολογισμό του «βέλτιστου beamformer» για το μοντέλο combined CMI-CCI), καθώς και τη στατιστική μελέτη της συνθήκης “optimality of beamforming” σε αστικά μικροκυψελωτά κανάλια με συνιστώσα οπτικής επαφής, (για απόσταση πομπού δέκτη $<300\text{m}$). Για τα εν λόγω κανάλια, τα οποία προσομοιώνουν στον βέλτιστο δυνατό βαθμό το «μακροπρόθεσμο» μοντέλο combined CMI-CCI, προέκυψαν τα ακόλουθα αποτελέσματα:

- Η συνθήκη “optimality of beamforming” ικανοποιείται με πολύ υψηλή πιθανότητα (>0.99), γεγονός το οποίο συνεπάγεται την αποκλειστική χρήση του «βέλτιστου beamformer» στο εν λόγω περιβάλλον για την επίτευξη της «εργοδικής χωρητικότητας».

- Το κέρδος του «βέλτιστου beamformer» ως προς τον “max SNR beamformer” είναι ασήμαντο σε μεγάλο εύρος του SNR, (η «εργοδική χωρητικότητα beamforming» σχεδόν ταυτίζεται με τη μέση αμοιβαία πληροφορία που επιτυγχάνει ο “max SNR beamformer”). Προκύπτει λοιπόν το συμπέρασμα ότι σε αστικά μικροκυψελωτά κανάλια με συνιστώσα οπτικής επαφής (LOS component) μπορεί να χρησιμοποιηθεί ως βέλτιστη πολιτική εκπομπής ο “max SNR beamformer”, (ο οποίος επιτυγχάνει την «εργοδική χωρητικότητα» με υψηλή πιθανότητα, βάσει της προηγούμενης παρατήρησης).

Τέλος, στο 6^ο Κεφάλαιο παρουσιάζονται συγκεντρωτικά τα σημαντικότερα συμπεράσματα της διατριβής.

CONTENTS

ABSTRACT	8
LIST OF TABLES	32
LIST OF FIGURES	35
1 INTRODUCTION	39
1.1 From smart antennas to MIMO systems	39
1.2 Spectral efficiency of MIMO systems	43
1.3 Thesis outline	46
1.4 Notation	47
2 CAPACITY OF MIMO CHANNELS	49
2.1 Introduction	49
2.2 MIMO channels capacity	52
2.2.1 Perfect CSI at the receiver and the transmitter	52
2.2.2 Perfect CSI at the receiver and unknown channel to the transmitter	54
2.2.3 Perfect Channel State Information (CSI) at the receiver and Channel Distribution Information at the transmitter (CDIT)	55
2.3 Rate-Optimum beamforming transmission in MIMO channels	62
3 RATE-OPTIMUM BEAMFORMING TRANSMISSION IN MISO Rician FADING CHANNELS	67
3.1 Introduction	67
3.2 System model and problem statement	69

3.3	Optimum beamforming transmission in MISO Rician fading channels	70
3.4	Simulation results	89
3.4.1	Simulation model	89
3.4.2	Calculation of the optimum beamformer	91
3.4.3	Computational complexity assessment	93
3.4.4	Simulation results for the ergodic beamforming capacity	98
4	RATE-OPTIMUM BEAMFORMING TRANSMISSION AND RESULTS FOR THE OPTIMALITY OF BEAMFORMING CONDITION FOR MIMO RICIAN FADING CHANNELS	105
4.1	Introduction	105
4.2	System model and problem statement	105
4.3	Optimum beamforming transmission in MIMO Rician fading channels	107
4.4	Simulation results for the optimum beamformer	112
4.4.1	Simulation model	112
4.4.2	Computational complexity assessment	113
4.4.3	Simulation results for the ergodic beamforming capacity	117
4.5	Simulation results for the optimality of beamforming	119
5	CAPACITY AND OPTIMALITY OF BEAMFORMING FOR DIFFERENT OPERATIONAL ENVIRONMENTS	127
5.1	Introduction	127
5.2	MIMO channel simulation model	127
5.3	Simulations for MISO 2×1 Rayleigh fading channels	132
5.3.1	Simulation results for the ergodic capacity	136
5.3.2	Simulation results for the optimality of beamforming	139

5.4	Simulations for MISO 4×1 Rician fading channels	142
5.4.1	Simulation results for the ergodic beamforming capacity	144
5.4.2	Simulation results for the optimality of beamforming	148
6	CONCLUSIONS AND FUTURE WORK	151
6.1	Rate-optimum beamforming transmission in MISO and MIMO Rician fading channels	151
6.2	Simulations for different operational environments	155
6.3	Future work	157
	LIST OF ABBREVIATIONS	159
	BIBLIOGRAPHY	161

LIST OF TABLES

3.1	Relation between correlation coefficient ρ and interelement distance D . . .	90
3.2	Simulation scenarios	94
3.3	Parameters of the 1-D algorithm for the calculation of the optimum beamformer	94
3.4	Parameters of the multidimensional algorithm for the calculation of the optimum beamformer	95
3.5	Parameters for the solution of the 2×2 (non-linear) system of equations in [50]	95
4.1	Parameters of the 1-D algorithm for the calculation of the optimum beamformer	113
4.2	Parameters of the multidimensional algorithm for the calculation of the optimum beamformer	114
5.2	Correlation coefficient statistics	131
5.3	Statistics of channel error variance and feedback quality	141
5.1	Channel simulation process	150

LIST OF FIGURES

1-1	Space Division Multiple Access (SDMA) [13].	40
1-2	Switched Beams technique [13].	40
1-3	Spatial Filtering for Interference Reduction (SFIR) technique [13].	41
1-4	MIMO techniques.	42
2-1	$N \times M$ MIMO system.	49
2-2	Transmission with Q_{opt}	52
2-3	Waterfilling algorithm.	53
2-4	Transmission for Unknown Channel to the transmitter.	54
2-5	CDIT models.	62
2-6	Beamforming transmission.	63
3-1	$\mathcal{I}_{\text{bf,avg}}$ vs. $m_{\mathbf{v}}$ and $\sigma_{\mathbf{v}}$	72
3-2	Geometric interpretation of Proposition 3.2.	74
3-3	Diagrammatic representation of the calculation of \mathbf{v}_{θ} (equation (3.23)) for Theorem 3.1 (<i>EIG</i> stands for eigen-decomposition).	86
3-4	Convergence of the infinite-series (3.77), for different $\{m_{\mathbf{v}}, \sigma_{\mathbf{v}}\}$ values and a MISO 4×1 system with SNR = 10dB.	89
3-5	MISO 4×1 system, where the multipath from a user (MS), at an angle ψ with respect to the transmit antenna boresight, arrives at the base station (BS) with an angular spread Δ	91
3-6	Unimodal (a), and non unimodal (b) cases of $\mathcal{I}_{\text{bf,avg}}(\theta)$	92

3.7	Runtime vs. the number of channel samples for a MISO 4×1 sytem (a), and the number of transmit antenna elements N (MISO $N \times 1$) with 2×10^4 channel samples (b).	97
3.8	$\mathcal{E}[\Delta\mathcal{I}_{\text{bf,avg}}]$ vs. $\ \boldsymbol{\mu}\ _2$ and ρ , for a MISO 4×1 system with $\{N = 4, \beta = 1, \phi = 85^\circ, \text{SNR} = 10\text{dB}\}$	99
3.9	$\mathcal{E}[\Delta\mathcal{I}_{\text{bf,avg}}]$ and $\mathcal{E}\left[\frac{\Delta\mathcal{I}_{\text{bf,avg}}}{\mathcal{I}_{\text{bf,avg}}(\text{SNR}, \mathbf{v}_{\text{maxSNR}})}\right]$ vs. the SNR, for a MISO 4×1 system with $\{\ \boldsymbol{\mu}\ _2 = 1.6, \rho = 0.9, \phi = 85^\circ, \beta = 1\}$	100
3.10	Ergodic capacity C_{erg} and ergodic beamforming capacity C_{bf} achieved by the asymptotic approach from [50] and the optimum beamformer, respectively, versus the SNR, for a MISO 4×1 system and different fading scenarios: (a) $\{K = 0.5, \rho = 0.9, \phi = 85^\circ\}$, (b) $\{K = 0.1, \rho = 0.5, \phi = 85^\circ\}$	102
3.11	Ergodic capacity C_{erg} and ergodic beamforming capacity C_{bf} achieved by the asymptotic approach from [50] and by the optimum beamformer, respectively, vs. the SNR, for a MISO 4×1 system, the transmit antenna array configuration used in [49] and different fading scenarios: $K = 0.1$ and $K = 1$	103
4.1	$\mathcal{I}_{\text{bf,avg}}$ vs. $\sigma_{\mathbf{z}}$ and $ \mathbf{q}\mathbf{v}^\dagger $, for $\{\mathbf{R}_r = \mathbf{I}_M, \mu = 1\}$	111
4.2	MIMO 4×4 system.	113
4.3	Runtime vs. the number of channel samples.	115
4.4	Runtime vs. the number of transmit antenna elements (N).	116
4.5	$\mathcal{E}[\Delta\mathcal{I}_{\text{bf,avg}}]$ vs. $\ \boldsymbol{\mu}\ _2$ and ρ_t , for a MIMO 4×4 system with $\{\phi = 85^\circ, \beta = 0.2, \text{SNR} = 10\text{dB}\}$	118
4.6	Optimality region $\mu - \rho_t$, for a MIMO 4×4 system and $\{\text{SNR} = 0/3\text{dB}, \phi = 35^\circ/65^\circ, \Delta_r = 68^\circ\}$	120
4.7	Pr_{bf} vs. SNR, for a MIMO 4×4 system and $\{\beta = 0.01, \phi = 45^\circ, \mu = 1.4, \rho_t = 0.1, \Delta_r = 68^\circ\}$	122

4.8	Pr_{bf} vs. SNR, for a MIMO 4×4 system and $\{\beta = 0.14, \phi = 45^\circ, \mu = 1.4, \rho_t = 0.1, \Delta_r = 68^\circ\}$.	123
4.9	Optimality region $\mu - \rho_t$, for a MIMO 4×4 system and $\{\text{SNR} = 0\text{dB}, \beta = 0.1, \Delta_r = 68^\circ\}$.	123
4.10	Optimality region $\mu - \rho_t$, for a MIMO 4×4 system and $\{\text{SNR} = 0\text{dB}, \beta = 0.2, \Delta_r = 68^\circ\}$.	124
4.11	Pr_{bf} vs. M , for $\{N = 4, \text{SNR} = 0\text{dB}, \Delta_r = 68^\circ\}$.	126
5.1	Two tier celular structure. s_i is the sector numbering, with $i = 1, \dots, 3$ for the 3-sector scenario or $i = 1, \dots, 6$ for the 6-sector scenario.	130
5.2	Rayleigh distribution of $ \mathbf{H}_{1,n} $.	131
5.3	Ergodic capacity vs. SNR, in a suburban environment.	137
5.4	Ergodic capacity vs. SNR, in an urban macro environment with $\mathcal{E}[\sigma_{AS}] = 8^\circ$.	138
5.5	Ergodic capacity vs. SNR, in an urban macro environment with $\mathcal{E}[\sigma_{AS}] = 15^\circ$.	138
5.6	Ergodic capacity vs. SNR, in an urban micro environment.	139
5.7	Propability of beamforming vs. SNR, for the CMI model.	140
5.8	Propability of beamforming vs. SNR, for the CCI model.	140
5.9	$\Delta\mathcal{I}_{\text{st}}$ vs. SNR.	146
5.10	$\Delta\mathcal{I}_{\text{it}}$ vs. SNR.	148
5.11	$C_{\text{bf}}^{\text{st}}, C_{\text{bf}}^{\text{lt}}$ and $\left(\frac{C_{\text{bf}}^{\text{st}} - C_{\text{bf}}^{\text{lt}}}{C_{\text{bf}}^{\text{lt}}} \times 100\right)$ vs. SNR.	149

Chapter 1

INTRODUCTION

1.1 From smart antennas to MIMO systems

Since the early nineties adaptive/smart antennas have been a technical breakthrough in wireless communications. Smart antennas were used in RADAR and SONAR systems during the 2nd World War, mainly for the “shaping” of the antenna radiation pattern. Van Atta was the first who introduced in 1959 the term “adaptive antenna”, in order to describe antennas able to transmit along the direction of reception [1]. Later on, in the sixties, Howells [2]-[3], Applebaum [4] and Widrow [5]-[7] developed algorithms for the adaptive mitigation of interference and Capon [8] for finding the direction of mobile stations, using adaptive antennas. In the seventies and eighties there was a lot of research on algorithms for adaptive antennas (optimum combining, direction finding [9], etc.). This technology was heavily promoted in the European Union in the nineties by three collaborative R&D programs (TSUNAMI) [10]-[11] with key players the universities of Bristol, Aalborg and Catalonia, while the university of Stanford along with companies like Metawave, Nortel Networks and Arraycomm [12] were the main proponents on the other side of the Atlantic.

Smart antennas used at the base stations of cellular systems can enhance the SNR (Signal to Noise Ratio) or the SINR (Signal to Interference plus Noise Ratio) for both links. Interference in cellular systems is considered to be the received signal from “undesired” mobile stations/users of the same cell (intracell interference) or different cells (intercell interference) or other base stations. An increase in the SNR/SINR increases the downlink/uplink channel capacity and/or reduces the bit-error-rate (BER), increases the communication range or reduces the downlink and/or uplink transmit power.

The aforementioned benefits can be achieved by employing various techniques like Space Division Multiple Access (SDMA) as shown in Figure 1.1 [13], Switched Beams

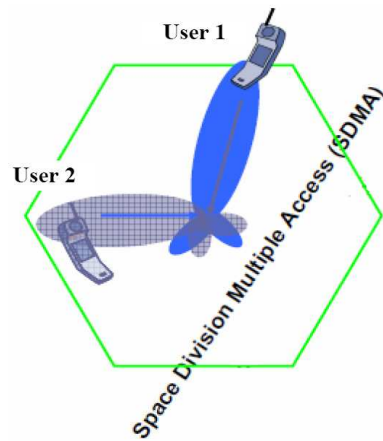


Figure 1-1: Space Division Multiple Access (SDMA) [13].

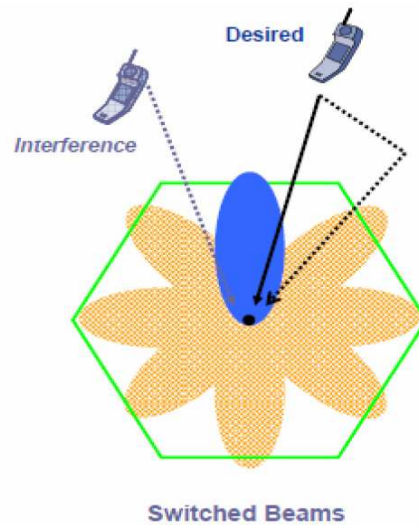


Figure 1-2: Switched Beams technique [13].

as shown in Figure 1.2 [13], and Spatial Filtering for Interference Reduction (SFIR) as shown in Figure 1.3 [13]. For the SFIR technique and the calculation of the optimum steady-state solution for the weight vector of the adaptive/smart antenna, the following performance measures can be employed, which were discussed and analyzed in [14]:

- a. Mean Square Error (MSE) criterion.
- b. Signal to Noise Ratio (SNR) criterion.
- c. Maximum Likelihood (ML) criterion.
- d. Minimum Variance (MV) criterion.

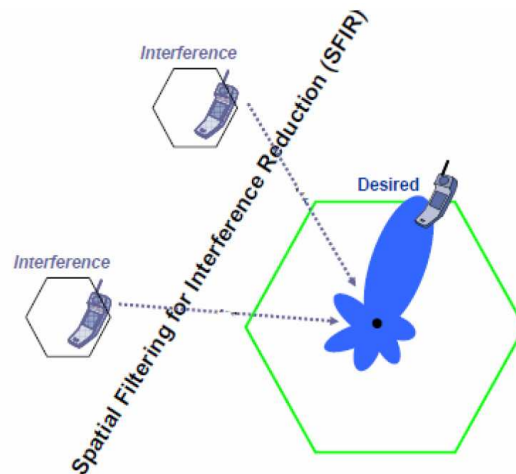


Figure 1.3: Spatial Filtering for Interference Reduction (SFIR) technique [13].

There are several examples of generic smart antenna systems reported in the open literature, with one basic thing in common: the mobile station is equipped with a single-element antenna (e.g. a dipole antenna). The idea of using antennas with multiple elements also at the mobile station opened the way for the transition from smart/adaptive antennas to multiple-input multiple-output (MIMO) systems, which are able to employ more intelligent algorithms that further improve system performance (capacity, BER and coverage) in “harsh” multipath environments, without the expense of additional bandwidth.

It is true that the last few years we are witnessing an unprecedented growth in user demand for high speed wireless communications and novel communication paradigms and applications create an ever increasing volume of data traffic. The desired characteristics of broadband wireless communication systems are:

- high spectral efficiency and data rates,
- high Quality Of Service (e.g. small bit-error-rate (BER)),
- wide coverage,
- low deployment, maintenance and operation costs.

However, in most cases, the wireless channel is very “hostile” and causes severe fluctuations in the (received) signal level, due to multipath propagation (multipath fading).

ing). Effects like path-loss (i.e. the signal power decrease with distance), shadowing (i.e. the path-loss fluctuation at the same distance), noise and interference, all degrade the performance of wireless communication systems. Moreover, the desired communication bandwidth may not be always available.

MIMO systems employ multiple transmit and receive antennas to combat/exploit the aforementioned “hostility” of the wireless channel: MIMO systems increase spectral efficiency, Quality of Service and coverage, whereas they are capable of mitigating interference. MIMO systems exploit multipath propagation to achieve these benefits, without the expense of additional bandwidth. (These advantages make MIMO a very attractive and promising option for future mobile communication systems especially when combined with the benefits of orthogonal frequency-division multiplexing (OFDM)). The techniques employed by MIMO systems in order to achieve the aforementioned benefits are the following (see also Figure 1.4):

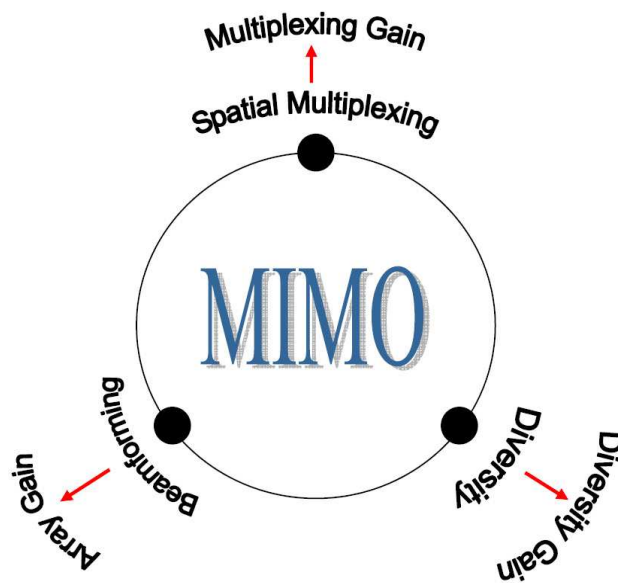


Figure 1.4: MIMO techniques.

a. **Beamforming.** Transmit and/or receive beamforming (i.e. transmission and/or reception along a unique direction/vector) is mainly designed to offer *array gain*, i.e. increase of the SNR, when the channel is known at both ends of the radio link, (at the trans-

mitter/receiver for transmit/receive beamforming, respectively). However, beamforming can also offer *diversity gain*. Both gains enhance system coverage and BER. Moreover, SNR maximization through transmit beamforming may - under certain conditions (e.g. for MISO systems with channel knowledge at the transmitter) - maximize system's spectral efficiency, (i.e. achieve maximization of the mutual information).

b. **Diversity.** Transmit diversity techniques (for MISO and MIMO systems) - when the channel is unknown to the transmitter - exploit transmission along Space and Time, and for this reason the related transmission is referred to in the literature as Space-Time Coding (STC) [15]-[22]. The Alamouti transmission scheme, Space-Time Block Codes (STBC) and Space-Time Trellis Codes (STTC) are some examples of STC transmission. Receive diversity techniques (for SIMO systems), like Maximum Ratio Combining (MRC) [23]-[24], can also be employed. Transmit and receive diversity techniques offer both diversity and array gain, enhancing in this manner system coverage and BER.

c. **Spatial multiplexing.** Spatial multiplexing techniques are transmission techniques mainly designed to enhance spectral efficiency, i.e. maximize the mutual information between transmitter and receiver, based on the available Channel State Information (CSI) at both ends of the radio link, (e.g. full- or partial- or no-CSI at the transmitter combined with full-CSI at the receiver are the most studied cases in the open literature).

It is important to note here, that in any of the aforementioned cases, where transmit precoding is employed by the MIMO system (i.e. transmit beamforming, transmit diversity and spatial multiplexing) the achieved diversity and array gain and hence, the achieved throughput (i.e. effective data rate, which is related to the BER) depends also on the detection method that is employed at the receiver (e.g. ZF, MMSE, ML etc.). Trade-offs between diversity, array and multiplexing gain are discussed in [25]-[26].

1.2 Spectral efficiency of MIMO systems

As it was discussed in the previous section of this chapter, MIMO systems can be exploited to significantly increase channel capacity, through spatial multiplexing techniques.

Pioneering works by Winters [27], Foschini [28] and Telatar [29] ignited much interest in this area by predicting remarkable spectral efficiencies for wireless systems with multiple antennas when the channel exhibits rich scattering and its variations can be accurately tracked. This resulted in an explosion of research activity to characterize the theoretical and practical issues associated with MIMO wireless channels [30].

Many MIMO techniques have been developed to capitalize on the theoretical capacity gains predicted by Shannon theory. A major focus of such work is space-time coding [31]. Other techniques for MIMO systems include space-time modulation [32], [33], adaptive modulation and coding [34], space-time equalization [35], [36], space-time signal processing [37], space-time CDMA [38], [39], and space-time OFDM [40], [41], [42]. A good overview in these areas and other practical techniques along with their performance can be found in [43].

A MIMO system with N transmit and M receive antenna elements, can achieve (for the same channel and transmit power), much higher capacity than a conventional Single-Input Single-Output (SISO) system. It has been shown in [28]-[29] that under certain conditions, the capacity achieved by MIMO systems increases linearly with the $\min\{N, M\}$. For MIMO systems with perfect CSI at both ends of the link (transmitter/receiver), the spatial pre-coding transmission scheme that achieves capacity was presented in [28]-[29]. However, perfect CSI at the transmitter is practically unrealistic, mainly due to the inevitable delay in the control channel which is used to feed back the CSI from the receiver [44] or due to the delay in the channel estimation algorithm employed at the transmitter [45]. Instead, it is more realistic and practical to assume that the transmitter has knowledge of the parameters of the MIMO channel distribution, since the channel statistics usually remain invariant in a large time window, (tens to hundreds of times larger than the coherence time [44]). This channel feedback information model is referred to as “Transmitter Channel Distribution Information” or CDIT model [30]. In a CDIT model the optimum transmission maximizes the average mutual information (between transmitter and receiver) and the rate (in bps/Hz) achieved in this case is referred to as “ergodic

capacity”.

The (optimum) spatial pre-coding transmission scheme that achieves ergodic capacity has been addressed in the literature for the following complex Gaussian CDIT models:

a. Channel Covariance Information or CCI model. This model represents MIMO Rayleigh fading channels and was studied in [46]-[48].

b. Channel Mean Information or CMI model. This model represents spatially uncorrelated MIMO Rician fading channels with unit covariance matrix (i.e. of the form $a\mathbf{I}$) and was studied in [46]-[47].

c. Combined CMI-CCI model. This model represents spatially correlated or uncorrelated with non-unit covariance matrix MIMO Rician fading channels and was studied in [49] and [50].

Several modern wireless systems incorporate MIMO techniques [51]:

a. **IEEE 802.11n WiFi** [52]-[53]. MIMO-OFDM wireless LAN products based on the IEEE 802.11n WiFi (5GHz band) standard are available and achieve throughput up to 600 Mbps. The MIMO techniques adopted in this standard are open-loop (i.e. CSI at the transmitter is not required) and include transmit beamforming, spatial multiplexing (maximum 4 spatial streams in a 40MHz channel) and diversity techniques (STBC and Cyclic Shift Diversity (CSD), and the conventional receive diversity technique MRC).

b. **IEEE 802.16 WiMAX** [54]-[56]. The IEEE 802.16 wireless MAN standard known as WiMAX also includes MIMO features (used along with OFDM/OFDMA or TDM/TDMA transmission). Fixed WiMAX services are being offered by operators worldwide. Mobile WiMAX networks based on IEEE 802.16e are being deployed (2-6GHz band for mobile applications and 2-11GHz band for fixed applications), while IEEE 802.16m is under development (it enables interoperability between WiMAX and LTE, supports high mobility up to 350 km/h and data rates up to 300 Mbps). WiMAX supports open and closed-loop MIMO techniques. The open-loop techniques include spatial multiplexing (4 spatial streams with a 4×4 MIMO configuration) and STC transmission based on the Alam-

outi scheme. The closed-loop techniques include spatial multiplexing, STC, and adaptive beamforming.

c. **IEEE 802.20 MBWA** [57]-[58]. IEEE 802.20 mobile broadband wireless access (MBWA) standard ($<3.5\text{GHz}$) proposes a complete cellular structure and is designed to support mobility including high-speed mobile users (250 km/h). The standard incorporates MIMO-OFDM/OFDMA and MIMO-CDMA transmission, (OFDM/OFDMA for the downlink/uplink and CDMA for the uplink). For the single-user MIMO (SU-MIMO) transmission, 802.20 supports spatial multiplexing and diversity techniques, utilizing up to 4 transmit antennas. The standard also supports multi-user MIMO (MU-MIMO) transmission, by employing Space Division Multiple Access (SDMA).

d. **LTE** [59]-[60]. The 3GPP Long Term Evolution (LTE) adopts MIMO transmission (OFDM /OFDMA for the downlink and SC-FDMA for the uplink transmission), which includes spatial multiplexing, diversity and beamforming. LTE achieves typical throughputs of 100 Mbps and 50 Mbps in the downlink and the uplink, respectively, in the 20MHz channel (1.25, 2.5, 5, 10 and 20 MHz bandwidths are supported), and specifies full performance in a 5 km radius (with slight degradation from 5-30 km, while operation up to 100 km may be possible). Moreover, it supports high-speed mobility (high performance at speeds up to 120 km/h, while connectivity is maintained up to 350 km/h or up to 500 km/h).

1.3 Thesis outline

The present doctoral thesis discusses the capacity of MIMO systems for single-user systems (i.e. SU-MIMO) and different channel information models. The main focus is on the calculation of the (optimum) beamforming transmission that maximizes the average mutual information (between transmitter and receiver) in spatially correlated MIMO Rician flat fading channels (i.e. under the combined CMI-CCI model).

The doctoral thesis is organized as follows:

In Chapter 2, basic definitions and known results on the capacity of MIMO systems

are provided. Moreover, the channel feedback information models considered throughout the doctoral thesis are discussed.

In Chapters 3 and 4, the algorithm for the calculation of the optimum beamformer that achieves ergodic beamforming capacity (i.e. maximizes the average mutual information under the *rank*-1 transmission constraint) for spatially correlated or uncorrelated with non-unit covariance matrix MIMO Rician flat fading channels (i.e. the combined CMI-CCI model) is presented. Moreover, simulations are produced for the proposed algorithm and the optimum beamformer as follows:

- a. The computational complexity of the proposed algorithm is compared with the corresponding complexity of other (currently employed) multi-dimensional algorithms.
- b. The ergodic beamforming capacity achieved by the optimum beamformer is compared with the ergodic capacity (achieved by higher rank transmission schemes) and the corresponding average mutual information achieved by the max SNR beamformer.
- c. The optimality of beamforming condition is studied.

In Chapter 5, the ergodic capacity, the ergodic beamforming capacity and the optimality of beamforming condition are studied via simulations for different channel feedback information models and different operational scenarios, which are produced using the MIMO channel simulation model of 3GPP.

Chapter 6 summarizes the most important conclusions of this doctoral thesis and discusses some ideas for future work.

1.4 Notation

Throughout this doctoral thesis the following notation is used: Vectors are denoted with bold small letters and matrices with bold capital letters. All vectors are row vectors and matrix eigenvectors are column vectors. $(\cdot)^T$, $(\cdot)^*$, $(\cdot)^\dagger$ stand for transposition, complex conjugation and complex conjugate transposition, respectively. \mathbf{I}_N is the $N \times N$ unit matrix. $\mathbf{M}_{\bullet i} / \mathbf{M}_{i \bullet}$ is the i^{th} column/row of matrix \mathbf{M} , respectively. \mathbf{M}_{ij} is the i^{th} row and j^{th}

column element of matrix \mathbf{M} . \mathbf{x}_i is the i^{th} element of vector \mathbf{x} . The i^{th} eigenvalue of matrix \mathbf{M} is denoted as $\lambda_i(\mathbf{M})$ and $\lambda_{max}(\mathbf{M})$ stands for the maximum eigenvalue of matrix \mathbf{M} . $\mathbb{H}_{++}^N / \mathbb{H}_+^N$ is the set of positive definite/semi-definite Hermitian $N \times N$ matrices, respectively. $\mathbb{C} / \mathbb{C}^{M \times N}$ is the set of complex numbers / $M \times N$ complex matrices, respectively. $\|\cdot\|_2$ stands for the l_2 -norm on $\mathbb{C}^{1 \times N}$. $\|\mathbf{M}\|_F$ stands for the Frobenius norm of matrix \mathbf{M} . $f(\mathbf{x})|_{\mathbf{x}=\mathbf{x}_o}$ stands for the value of $f(\mathbf{x})$ at $\mathbf{x} = \mathbf{x}_o$. $\mathcal{E}[\cdot]$ is the expectation operator. $\mathcal{N}(\cdot, \cdot)$ denotes the complex normal distribution. $tr\{\cdot\}$ and $rank\{\cdot\}$ are the trace and rank of a matrix, respectively. $\mathbf{M} \succeq 0$ denotes that matrix \mathbf{M} is positive semi-definite. $vec(\mathbf{M})$ is the $NM \times 1$ vector formed by sorting the N columns of matrix $\mathbf{M} \in \mathbb{C}^{M \times N}$ one below the other, forming a column vector. $diag[\mathbf{x}]$ is a diagonal matrix with the elements of vector \mathbf{x} in its diagonal.

Chapter 2

CAPACITY OF MIMO CHANNELS

2.1 Introduction

Consider a MIMO $N \times M$ flat fading wireless channel, with $N \geq 2$ and $M \geq 1$ the number of transmit and receive array antenna elements, respectively. The received signal is a vector $\mathbf{y} \in \mathbb{C}^{1 \times M}$ expressed by the following equation:

$$\mathbf{y}^T = \mathbf{H}\mathbf{x}^T + \mathbf{n}^T \quad (2.1)$$

where $\mathbf{H} \in \mathbb{C}^{M \times N}$ is the channel matrix, $\mathbf{x} \in \mathbb{C}^{1 \times N}$ is the transmit signal vector and $\mathbf{n} \in \mathbb{C}^{1 \times M}$ is the received noise vector (see Figure 2.1). Vectors \mathbf{x} and \mathbf{n} follow zero-mean, circularly symmetric, complex Gaussian distributions with covariance matrices $\Sigma = \mathcal{E}[\mathbf{x}^\dagger \mathbf{x}]$ and $\mathcal{E}[\mathbf{n}^\dagger \mathbf{n}] = \sigma^2 \mathbf{I}_M$, respectively.

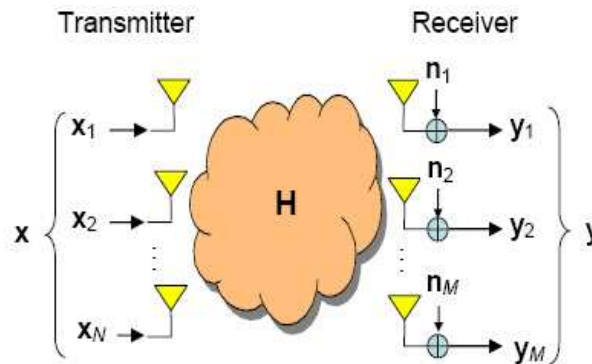


Figure 2.1: $N \times M$ MIMO system.

The transmit covariance matrix Σ is constrained by the total transmitted power P as follows:

$$\text{tr}(\Sigma) \leq P \quad (2.2)$$

The normalized transmit covariance matrix \mathbf{Q} is expressed by the following equation:

$$\mathbf{Q} = \frac{1}{P} \Sigma \quad (2.3)$$

\mathbf{Q} is a Hermitian positive semi-definite matrix ($\mathbf{Q} \succeq 0$) with $tr\{\mathbf{Q}\} \leq 1$.

In MIMO systems the mutual information between transmitter and receiver, when the receiver has perfect CSI, is expressed by the following equation ([28]-[29]):

$$\mathcal{I}(\text{SNR}, \mathbf{Q}, \mathbf{H}) = \log_2 \det(\mathbf{I}_M + \text{SNR} \mathbf{H} \mathbf{Q} \mathbf{H}^\dagger) \quad (2.4)$$

where $\text{SNR} = P/\sigma^2$, (the mathematical background for the proof of (2.4) is omitted and the mutual information \mathcal{I} is presented throughout this doctoral thesis as a function of the parameters $\{\text{SNR}, \mathbf{Q}, \mathbf{H}\}$).

When both the transmitter and the receiver have perfect CSI¹, the mutual information $\mathcal{I}(\text{SNR}, \mathbf{Q}, \mathbf{H})$ can be maximized with respect to \mathbf{Q} (for a given channel matrix and SNR). The maximum mutual information is the “channel capacity”:

$$C = \max_{tr\{\mathbf{Q}\} \leq 1, \mathbf{Q} \succeq 0} \log_2 \det(\mathbf{I}_M + \text{SNR} \mathbf{H} \mathbf{Q} \mathbf{H}^\dagger) \quad (2.5)$$

In the context of this thesis only flat fading channels are studied. However, it must be mentioned that in frequency selective channels the frequency band of interest can be divided into L narrower flat sub-channels and the channel capacity can be expressed as follows:

$$C_{\text{FS}} = \frac{1}{L} \max_{tr\{\mathbf{R}\} \leq L, \mathbf{R} \succeq 0} \log_2 \det(\mathbf{I}_{ML} + \text{SNR} \mathcal{H} \mathbf{R} \mathcal{H}^\dagger) \quad (2.6)$$

where:

a. \mathcal{H} is an $ML \times NL$ block diagonal matrix with the L sub-channels $\mathbf{H}_i \in \mathbb{C}^{M \times N}$ ($i = 1, \dots, L$) as the block diagonal elements,

¹Usually, it is assumed that the receiver is able to estimate the channel in the context of a data training period and then it feeds back the channel to the transmitter via a low rate control channel.

b. \mathbf{R} is the transmit covariance matrix defined as $\mathbf{R} = \mathcal{E}[\mathcal{S}\mathcal{S}^\dagger]$, where $\mathcal{S} = [\mathbf{s}_1^T, \mathbf{s}_2^T, \dots, \mathbf{s}_L^T]^T$, with $\mathbf{s}_i \in \mathbb{C}^{N \times 1}$ ($i = 1, \dots, L$) the signal transmitted in each (flat) sub-channel.

As it was mentioned in the introduction of this chapter, the assumption for perfect CSI at the transmitter is practically unrealistic (due to the delay in the control channel which is used to feed back the CSI from the receiver) and it is more realistic to assume a CDIT model. In a CDIT model, the transmitter cannot achieve capacity in the sense discussed in the previous paragraphs. In this case, the mutual information is maximized by the transmitter statistically with respect to \mathbf{Q} . The achieved maximum average mutual information is referred to as “ergodic capacity” and is defined as:

$$C_{\text{erg}} = \max_{\text{tr}\{\mathbf{Q}\} \leq 1, \mathbf{Q} \succeq 0} \mathcal{E}_{\mathbf{H}} [\log_2 \det (\mathbf{I}_M + \text{SNR} \mathbf{H}\mathbf{Q}\mathbf{H}^\dagger)] \quad (2.7)$$

The expectation $\mathcal{E}_{\mathbf{H}} [\cdot]$ in (2.7) is calculated using Monte Carlo integration over a set of channel samples that follow the channel distribution.

The optimum transmit covariance matrix \mathbf{Q} that achieves the C_{erg} in (2.7) will be denoted throughout this chapter as \mathbf{Q}_{opt} . The transmission of a MIMO system using $\mathbf{Q}_{\text{opt}} = \mathbf{V}\mathbf{\Lambda}_{\text{opt}}\mathbf{V}^\dagger$ - with \mathbf{V} and $\mathbf{\Lambda}_{\text{opt}}$ the eigenvectors and eigenvalues matrices of \mathbf{Q}_{opt} , respectively - is shown in Figure 2.2.

Moreover, C_{erg} is the best knowledge that the transmitter can have for the “allowed” achievable rate (bps/Hz) and is not “capacity” with the strict sense of the term, as defined by and used in (2.5). For every channel realization \mathbf{H} , C_{erg} will be less than or equal to the channel capacity defined by (2.5).

Finally, it is important to note again that equations (2.4)-(2.7) are valid only when the receiver has perfect CSI. Any other case/model, where the receiver has not perfect CSI, is out of the scope of the present doctoral thesis. In [61]-[63] the MIMO channel capacity is studied when both the receiver and the transmitter have channel distribution information (i.e. a CDIR-CDIT model is assumed).

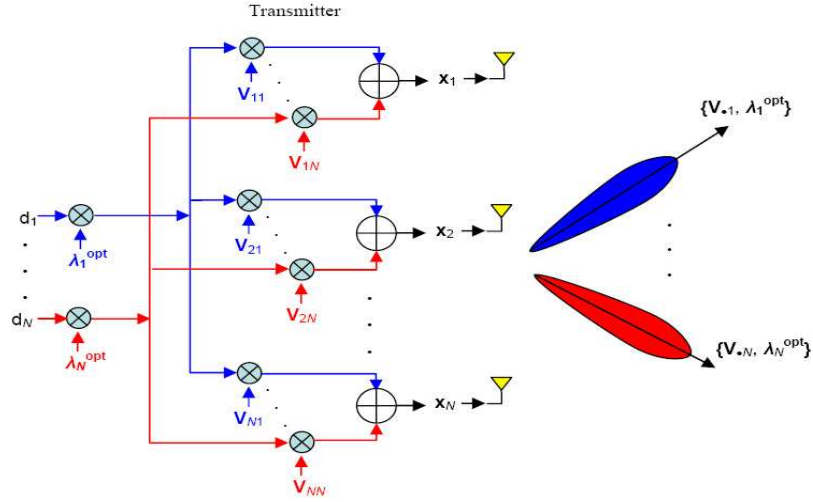


Figure 2-2: Transmission with \mathbf{Q}_{opt} .

2.2 MIMO channels capacity

2.2.1 Perfect CSI at the receiver and the transmitter

It has been proven in [29] that when perfect CSI is assumed at both ends of the MIMO link the channel capacity (expressed by (2.5)) is achieved by transmitting along the right singular vectors of the MIMO channel matrix and allocating power optimally to the (orthogonal) transmit directions. In this case the channel capacity is expressed by the following equation:

$$C = \max_{\sum_{i=1}^r \gamma_i = 1} \sum_{i=1}^r \log_2(1 + \text{SNR} \gamma_i \lambda_i) \quad (2.8)$$

with λ_i ($i = 1, \dots, r$) the non-zero eigenvalues of matrix $\mathbf{H}\mathbf{H}^\dagger$ and γ_i ($i = 1, \dots, r$) the power allocated to each channel mode (i.e. λ_i) and hence, to each of the r transmit directions (i.e. the right singular vectors of the channel matrix \mathbf{H}).

The maximization/optimization problem in (2.8) (with respect to γ_i ($i = 1, \dots, r$)) is solved using the Lagrange method, exploiting the concavity of (2.8) with respect to γ_i . The optimal power allocation (i.e. γ_i^{opt} ($i = 1, \dots, r$)) is determined through an iterative

algorithm referred to as “water-pouring” (or “water-filling”), ([29], [64]-[66]) and satisfies:

$$\gamma_i^{\text{opt}} = \left(\mu - \frac{1}{\text{SNR}\lambda_i} \right)_+ \quad (2.9)$$

where μ is a constant and $(x)_+$ implies

$$(x)_+ = \begin{cases} x & \text{if } x \geq 0 \\ 0 & \text{if } x < 0 \end{cases} \quad (2.10)$$

According to the water-pouring algorithm, power may not be allocated to all channel modes, as shown in Figure 2.3. Moreover, the lower the SNR and/or the disparity between the channel singular values ($\lambda_i (i = 1, \dots, r)$), the fewer the transmit directions that the available power is allocated to.

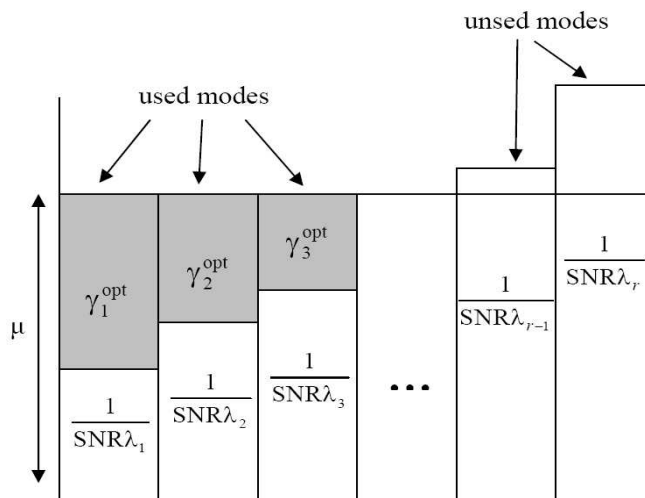


Figure 2.3: Waterfilling algorithm.

The ergodic capacity can also be defined for this channel information model. For any given channel distribution and assuming an ergodic channel (i.e. the channel realizations are independent) the ergodic capacity of the channel is the ensemble average of (2.8) over the channel distribution:

$$C_{\text{erg}}^{CSIT} = \mathcal{E}_{\mathbf{H}} \left[\max_{\sum_{i=1}^r \gamma_i = 1} \sum_{i=1}^r \log_2 (1 + \text{SNR} \gamma_i \lambda_i) \right] \quad (2.11)$$

2.2.2 Perfect CSI at the receiver and unknown channel to the transmitter

When the channel is totally unknown to the transmitter, practically the transmitter cannot maximize the mutual information and hence, achieve the channel capacity. In this case, the best choice for the transmitter is to transmit independent signals with equal power from its antenna elements, as it is shown in Figure 2.4. In this case the achieved mutual information, (which is also referred to as “capacity” for simplicity reasons), is expressed by the following equation:

$$C_{\text{un}} = \sum_{i=1}^r \log_2 \left(1 + \frac{\text{SNR}}{N} \lambda_i \right) \quad (2.12)$$

where λ_i ($i = 1, \dots, r$) the eigenvalues of matrix $\mathbf{H}\mathbf{H}^\dagger$.

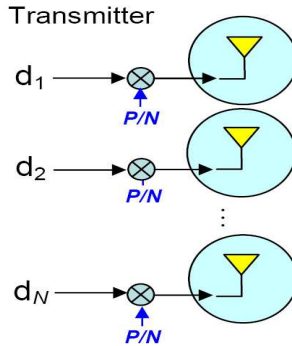


Figure 2-4: Transmission for Unknown Channel to the transmitter.

The ergodic capacity can also be defined in this case. For any given channel distribution and assuming an ergodic channel (i.e. the channel realizations are independent) the ergodic capacity of the channel is the ensemble average of (2.12) over the channel distribution:

$$C_{\text{erg}}^{\text{un}} = \mathcal{E}_{\mathbf{H}} \left[\sum_{i=1}^r \log_2 \left(1 + \frac{\text{SNR}}{N} \lambda_i \right) \right] \quad (2.13)$$

Assuming a channel with complex Gaussian distribution $\text{vec}(\mathbf{H}) \sim (\mathbf{0}, \mathbf{I}_{MN})$, (i.e. spa-

tially uncorrelated Rayleigh distributed channel), it can be proven through simulations that were presented in [66], that the ergodic capacity for unknown channel to the transmitter is lower than the ergodic capacity for known channel to the transmitter (i.e. perfect CSI), for any SNR. Moreover, in this case and when $N = M$ the aforementioned ergodic capacities converge for high SNR values.

Consider now a MIMO channel with complex Gaussian distribution $\text{vec}(\mathbf{H}) \sim (\mathbf{0}, \mathbf{I}_{MN})$ and $N = M$. According to the strong law of large numbers [67] we have:

$$\frac{1}{M} \mathbf{H} \mathbf{H}^\dagger \rightarrow \mathbf{I}_M, \text{ as } M \rightarrow \infty \quad (2.14)$$

Therefore, when $M \rightarrow \infty$ and the channel is unknown to the transmitter, the capacity expressed by (2.13) approaches:

$$C_{\text{un}} \rightarrow M \log_2(1 + \text{SNR}) \quad (2.15)$$

From (2.15) it can be observed that the capacity increases linearly with M for a fixed SNR and consequently we have M times higher capacity than the capacity achieved by a SISO system. Moreover, for a fixed M , for every 3dB increase in SNR we get M bps/Hz in capacity for a MIMO channel, compared with 1 bps/Hz for a SISO channel [66].

2.2.3 Perfect Channel State Information (CSI) at the receiver and Channel Distribution Information at the transmitter (CDIT)

Assuming a CDIT model, the solution of the optimization problem defined in (2.7), i.e. the calculation of the optimum transmit covariance matrix \mathbf{Q}_{opt} , depends on the channel distribution. In the following, the solution of the aforementioned problem is presented for complex Gaussian channels.

Channel Covariance Information (CCI) model

This CDIT model describes MIMO Rayleigh fading channels. The (spatial) correlation of the channel matrix is expressed by the $NM \times NM$ channel covariance matrix, defined

as:

$$\mathbf{R} = \mathcal{E} \left[\text{vec}(\mathbf{H}) \text{vec}(\mathbf{H})^\dagger \right] \quad (2.16)$$

\mathbf{R} is positive semi-definite and Hermitian matrix. Therefore, the channel distribution is expressed as $\text{vec}(\mathbf{H}) \sim \mathcal{N}(\mathbf{0}, \mathbf{R})$, where $\mathbf{0}$ is (in this case) a zero column vector with NM elements. In this CDIT model, \mathbf{R} is calculated by the receiver in the context of long-term statistics (since the receiver has perfect CSI) and then it is fed back to the transmitter (i.e. the transmitter is “informed” for the channel covariance).

The channel matrix realizations of this model can be produced by the following equation:

$$\text{vec}(\mathbf{H}) = \mathbf{R}^{1/2} \text{vec}(\mathbf{H}_w) \quad (2.17)$$

where $\mathbf{H}_w \in \mathbb{C}^{M \times N}$ is a zero-mean complex Gaussian matrix, spatially uncorrelated and its complex elements have independent real and imaginary parts, each with 1/2 variance. Namely, it is $\text{vec}(\mathbf{H}_w) \sim \mathcal{N}(\mathbf{0}, \mathbf{I}_{MN})$.

Moreover, \mathbf{R} can also be expressed by the following equation:

$$\mathbf{R} = \mathbf{R}_t^T \otimes \mathbf{R}_r \quad (2.18)$$

where \mathbf{R}_t and \mathbf{R}_r are the channel transmit and receive covariance matrices, which are defined as $\mathbf{R}_t = \mathcal{E}[\mathbf{H}^\dagger \mathbf{H}]$ and $\mathbf{R}_r = \mathcal{E}[\mathbf{H} \mathbf{H}^\dagger]$.

Although the model described above by (2.17) is capable of capturing any correlation effect between the elements of \mathbf{H} , the following simpler model may be used:

$$\mathbf{H} = \mathbf{R}_r^{1/2} \mathbf{H}_w \mathbf{R}_t^{1/2} \quad (2.19)$$

The model expressed by (2.19), although not completely general, it has been validated through field measurements as a sufficiently accurate representation of the fade correlations seen in actual cellular systems [68]. This model will be assumed throughout this doctoral thesis.

For the CCI model the solution of the optimization problem (2.7) is expressed by the following theorem:

Theorem 2.1. Let $\mathbf{R}_t = \mathbf{U}_t \mathbf{\Lambda}_t \mathbf{U}_t^\dagger$ the eigen-decomposition of \mathbf{R}_t , where \mathbf{U}_t and $\mathbf{\Lambda}_t$ stand for the eigenvectors and eigenvalues matrices, respectively. The optimum transmit covariance matrix that achieves ergodic capacity is expressed as $\mathbf{Q}_{\text{opt}} = \mathbf{U}_t \mathbf{\Lambda}_{\text{opt}} \mathbf{U}_t^\dagger$, where $\mathbf{\Lambda}_{\text{opt}}$ is determined through numerical optimization techniques.

The proof of the above theorem was first presented for MISO systems in [46]. Then it was extended in [47] for MIMO systems with $\mathbf{R}_r = \mathbf{I}_M$ (i.e. it was assumed that there is no correlation at the receive antenna) and finally, in [48] it was generalized to include any \mathbf{R}_r . For the calculation of $\mathbf{\Lambda}_{\text{opt}}$ the iterative algorithm proposed in [69] can be employed.

Channel Mean Information (CMI) model

This CDIT model describes spatially uncorrelated with unit covariance matrix MIMO Rician fading channels. The CMI model was first introduced in [46] for MISO systems as a “short-term feedback model”, where the receiver feeds back to the transmitter a channel measurement (made at time t_0) and then the transmitter, based on this channel measurement, on long-term statistics and the MMSE estimation theory [70], estimates the channel realization at time t_s (with an estimation error). The reason for using this estimation process is the feedback delay (s) of the channel measurement² (made by the receiver at time t_0). Theoretically, if there was no delay in the feedback control channel, there would be no need for channel estimation and the model described in paragraph 2.3.1 would be employed (perfect CSI at the receiver and the transmitter).

According to the MMSE estimation theory and as referred to in [44], an estimation of the channel \mathbf{H}_s at the transmit time s (which is practically the feedback delay) - denoted as $\hat{\mathbf{H}}_s$ - is based on the channel measurement \mathbf{H}_0 at time t_0 , and on the long-term statistics $\bar{\mathbf{H}}$, \mathbf{R} and \mathbf{R}_s , i.e. the channel mean, covariance and auto-covariance matrices, respectively, calculated by the receiver by averaging instantaneous channel measurements over

²The channel measurement is fed back to the transmitter via a low-rate control channel

tens of channel coherence times. \mathbf{R} and \mathbf{R}_s are expressed by the following equations:

$$\mathbf{R} = \mathcal{E} \left[(\text{vec}(\mathbf{H}) - \text{vec}(\overline{\mathbf{H}})) (\text{vec}(\mathbf{H}) - \text{vec}(\overline{\mathbf{H}}))^{\dagger} \right] \quad (2.20)$$

$$\mathbf{R}_s = \mathcal{E} \left[\text{vec}(\mathbf{H}_0) \text{vec}(\mathbf{H}_s)^{\dagger} \right] \quad (2.21)$$

Moreover, \mathbf{R} is again expressed by (2.18), where the channel transmit and receive covariance matrices are defined as $\mathbf{R}_t = \mathcal{E} \left[(\mathbf{H} - \overline{\mathbf{H}})^{\dagger} (\mathbf{H} - \overline{\mathbf{H}}) \right]$ and $\mathbf{R}_r = \mathcal{E} \left[(\mathbf{H} - \overline{\mathbf{H}}) (\mathbf{H} - \overline{\mathbf{H}})^{\dagger} \right]$, respectively.

The channel estimation $\widehat{\mathbf{H}}_s$ is expressed as follows:

$$\widehat{\mathbf{h}}_s = \overline{\mathbf{h}} + \mathbf{R}_s^{\dagger} \mathbf{R}^{-1} [\mathbf{h}_0 - \overline{\mathbf{h}}] \quad (2.22)$$

while the estimation error is expressed by the error covariance matrix $\mathbf{R}_{e,s}$:

$$\mathbf{R}_{e,s} = \mathbf{R} + \mathbf{R}_s^{\dagger} \mathbf{R}^{-1} \mathbf{R}_s \quad (2.23)$$

where:

$$\widehat{\mathbf{h}}_s = \text{vec}(\widehat{\mathbf{H}}_s) \quad (2.24)$$

$$\mathbf{h}_0 = \text{vec}(\mathbf{H}_0) \quad (2.25)$$

$$\overline{\mathbf{h}} = \text{vec}(\overline{\mathbf{H}}) \quad (2.26)$$

In the CMI model, the error covariance matrix $\mathbf{R}_{e,s}$ is a white matrix with equal diagonal elements, i.e. it is expressed as $\mathbf{R}_{e,s} = a\mathbf{I}_{MN}$, where a is referred to as the “estimation error”³. The transmitter exploits the (current) channel estimation $\widehat{\mathbf{H}}_s$ and calculates the optimum transmission \mathbf{Q}_{opt} at time s , as the transmission scheme that achieves ergodic capacity (i.e. it solves the optimization problem in (2.7)) assuming a channel distribution $\text{vec}(\mathbf{H}) \sim \mathcal{N}(\text{vec}(\mathbf{H}_m), a\mathbf{I}_{MN})$, with $\mathbf{H}_m = \widehat{\mathbf{H}}_s$. It can be observed that for the calculation of \mathbf{Q}_{opt} (whenever a channel measurement \mathbf{H}_0 is fed back from the receiver) the channel

³This may be mathematically valid and occur for some values of \mathbf{R} and \mathbf{R}_s (see (2.23)) or it can be an assumption, i.e. the error correlation effects are ignored.

that is assumed at the transmitter is always spatially uncorrelated (with unit covariance matrix) and has a Rician distribution, (since $\mathbf{H}_m = \widehat{\mathbf{H}}_s \neq \mathbf{0}$). On the other hand, the long-term distribution of the channel is not necessarily Rician, but it can also be a Rayleigh distribution if $\overline{\mathbf{H}} = \mathbf{0}$.

Observe from (2.22) and (2.23) that when $\mathbf{R}_s = \mathbf{0}$ (i.e. there is no correlation between channel realizations with time difference s), then it is always $\widehat{\mathbf{h}}_s = \overline{\mathbf{h}}$ and $\mathbf{R}_{e,s} = \mathbf{R}$, regardless of the channel measurement \mathbf{H}_0 . Moreover, if it is also $\overline{\mathbf{H}} \neq \mathbf{0}$ and $\mathbf{R} = a\mathbf{I}_{MN}$ (or, equivalently, $\mathbf{R}_r = \beta_r\mathbf{I}_M$ and $\mathbf{R}_t = \beta_t\mathbf{I}_N$, with $a = \beta_r\beta_t$), then we have a “long-term feedback” CMI model, where the instantaneous channel measurements \mathbf{H}_0 need not be fed back by receiver. In this case only the long-term channel mean $\overline{\mathbf{H}}$ is fed back by the receiver and is exploited by the transmitter in order to calculate and employ \mathbf{Q}_{opt} for the time period that the statistic $\overline{\mathbf{H}}$ is valid. A new feedback occurs only when $\overline{\mathbf{H}}$ changes. Obviously, if $\overline{\mathbf{H}} = \mathbf{0}$, then the long-term feedback CMI model becomes a CCI model (i.e. $\text{vec}(\mathbf{H}) \sim \mathcal{N}(\mathbf{0}, a\mathbf{I}_{MN})$), which is inherently a long-term feedback model.

The channel matrix realizations of the CMI model can be produced by the following equation, for both the long and the short-term feedback models:

$$\mathbf{H} = \mathbf{H}_m + \sqrt{a}\mathbf{H}_w \quad (2.27)$$

where $\mathbf{H}_m = \widehat{\mathbf{H}}_s$ for the short-term feedback model and $\mathbf{H}_m = \overline{\mathbf{H}}$ for the long-term feedback model.

For the CMI model the solution of the optimization problem (2.7) is expressed by the following theorem:

Theorem 2.2. The optimum transmit covariance matrix \mathbf{Q}_{opt} for the CMI model (described by (2.27)) is decomposed as $\mathbf{Q}_{\text{opt}} = \mathbf{U}\mathbf{\Lambda}_{\text{opt}}\mathbf{U}^\dagger$ (\mathbf{U} and $\mathbf{\Lambda}_{\text{opt}}$ stand for the eigenvectors and eigenvalues matrices, respectively), where the first column of \mathbf{U} is the dominant right singular vector of \mathbf{H}_m and the rest of its columns are arbitrarily chosen (with the restriction that \mathbf{U} should be a unitary matrix). Furthermore, the eigenvalues matrix $\mathbf{\Lambda}_{\text{opt}} = \text{diag}[\lambda_1^o, \lambda_2^o, \dots, \lambda_N^o]$ is determined through numerical optimization techniques, with $\lambda_2^o =$

$$\dots = \lambda_N^o = \lambda \text{ and } \lambda = \frac{P - \lambda_1^o}{N-1}.$$

The proof of the above theorem was first presented for MISO systems in [46]. Then it was extended in [47] for MIMO systems with $\text{rank}\{\mathbf{H}_m\} = 1$ (i.e. for physical Rician channels where \mathbf{H}_m represents the Line of Sight (LOS) component) and finally, in [71] it was generalized to include any \mathbf{H}_m matrix.

Combined CMI-CCI model

This CDIT model describes spatially correlated or uncorrelated with non-unit covariance matrix MIMO Rician fading channels. For the combined CMI-CCI model there is no closed-form expression for the optimum transmit directions and hence, both the eigenvectors and the eigenvalues of the optimum transmit covariance matrix must be calculated numerically.

The channel matrix samples of the combined CMI-CCI model can be produced by the following equation:

$$\text{vec}(\mathbf{H}) = \text{vec}(\mathbf{H}_m) + \mathbf{R}_0^{1/2} \text{vec}(\mathbf{H}_w) \quad (2.28)$$

(i.e. $\text{vec}(\mathbf{H}) \sim \mathcal{N}(\text{vec}(\mathbf{H}_m), \mathbf{R}_0)$) and assuming a (simplified) model with separable transmit and receive correlations, (2.28) is written as:

$$\mathbf{H} = \mathbf{H}_m + \mathbf{R}_{0,r}^{1/2} \mathbf{H}_w \mathbf{R}_{0,t}^{1/2} \quad (2.29)$$

where:

a. If $\mathbf{R}_s \neq 0$, then $\mathbf{H}_m = \widehat{\mathbf{H}}_s$, $\mathbf{R}_{0,r} = \mathbf{R}_{e,s}^r$, $\mathbf{R}_{0,t} = \mathbf{R}_{e,s}^t$, with \mathbf{R}_s , $\widehat{\mathbf{H}}_s$ previously defined in the discussion for the CMI model and

$$\mathbf{R}_{e,s} = (\mathbf{R}_{e,s}^t)^T \otimes \mathbf{R}_{e,s}^r \quad (2.30)$$

$\mathbf{R}_{e,s}$ is defined by (2.23). In this case we have a the short-term feedback model, namely, $\widehat{\mathbf{H}}_s$, $\mathbf{R}_{e,s}^r$ and $\mathbf{R}_{e,s}^t$ are calculated dynamically by the transmitter for every channel measurement (\mathbf{H}_0) which is fed back by the receiver. Moreover, with (2.30) it is implied that

the error covariance matrix $\mathbf{R}_{e,s}$ may have a Kronecker structure⁴.

b. If $\mathbf{R}_s = \mathbf{0}$, then $\mathbf{H}_m = \bar{\mathbf{H}}$, $\mathbf{R}_{0,r} = \mathbf{R}_r$ and $\mathbf{R}_{0,t} = \mathbf{R}_t$, with $\bar{\mathbf{H}}$ previously defined in the discussion for the CMI model and $\mathbf{R}_r/\mathbf{R}_t$ defined in (2.18). In this case we have a long-term feedback model, namely, only the long-term channel statistics $\bar{\mathbf{H}}$ and \mathbf{R} are fed back by the receiver and are exploited by the transmitter in order to calculate and employ \mathbf{Q}_{opt} for the time period that these statistics are valid. A new feedback occurs when $\bar{\mathbf{H}}$ and \mathbf{R} change. Obviously, if $\bar{\mathbf{H}} = \mathbf{0}$, then the long-term feedback combined CMI-CCI model becomes a CCI model and if $\{\bar{\mathbf{H}} \neq \mathbf{0}, \mathbf{R} = a\mathbf{I}_{MN}\}$ then the long-term feedback combined CMI-CCI model becomes a long-term feedback CMI model.

In [30] it was mentioned that the calculation of \mathbf{Q}_{opt} for the combined CMI-CCI model was an open problem. In [49] a solution was proposed, employing an interior barrier point algorithm. However, the algorithm in [49] was characterized by high computational complexity and hence, it is prohibitively complex for real-time applications. In [50] an asymptotic approach was proposed for the solution of the aforementioned optimization problem, where it was shown that it has very good performance (i.e. the achieved average mutual information is close to the ergodic capacity achieved by the algorithm in [49]) and low complexity, compared with the algorithm in [49]. Moreover, in [44] closed-form solutions for asymptotic SNR values were provided. More precisely, assuming that $\mathbf{R}_r = \mathbf{I}_M$, it was proven that:

a. When $\text{SNR} \rightarrow 0$, the optimum transmission is along the dominant eigenvector of the channel transmit correlation matrix $\mathcal{E}[\mathbf{H}^\dagger \mathbf{H}]$, (this is a beamforming transmission referred to also in the literature as “max SNR beamformer”).

b. When $\text{SNR} \rightarrow \infty$ and for MIMO systems with $N \leq M$, it is $\mathbf{Q}_{\text{opt}} = \frac{1}{N}\mathbf{I}_N$.

Figure 2.5 presents an overview of the aforementioned Gaussian CDIT models.

⁴If it is assumed that all scalar channels between the N transmit and M receive antennas have the same temporal correlation factor ρ_s (i.e. if homogeneous temporal correlation is assumed), then it is $\mathbf{R}_s = \rho_s \mathbf{R}$ and from (2.23) it follows that $\mathbf{R}_{e,s} = (1 - \rho_s^2) \mathbf{R}$. From the last equation it can be concluded that $\mathbf{R}_{e,s}$ may have the Kronecker structure of (2.30) with $\mathbf{R}_{e,s}^t = \sqrt{(1 - \rho_s^2)} \mathbf{R}_t$ and $\mathbf{R}_{e,s}^r = \sqrt{(1 - \rho_s^2)} \mathbf{R}_r$.

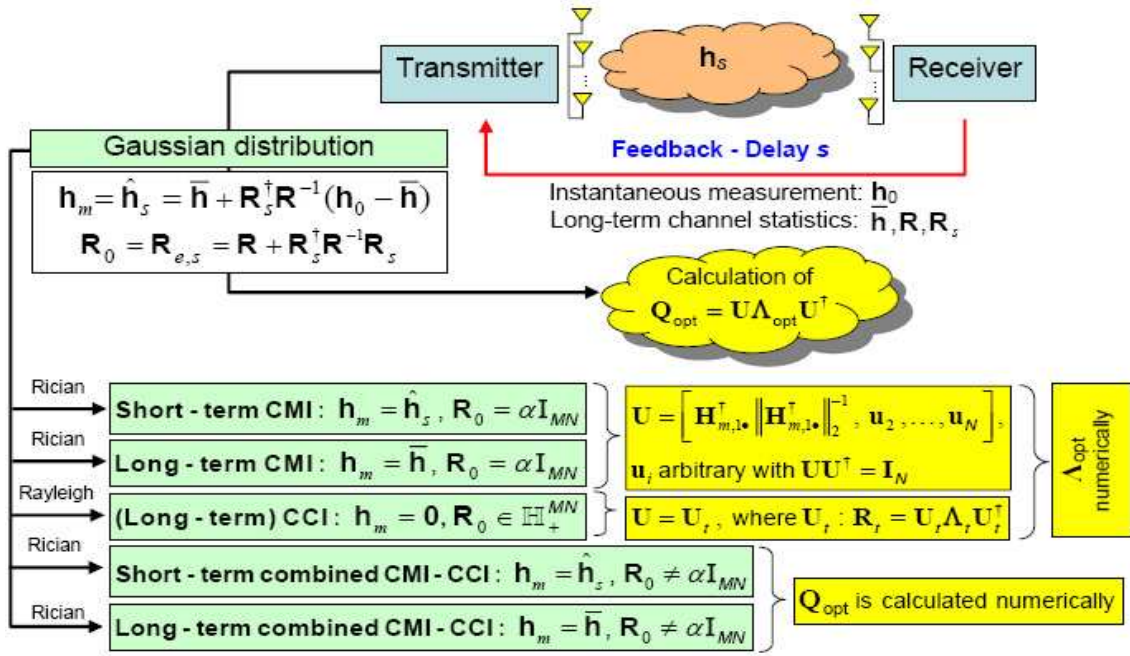


Figure 2.5: CDIT models.

2.3 Rate-Optimum beamforming transmission in MIMO channels

When the transmit covariance matrix \mathbf{Q} is restricted to be *rank-1* then we have a beamforming scenario where all the available power is allocated to a unique direction via the beamforming vector, as it is shown in Figure 2.6. In this case, (2.3) becomes:

$$\mathbf{Q} = \frac{1}{P} \mathbf{v} \mathbf{v}^\dagger \quad (2.31)$$

where $\mathbf{v} \in \mathbb{C}^{1 \times N}$ (with $\|\mathbf{v}\|_2 = 1$) is the beamforming vector/direction.

The corresponding mutual information for this transmission scheme is referred to throughout this doctoral thesis as “beamforming mutual information” and will be denoted as $\mathcal{I}_{\text{bf}}(\text{SNR}, \mathbf{v}, \mathbf{H})$. Substituting (2.31) into (2.4), $\mathcal{I}(\text{SNR}, \mathbf{v}, \mathbf{H})$ is expressed as follows:

$$\mathcal{I}_{\text{bf}}(\text{SNR}, \mathbf{v}, \mathbf{H}) = \log_2 \det (\mathbf{I}_M + \text{SNR} \mathbf{H} \mathbf{v} \mathbf{v}^\dagger \mathbf{H}^\dagger) \quad (2.32)$$

Moreover, in the context of CDIT models, the corresponding ergodic capacity for this restricted case of transmission is referred to throughout this doctoral thesis as “ergodic beamforming capacity” (the same terminology was also used in [72]), will be denoted as

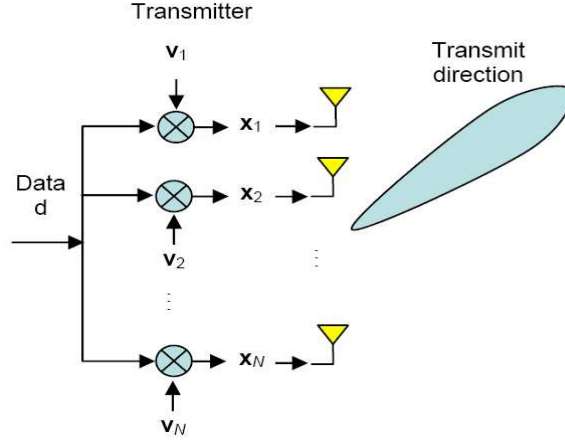


Figure 2.6: Beamforming transmission.

C_{bf} , and substituting (2.32) into (2.7), C_{bf} is expressed by the following equation:

$$\begin{aligned}
 C_{\text{bf}} &= \max_{\|\mathbf{v}\|_2=1} \mathcal{E}_{\mathbf{H}} [\mathcal{I}_{\text{bf}}(\text{SNR}, \mathbf{v}, \mathbf{H})] = \max_{\|\mathbf{v}\|_2=1} \mathcal{I}_{\text{bf,avg}}(\text{SNR}, \mathbf{v}) = \\
 &= \max_{\|\mathbf{v}\|_2=1} \mathcal{E}_{\mathbf{H}} [\log_2 \det (\mathbf{I}_M + \text{SNR} \mathbf{H} \mathbf{v} \mathbf{v}^\dagger \mathbf{H}^\dagger)] \quad (2.33)
 \end{aligned}$$

Note that in (2.33) it is defined $\mathcal{E}_{\mathbf{H}} [\mathcal{I}_{\text{bf}}(\text{SNR}, \mathbf{v}, \mathbf{H})] = \mathcal{I}_{\text{bf,avg}}(\text{SNR}, \mathbf{v})$. The beamforming vector that achieves ergodic beamforming capacity (i.e. is the solution of the optimization problem in (2.33)) will be referred to as “optimum beamformer”, denoted as \mathbf{v}_{opt} .

There are several reasons why it is important to consider the optimum beamforming transmission in MIMO systems:

a. The complexity of the system and as a consequence the overall cost, are significantly reduced.

b. Results presented in the following chapters of this doctoral thesis show that there are operational scenarios where the ergodic beamforming capacity is very close to the ergodic capacity, achieved by higher rank transmission schemes.

c. There are operational scenarios where the optimum beamformer achieves ergodic capacity, namely it is $C_{\text{bf}} = C_{\text{erg}}$ and $\mathbf{Q}_{\text{opt}} = \frac{1}{P} \mathbf{v}_{\text{opt}} \mathbf{v}_{\text{opt}}^\dagger$. This is achieved when the following

necessary and sufficient condition is satisfied [73]:

$$\lambda_{max} \left((\mathbf{I}_N - \mathbf{v}_{opt}^\dagger \mathbf{v}_{opt}) \mathbf{K} (\mathbf{I}_N - \mathbf{v}_{opt}^\dagger \mathbf{v}_{opt})^\dagger \right) \leq \mathbf{v}_{opt} \mathbf{K} \mathbf{v}_{opt}^\dagger \quad (2.34)$$

with $\mathbf{K} \in \mathbb{H}_+^N$ expressed as:

$$\mathbf{K} = \mathcal{E}_{\mathbf{H}} \left[\mathbf{H}^\dagger (\mathbf{I}_M + \text{SNR} \mathbf{H} \mathbf{v}_{opt}^\dagger \mathbf{v}_{opt} \mathbf{H}^\dagger)^{-1} \mathbf{H} \right] \quad (2.35)$$

Inequality (2.34), known in the literature as “optimality of beamforming condition” [30], is valid for any CDIT model. In [47]-[48] more specific expressions of (2.34) were derived, for the (complex Gaussian) CCI and CMI models:

a. **CCI model.** The necessary and sufficient condition for optimality of beamforming can be expressed by the following inequality:

$$\frac{1}{\text{SNR} \lambda_2(\mathbf{R}_t)} \geq \frac{M}{1 - \left(\frac{1}{\text{SNR} \lambda_1(\mathbf{R}_t)} \right)^M \exp \left(\frac{1}{\text{SNR} \lambda_1(\mathbf{R}_t)} \right) \Gamma \left(1 - M, \frac{1}{\text{SNR} \lambda_1(\mathbf{R}_t)} \right)} - 1 \quad (2.36)$$

where $\Gamma(k, x) = \int_x^\infty t^{k-1} e^{-t} dt$ is the upper incomplete Gamma function.

b. **CMI model.** The necessary and sufficient condition for optimality of beamforming can be expressed by the following inequality:

$$\mathcal{E} \left[\frac{1}{1 + \text{SNR} \mu w} \right] \leq \frac{1 + \text{SNR} (1 - M)}{1 + \text{SNR}} \quad (2.37)$$

where μ is the non-zero (and unique) eigenvalue of \mathbf{H}_m and w is a non-central chi-squared distributed random variable with $2M$ degrees of freedom and non-centrality parameter $\delta = \mu^2$. It must be mentioned here that condition (2.37) is valid for the long-term feedback CMI model, where $\mathbf{H}_m = \overline{\mathbf{H}}$, $\text{rank}\{\mathbf{H}_m\} = 1$ and \mathbf{H}_m represents the LOS component of the Rician channel.

As far as the solution of the optimization problem in (2.33) and the calculation of \mathbf{v}_{opt} is concerned, the optimum beamformer can be determined in closed-form for the CCI and CMI models: in both cases \mathbf{v}_{opt} is the dominant eigenvector of the channel transmit

correlation matrix $\mathcal{E} [\mathbf{H}^\dagger \mathbf{H}]$ ([72], [74]), and consequently, it coincides with the max SNR beamformer. For the combined CMI-CCI model there is no closed-form expression for \mathbf{v}_{opt} . In this case \mathbf{v}_{opt} must be calculated numerically by solving a multi-dimensional optimization problem (see (2.33)), which is prohibitively complex for real-time systems and applications [75]. In Chapters 3 and 4 of the present doctoral thesis, a solution for this problem is proposed for MISO and MIMO channels, respectively, and it is proven that \mathbf{v}_{opt} can be calculated numerically in the context of a simple 1-D optimization problem, which can be solved very fast by employing any standard 1-D search algorithm [76].

Chapter 3

RATE-OPTIMUM BEAMFORMING TRANSMISSION IN MISO RICIAN FADING CHANNELS

3.1 Introduction

In MIMO channels with perfect CSI at the receiver (CSIR) and partial CSI at the transmitter (CDIT), when the transmit covariance matrix is constrained to be a *rank-1* matrix, all the available power should be transmitted along a unique direction with the help of a “beamforming vector”, and hence we have a beamforming scenario. The transmission scheme that maximizes the average mutual information for this (constrained) scenario is referred to as “optimum beamforming” and the relative beamforming vector is referred to as “optimum beamformer”. The maximum average mutual information achieved by the optimum beamformer is referred to as “ergodic beamforming capacity” and is defined by (2.29). It must be noted that the ergodic beamforming capacity does not coincide with the ergodic capacity of the channel generally, however, this is possible when the optimality of beamforming condition (2.34) is satisfied. The reasons why it is important to consider optimum beamforming transmission in MIMO systems were explained in Chapter 2.

As it was also mentioned in Chapter 2, for the CCI and CMI models the optimum beamformer is the dominant eigenvector of the channel transmit correlation matrix [72]. However, for the combined CMI-CCI model, a closed-form expression for the optimum beamformer has not been presented in the open literature until now. In this case, the optimum beamformer must be determined numerically as the solution of a convex multi-dimensional optimization problem, (the N complex elements of the optimum beamformer must be calculated, i.e. $2N$ real parameters). As a result, the solution of this problem (using standard algorithms¹), which is referred to as “optimum beamforming problem”, is

¹e.g. interior-point methods [77].

relatively slow and is characterized by high computational complexity, (it is stated in [75] that the solution of this problem is “prohibitively complex”). Furthermore, the optimum beamforming problem must be solved at the transmitter a lot faster than the channel statistics change, which is a very strict constraint for channels with small coherence times. For this reason, a faster and more efficient solution is required. Until now, a method for the simplification of the aforementioned solution has not been presented in the open literature.

Moreover, the algorithms that have been presented in [49]-[50] for the combined CMI-CCI model, are not dedicated solutions to the optimum beamforming problem, since they do not consider the *rank-1* constraint for the transmit covariance matrix (i.e. beamforming), and hence, they do not solve this problem. However, they are able to calculate the optimum beamformer when the optimality of beamforming condition (2.34) is satisfied, but even in this case, the problem they solve is still multi-dimensional and hence, computationally complex.

In this chapter a novel simple one-dimensional (1-D) method is addressed for the straightforward and unconditional solution of the optimum beamforming problem (i.e. the maximization of the average mutual information for the beamforming transmission scenario) with MISO systems under the combined CMI-CCI model². Moreover, in the context of this work, it is demonstrated via simulations that:

a. The proposed method has significantly lower computational complexity compared to other currently employed multi-dimensional algorithms, e.g. an interior-point method or the asymptotic approach [50], which provide optimum and sub-optimum solution, respectively, to the same problem under specific conditions (i.e. when the optimality condition (2.34) is satisfied).

b. The ergodic beamforming capacity is always higher compared to the average mutual information achieved by the beamforming transmission that maximizes the expected

²The proposed method will provide a solution regardless of whether the optimality condition (2.34) is satisfied or not.

received SNR (referred to as “max SNR beamformer”), and moreover, as already mentioned above, it is very close to the ergodic capacity³ in many operational scenarios or equal to the ergodic capacity when the optimality condition (2.34) is satisfied.

The rest of this chapter is organized as follows: In Section 3.2 the system model and the optimum beamforming problem are introduced. In Section 3.3, a novel method for the calculation of the optimum beamformer for MISO systems under the combined CMI-CCI model is proven. Section 3.4 presents simulation results related to the computational complexity of the proposed method and the capacity performance of the optimum beamformer.

3.2 System model and problem statement

In a flat fading channel the received signal y of a MISO system with N transmit antenna elements is expressed as:

$$y = \mathbf{h}\mathbf{x}^T + n \quad (3.1)$$

where $\mathbf{x} \in \mathbb{C}^{1 \times N}$ is the transmitted signal, $\mathbf{h} \in \mathbb{C}^{1 \times N}$ is the channel vector and n is the received noise. n is complex Gaussian random variable with zero-mean and variance $\mathcal{E}[n^2] = n_o$. \mathbf{x} is complex Gaussian random vector with zero-mean and circularly symmetric covariance matrix $\Sigma = \mathcal{E}[\mathbf{x}^\dagger \mathbf{x}]$.

When beamforming is considered, Σ has *rank*-1 and is expressed as:

$$\Sigma = P\mathbf{v}^\dagger \mathbf{v} \quad (3.2)$$

where P is the (total) transmitted power and $\mathbf{v} \in \mathbb{C}^{1 \times N}$ is the unit-norm beamforming vector.

Assuming perfect CSI at the receiver and CDIT, the ergodic beamforming capacity is

³The algorithms in [49]-[50] can be used for the calculation of the ergodic capacity.

expressed by (2.29):

$$C_{\text{bf}} = \max_{\|\mathbf{v}\|_2=1} \mathcal{E}_{\mathbf{h}} [\mathcal{I}_{\text{bf}}(\text{SNR}, \mathbf{v}, \mathbf{h})] = \max_{\|\mathbf{v}\|_2=1} \mathcal{I}_{\text{bf,avg}}(\text{SNR}, \mathbf{v}) = \max_{\|\mathbf{v}\|_2=1} \mathcal{E}_{\mathbf{h}} [\log_2 \det (\mathbf{I}_M + \text{SNR} \mathbf{h} \mathbf{v}^\dagger \mathbf{v} \mathbf{h}^\dagger)] \quad (3.3)$$

The optimum beamformer, \mathbf{v}_{opt} , is the beamforming vector that maximizes (3.3), and is expressed as the solution of the following convex optimization problem:

$$\mathbf{v}_{\text{opt}} = \arg \max_{\mathbf{v} \in \mathbf{S}} \mathcal{I}_{\text{bf,avg}}(\text{SNR}, \mathbf{v}) \quad (3.4)$$

$$\mathbf{S} = \{\mathbf{v}; \mathbf{v} \in \mathbb{C}^{1 \times N}, \|\mathbf{v}\|_2 = 1\} \quad (3.5)$$

The solution of (3.4) depends on the distribution of \mathbf{h} (i.e. the CDIT model) and - as mentioned in Section 3.1 - closed-form solutions exist only for the CMI and CCI feedback models. In the following section, the optimization problem in (3.4) is solved for MISO systems under the combined CMI-CCI model [74], [78].

3.3 Optimum beamforming transmission in MISO Rician fading channels

Consider a frequency flat MISO channel, with CDIT $\mathbf{h} \sim \mathcal{N}(\boldsymbol{\mu}, \mathbf{R})$, where $\boldsymbol{\mu} \in \mathbb{C}^{1 \times N}$ ($\boldsymbol{\mu} \neq \mathbf{0}$) is the channel mean and $\mathbf{R} \in \mathbb{H}_+^N$ ($\mathbf{R} \neq \mathbf{I}_N$) is the channel transmit covariance matrix, ($\boldsymbol{\mu}$ and \mathbf{R} represent the long-term channel statistics). The same CDIT model can also be used when the receiver feeds back to the transmitter instantaneous channel measurements, which are subject to delay and distortion [44], [75]. In this case, $\boldsymbol{\mu}$ and \mathbf{R} do not represent the long-term channel statistics, but $\boldsymbol{\mu}$ is the estimated channel value and \mathbf{R} is the error covariance matrix. Moreover, in this case, the long-term channel statistics are not necessarily a Rician distribution. In both aforementioned cases, the CDIT model under consideration is the combined CMI-CCI model, (long and short-term, respectively), and represents spatially correlated or uncorrelated with non-unit (transmit) covariance matrix MISO Rician fading channels, (see discussion in Chapter 2).

The channel samples are produced by the model expressed by (2.25):

$$\mathbf{h} = \boldsymbol{\mu} + \mathbf{h}_w \mathbf{R}^{1/2} \quad (3.6)$$

where $\mathbf{h}_w \in \mathbb{C}^{1 \times N}$ has i.i.d zero-mean complex Gaussian elements, with independent real and imaginary parts, each with variance 0.5.

It is proven in the following that the optimization problem in (3.4) under the channel model (3.6) can be reduced to only one dimension and subsequently solved using standard 1-D search algorithms [76].

Setting $z = \mathbf{h}\mathbf{v}^\dagger$, (3.3) becomes:

$$\mathcal{I}_{\text{bf,avg}}(\text{SNR}, \mathbf{v}) = \mathcal{E}_{|z|} [\log_2 (1 + \text{SNR} |z|^2)] \quad (3.7)$$

where $z \sim \mathcal{N}(\boldsymbol{\mu}\mathbf{v}^\dagger, \mathbf{v}\mathbf{R}\mathbf{v}^\dagger)$, and hence, $|z|$ follows a Rician distribution:

$$|z| \sim \frac{2x}{\sigma_{\mathbf{v}}} I_0 \left(\frac{2m_{\mathbf{v}}x}{\sigma_{\mathbf{v}}} \right) \exp \left(-\frac{x^2 + m_{\mathbf{v}}^2}{\sigma_{\mathbf{v}}} \right) \quad (3.8)$$

with

$$m_{\mathbf{v}} = |\boldsymbol{\mu}\mathbf{v}^\dagger| \quad (3.9)$$

$$\sigma_{\mathbf{v}} = \mathbf{v}\mathbf{R}\mathbf{v}^\dagger \quad (3.10)$$

Proposition 3.1 $\mathcal{I}_{\text{bf,avg}}(\text{SNR}, \mathbf{v})$ in (3.7) increases monotonically with $m_{\mathbf{v}}$ and $\sigma_{\mathbf{v}}$.

Proof: The proof is given in [75]. Figure 3.1 demonstrates graphically the validity of the proposition. ■

Proposition 3.1 implies that $\mathcal{I}_{\text{bf,avg}}(\text{SNR}, \mathbf{v})$ is a function of $m_{\mathbf{v}}$ and $\sigma_{\mathbf{v}}$ and it can be maximized with respect to these two parameters. However, in the context of the combined CMI-CCI model, $m_{\mathbf{v}}$ and $\sigma_{\mathbf{v}}$ cannot be maximized (simultaneously) for the same $\mathbf{v} \in \mathcal{S}$, and hence, the solution of the optimum beamforming problem is not trivial, (as for the CMI and CCI models).

Using the definition of the angle between vectors in N -dimensional complex vector

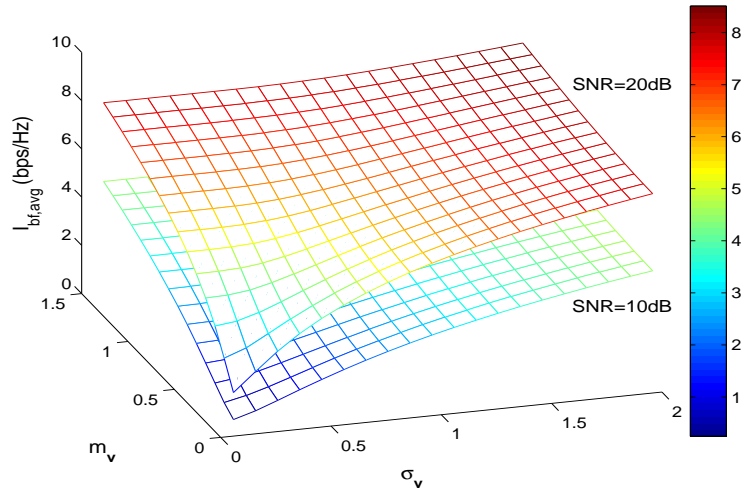


Figure 3-1: $\mathcal{I}_{\text{bf,avg}}$ vs. $m_{\mathbf{v}}$ and $\sigma_{\mathbf{v}}$.

spaces, (3.9) can be written as:

$$m_{\mathbf{v}} = \|\boldsymbol{\mu}\|_2 \cos \theta \quad (3.11)$$

where $\theta \in [0, \pi/2]$ is the (generalized) angle between $\boldsymbol{\mu}$ and \mathbf{v} . All vectors \mathbf{v} that belong to \mathcal{S} (as defined in (3.5)) and have an angle θ with $\boldsymbol{\mu}$, define a (non-convex) set \mathcal{S}_{θ} , with $\mathcal{S}_{\theta} \subset \mathcal{S}$, (Figure 3.2). In \mathcal{S}_{θ} , $m_{\mathbf{v}}$ has a fixed value (given by (3.11)) and hence, $\mathcal{I}_{\text{bf,avg}}(\text{SNR}, \mathbf{v})$ is maximized with \mathbf{v} , if and only if $\sigma_{\mathbf{v}}$ is maximized with \mathbf{v} . The beamforming vector that solves this optimization problem, restricted in \mathcal{S}_{θ} , is denoted as \mathbf{v}_{θ} (Figure 3.2):

$$\mathbf{v}_{\theta} = \arg \max_{\mathbf{v} \in \mathcal{S}_{\theta}} \sigma_{\mathbf{v}} = \arg \max_{\mathbf{v} \in \mathcal{S}_{\theta}} \mathbf{v} \mathbf{R} \mathbf{v}^{\dagger} \quad (3.12)$$

Solving (3.12) for all $\theta \in [0, \pi/2]$, the following (non-convex) set of vectors is defined:

$$\mathcal{S}_{\text{opt}} = \{\mathbf{v}_{\theta}; \theta \in [0, \pi/2]\} \quad (3.13)$$

In the proposition that follows, it is proven that the search of the optimum beamformer can be restricted in a subset of \mathcal{S}_{opt} , denoted as \mathcal{S}_o (Figure 3.2).

Proposition 3.2 The optimum beamformer \mathbf{v}_{opt} belongs to \mathcal{S}_o , (a subset of \mathcal{S}_{opt}), which is

defined as:

$$\mathbf{v}_{\text{opt}} \in \mathbf{S}_o = \{\mathbf{v}_\theta; \theta \in [0, \phi]\} \quad (3.14)$$

where:

a. ϕ is the angle between the normalized channel mean vector $\mathbf{m} = \boldsymbol{\mu}/\|\boldsymbol{\mu}\|_2$ and the complex conjugate transpose of the dominant eigenvector of the channel transmit covariance matrix \mathbf{R} , denoted as $\mathbf{U}_{\bullet 1}^\dagger$, i.e.

$$\phi = \cos^{-1}(|\mathbf{m}\mathbf{U}_{\bullet 1}|) \quad (3.15)$$

b. \mathbf{v}_θ is the solution of the optimization problem (3.12).

Proof: Assume an arbitrary $\mathbf{v} \in \mathbf{S}$ that has an angle θ with $\boldsymbol{\mu}$. Since $\mathbf{v} \in \mathbf{S}_\theta$, it is:

$$\begin{aligned} \mathcal{I}_{\text{bf,avg}}(\text{SNR}, \mathbf{v}) &\leq \mathcal{I}_{\text{bf,avg}}(\text{SNR}, \mathbf{v}_\theta) \leq \max_{\mathbf{v} \in \mathbf{S}_{\text{opt}}} \mathcal{I}_{\text{bf,avg}}(\text{SNR}, \mathbf{v}) \Rightarrow \\ \max_{\mathbf{v} \in \mathbf{S}} \mathcal{I}_{\text{bf,avg}}(\text{SNR}, \mathbf{v}) &\leq \max_{\mathbf{v} \in \mathbf{S}_{\text{opt}}} \mathcal{I}_{\text{bf,avg}}(\text{SNR}, \mathbf{v}) \end{aligned} \quad (3.16)$$

where the last inequality results from the fact that \mathbf{v} has been chosen arbitrarily in \mathbf{S} . However, since $\mathbf{S}_{\text{opt}} \subset \mathbf{S}$, (3.16) becomes a strict equality, which implies that $\mathbf{v}_{\text{opt}} \in \mathbf{S}_{\text{opt}}$. Now, for $\theta = \phi$, the (beamforming) vector of the set \mathbf{S}_ϕ that maximizes $\sigma_{\mathbf{v}}$ is $\mathbf{v}_\phi = \mathbf{U}_{\bullet 1}^\dagger$, with

$$\sigma_{\mathbf{v}}|_{\mathbf{v}=\mathbf{v}_\phi} = \max_{\mathbf{v} \in \mathbf{S}} \sigma_{\mathbf{v}} = \lambda_1(\mathbf{R}) \quad (3.17)$$

From (3.11) and (3.17), it can be concluded that $\forall \theta > \phi$, $m_{\mathbf{v}}|_{\mathbf{v}=\mathbf{v}_\theta} < m_{\mathbf{v}}|_{\mathbf{v}=\mathbf{v}_\phi}$ and $\sigma_{\mathbf{v}}|_{\mathbf{v}=\mathbf{v}_\theta} < \sigma_{\mathbf{v}}|_{\mathbf{v}=\mathbf{v}_\phi}$, respectively, and hence, since $\mathcal{I}_{\text{bf,avg}}(\text{SNR}, \mathbf{v})$ increases with $m_{\mathbf{v}}$ and $\sigma_{\mathbf{v}}$ (Proposition 3.1), it will be also:

$$\mathcal{I}_{\text{bf,avg}}(\text{SNR}, \mathbf{v}_\theta) \leq \mathcal{I}_{\text{bf,avg}}(\text{SNR}, \mathbf{v}_\phi) \quad (3.18)$$

Since (3.18) holds $\forall \theta > \phi$, it can be concluded that the angle of the optimum beamformer with respect to \mathbf{m} , (denoted as $\theta_{\text{opt}}(\mathbf{v}_{\text{opt}} = \mathbf{v}_{\theta_{\text{opt}}})$), should be constrained as $\theta_{\text{opt}} \leq \phi$. This conclusion is equivalently expressed by (3.14). ■

Proposition 3.2 implies that the optimum beamformer belongs to a continuous trajectory⁴ that is defined by the vectors of \mathcal{S}_o (see (3.14)), which lies on the surface of the unit-radius Euclidean ball, starts from \mathbf{m} (for $\theta = 0$) and ends to $\mathbf{U}_{\bullet,1}^\dagger$ (for $\theta = \phi$). This is visualized in Figure 3.2.

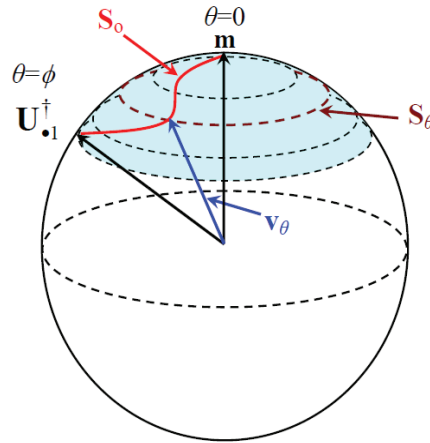


Figure 3.2: Geometric interpretation of Proposition 3.2.

Using (3.14), the optimization problem (3.4) can be re-formulated as:

$$\mathbf{v}_{\text{opt}} = \arg \max_{\mathbf{v} \in \mathcal{S}_o} \mathcal{I}_{\text{bf,avg}}(\text{SNR}, \mathbf{v}) \quad (3.19)$$

$$\mathcal{S}_o = \{\mathbf{v}_\theta; \theta \in [0, \phi]\} \quad (3.20)$$

where $\forall \theta \in [0, \phi]$, \mathbf{v}_θ is the solution of the optimization problem (3.12).

The optimization problem in (3.19) is 1-D with respect to the angle θ . The simplicity of (3.19) is now based on solving (3.12) and finding a convenient expression for \mathbf{v}_θ , for $\theta \in [0, \phi]$.

Theorems 3.1 and 3.2 below present the solution of the optimization problem (3.12), and \mathbf{v}_θ is expressed as a function of the CDIT parameters $\boldsymbol{\mu}$ and \mathbf{R} .

Theorem 3.1 ([74], [78]) The optimum beamformer \mathbf{v}_{opt} , for a MISO Rician flat fading channel with N transmit antenna elements ($N \geq 2$), mean value $\boldsymbol{\mu}$ ($\boldsymbol{\mu} \in \mathbb{C}^{1 \times N}$, $\boldsymbol{\mu} \neq \mathbf{0}$)

⁴The continuity of this trajectory is discussed in the following.

and transmit covariance matrix \mathbf{R} ($\mathbf{R} \in \mathbb{H}_+^N$, $\mathbf{R} \neq \mathbf{I}_N$), can be calculated from the following 1-D optimization problem:

$$\mathbf{v}_{\text{opt}} = \arg \max_{\mathbf{v} \in \mathbf{S}_o} \mathcal{I}_{\text{bf,avg}}(\text{SNR}, \mathbf{v}) \quad (3.21)$$

$$\mathbf{S}_o = \{\mathbf{v}_\theta; \theta \in [0, \phi]\} \quad (3.22)$$

where ϕ is calculated with the help (3.15) and \mathbf{v}_θ is expressed as:

$$\mathbf{v}_\theta = \cos \theta [1 \ \mathbf{Z}(r_\theta \mathbf{I}_{N-1} - \mathbf{G})^{-1}] \mathbf{W}^T \mathbf{U}^\dagger \quad (3.23)$$

where:

a. \mathbf{U} is the eigenvector matrix of \mathbf{R} and \mathbf{W} is a complex $N \times N$ orthonormal matrix with its first column defined as $\mathbf{W}_{\bullet 1} = \mathbf{U}^T \mathbf{m}^T$ ($\mathbf{m} = \boldsymbol{\mu} / \|\boldsymbol{\mu}\|_2$), whereas the rest of its columns ($\mathbf{W}_{\bullet i}$, $i = 2, \dots, N$) are arbitrarily chosen, with the restriction that $\mathbf{W}^\dagger \mathbf{W} = \mathbf{I}_N$. Moreover, \mathbf{G} and \mathbf{Z} are defined as:

$$\mathbf{G} = \begin{pmatrix} \mathbf{K}_{22} & \cdots & \mathbf{K}_{2N} \\ \vdots & \ddots & \vdots \\ \mathbf{K}_{N2} & \cdots & \mathbf{K}_{NN} \end{pmatrix} \quad (3.24)$$

$$\mathbf{Z} = [\mathbf{K}_{12} \ \mathbf{K}_{13} \ \cdots \ \mathbf{K}_{1N}] \quad (3.25)$$

where \mathbf{K}_{lm} is the l^{th} row and m^{th} column element of matrix \mathbf{K} , defined as:

$$\mathbf{K} = \sum_{i=1}^N \lambda_i(\mathbf{R}) \mathbf{W}_{i\bullet}^T \mathbf{W}_{i\bullet}^* \quad (3.26)$$

b. r_θ is the maximum real root of the $2(N-1)$ -degree polynomial:

$$P(x; \theta) = \cos^2 \theta \sum_{i=1}^{N-1} |\mathbf{Z} \mathbf{g}_i|^2 \left[\prod_{\substack{j=1 \\ j \neq i}}^{N-1} (x - \lambda_j(\mathbf{G}))^2 \right] - \sin^2 \theta \prod_{i=1}^{N-1} (x - \lambda_i(\mathbf{G}))^2 \quad (3.27)$$

where $\mathbf{g}_i \in \mathbb{C}^{(N-1) \times 1}$ is the i^{th} eigenvector of matrix \mathbf{G} .

Proof: The optimization problem (3.12) can also be expressed as:

$$\begin{aligned}
& \text{maximize} && \sigma_{\mathbf{v}} = \mathbf{v}\mathbf{R}\mathbf{v}^\dagger && (3.28) \\
& \text{subject to} && \mathbf{v}\mathbf{v}^\dagger = 1 \\
& && |m_{\mathbf{v}}|^2 = \|\boldsymbol{\mu}\|_2^2 \cos^2 \theta \Rightarrow \mathbf{v}\mathbf{M}\mathbf{v}^\dagger = \|\boldsymbol{\mu}\|_2^2 \cos^2 \theta
\end{aligned}$$

where $\mathbf{M} = \boldsymbol{\mu}^\dagger \boldsymbol{\mu}$. The optimization problem in (3.28) is a nonconvex Quadratically Constrained Quadratic Program (QCQP) and it can be generally solved numerically using a semidefinite relaxation (SDR) [79]. However, in this case where \mathbf{M} is *rank-1*, (3.28) can be solved analytically, as it is proven in the following. The solution of (3.28) is denoted as \mathbf{v}_θ .

Setting

$$\mathbf{v} = \mathbf{x}\mathbf{U}^\dagger \quad (3.29)$$

and recognizing that the l_2 -norms, the eigenvalues and the angles between vectors remain invariant under unitary transformations [80], (3.28) can be equivalently written:

$$\begin{aligned}
& \text{maximize} && \sigma_{\mathbf{x}} = \mathbf{x}\boldsymbol{\Lambda}\mathbf{x}^\dagger && (3.30) \\
& \text{subject to} && \mathbf{x}\mathbf{x}^\dagger = 1 \\
& && |\boldsymbol{\mu}_u \mathbf{x}^\dagger|^2 = \|\boldsymbol{\mu}\|_2 \cos \theta
\end{aligned}$$

where $\boldsymbol{\mu}_u = \boldsymbol{\mu}\mathbf{U}$ and $\boldsymbol{\Lambda}$ is the eigenvalue matrix of \mathbf{R} .

The solution of (3.30) is denoted as \mathbf{x}_θ . The constraints of (3.30) imply that \mathbf{x}_θ must be a unit-norm vector with an angle θ with $\boldsymbol{\mu}_u$. Hence, $\mathbf{x}_\theta \in \Sigma_\theta$, where Σ_θ represents the set of all unit-norm vectors that have an angle θ with $\boldsymbol{\mu}_u$. Let us now define the matrix $\mathbf{W} = [\mathbf{W}_{\bullet 1} \mathbf{W}_{\bullet 2} \dots \mathbf{W}_{\bullet N}]$, with its first column defined as $\mathbf{W}_{\bullet 1} = \boldsymbol{\mu}_u^T \|\boldsymbol{\mu}\|^{-1}$ and the rest of its columns $\mathbf{W}_{\bullet i} \in \mathbb{C}^{N \times 1}$, ($i = 2, \dots, N$), arbitrarily chosen with the restriction that $\mathbf{W}^\dagger \mathbf{W} = \mathbf{I}_N$. From the columns of matrix \mathbf{W} we form the orthonormal basis $\mathcal{B}_W =$

$[\mathbf{W}_{\bullet 1}^T \mathbf{W}_{\bullet 2}^T \dots \mathbf{W}_{\bullet N}^T]$ in $\mathbb{C}^{1 \times N}$. The set Σ_θ can be expressed with respect to this basis as:

$$\Sigma_\theta = \{[\mathbf{x}]_{\mathcal{B}_W} = [e^{ju_x} \cos \theta \ a_2 \ a_3 \ \dots \ a_N];$$

$$a_i \in \mathbb{C} \ (i = 2, \dots, N), \sum_{i=2}^N |a_i|^2 = \sin^2 \theta, \ u_x \in [0, 2\pi]\} \quad (3.31)$$

If we set

$$\mathbf{p} = [a_2 \ a_3 \ \dots \ a_N] \quad (3.32)$$

then any vector $[\mathbf{x}]_{\mathcal{B}_W} \in \Sigma_\theta$ can be written as:

$$[\mathbf{x}]_{\mathcal{B}_W} = [e^{ju_x} \mathbf{p}] \mathbf{D}_\theta \quad (3.33)$$

where \mathbf{D}_θ is $N \times N$ diagonal matrix with $\mathbf{D}_{\theta,11} = \cos \theta$ and $\mathbf{D}_{\theta,ii} = 1$, for $i = 2, \dots, N$.

Expressing now $[\mathbf{x}]_{\mathcal{B}_W} \in \Sigma_\theta$ with respect to the normal basis $\mathcal{B} = [\mathbf{e}_1 \ \mathbf{e}_2 \ \dots \ \mathbf{e}_N]$ we have:

$$\mathbf{x} = [\mathbf{x}]_{\mathcal{B}} = [\mathbf{x}]_{\mathcal{B}_W} {}_{\mathcal{B}}[\mathbf{I}]_{\mathcal{B}_W} = [e^{ju_x} \mathbf{p}] \mathbf{D}_\theta \mathbf{W}^T \quad (3.34)$$

where ${}_{\mathcal{B}}[\mathbf{I}]_{\mathcal{B}_W} = \mathbf{W}^T$ stands for the $\mathcal{B}_W \rightarrow \mathcal{B}$ basis transformation.

From (3.34), the optimization problem (3.30) can be transformed into the following equivalent optimization problem with respect to $\mathbf{p} \in \mathbb{C}^{1 \times N-1}$:

$$\begin{aligned} & \text{maximize} \quad \sigma_{\mathbf{p}} = [e^{ju_x} \mathbf{p}] \mathbf{D}_\theta \mathbf{K} \mathbf{D}_\theta [e^{ju_x} \mathbf{p}]^\dagger \\ & \text{subject to} \quad \mathbf{p} \mathbf{p}^\dagger = \sin^2 \theta \end{aligned} \quad (3.35)$$

where $\mathbf{K} \in \mathbb{H}_{++}^N$ and is given by the following equation:

$$\mathbf{K} = \sum_{i=1}^N \lambda_i(\mathbf{R}) \mathbf{W}_{i\bullet}^T \mathbf{W}_{i\bullet}^* \quad (3.36)$$

Now, partitioning \mathbf{K} properly and setting for simplicity $u_x = 0$ (u_x does not affect the solution of (3.35), due to the quadratic form of the objective function $\sigma_{\mathbf{p}}$), (3.35) can be

re-written as:

$$\begin{aligned} \text{maximize } \sigma_{\mathbf{p}} &= \mathbf{p}\mathbf{G}\mathbf{p}^\dagger + \cos\theta (\mathbf{p}\mathbf{Z}^\dagger + \mathbf{Z}\mathbf{p}^\dagger) + \cos^2\theta \mathbf{K}_{11} \\ \text{subject to } & \mathbf{p}\mathbf{p}^\dagger = \sin^2\theta \end{aligned} \quad (3.37)$$

where $\mathbf{G} \in \mathbb{H}_{++}^N$ is the principal submatrix of \mathbf{K} , i.e.

$$\mathbf{G} = \begin{pmatrix} \mathbf{K}_{22} & \cdots & \mathbf{K}_{2N} \\ \vdots & \ddots & \vdots \\ \mathbf{K}_{N2} & \cdots & \mathbf{K}_{NN} \end{pmatrix} \quad (3.38)$$

and

$$\mathbf{Z} = [\mathbf{K}_{12} \ \mathbf{K}_{13} \ \cdots \ \mathbf{K}_{1N}] \quad (3.39)$$

The solution of (3.37) is denoted as \mathbf{p}_θ and can be calculated using the Lagrange multipliers method. The Lagrangian of (3.37) is:

$$\mathcal{L}(\mathbf{p}) = \mathbf{p}\mathbf{G}\mathbf{p}^\dagger + \cos\theta \mathbf{p}\mathbf{Z}^\dagger + \cos\theta \mathbf{Z}\mathbf{p}^\dagger + \cos^2\theta \mathbf{K}_{11} + \kappa (\sin^2\theta - \mathbf{p}\mathbf{p}^\dagger) \quad (3.40)$$

where κ is the Lagrange multiplier, (real number⁵). $\mathcal{L}(\mathbf{p})$ does not satisfy the Cauchy-Riemann equations and is not complex differentiable. As a result the solution of (3.37) must satisfy the following necessary conditions [81]:

$$\nabla_{\mathbf{p}^*} \mathcal{L}(\mathbf{p}) = 0 \quad (3.41)$$

$$\mathbf{p}\mathbf{p}^\dagger = \sin^2\theta \quad (3.42)$$

where $\nabla_{\mathbf{p}^*} \mathcal{L}(\mathbf{p})$ is the complex gradient vector of $\mathcal{L}(\mathbf{p})$, given by the complex conjugate Wirtinger derivative [81]:

$$\nabla_{\mathbf{p}^*} \mathcal{L}(\mathbf{p}^*) = 2 \frac{d\mathcal{L}(\mathbf{p})}{d\mathbf{p}} = \frac{\partial \mathcal{L}(\mathbf{p})}{\partial \Re \mathbf{p}} + j \frac{\partial \mathcal{L}(\mathbf{p})}{\partial \Im \mathbf{p}} \quad (3.43)$$

⁵The Lagrange multiplier κ is a real number since the objective function $\sigma_{\mathbf{p}}$ and the constraint function $y(\mathbf{p}) = \mathbf{p}\mathbf{p}^\dagger - \sin^2\theta$ are real-valued functions of the complex variable \mathbf{p} [81].

where $\Re \mathbf{p}$ and $\Im \mathbf{p}$ are the real and imaginary parts of \mathbf{p} , respectively.

From (3.40), (3.41) and (3.43) we have:

$$\mathbf{p} (\kappa \mathbf{I}_{N-1} - \mathbf{G}) = \cos \theta \mathbf{Z} \quad (3.44)$$

In order (3.37) to have a solution, it must be:

$$|\kappa \mathbf{I}_{N-1} - \mathbf{G}| \neq 0 \quad (3.45)$$

and hence, (3.44) becomes:

$$\mathbf{p} = \cos \theta \mathbf{Z} (\kappa \mathbf{I}_{N-1} - \mathbf{G})^{-1} \quad (3.46)$$

Substituting (3.46) into the objective function of (3.37) we have:

$$\sigma_{\mathbf{p}} = \cos^2 \theta \mathbf{Z} (\kappa \mathbf{I}_{N-1} - \mathbf{G})^{-1} \mathbf{G} (\mathbf{Z} (\kappa \mathbf{I}_{N-1} - \mathbf{G})^{-1})^\dagger + 2 \cos^2 \theta \mathbf{Z} (\kappa \mathbf{I}_{N-1} - \mathbf{G})^{-1} \mathbf{Z}^\dagger + \cos^2 \theta \mathbf{K}_{11} \quad (3.47)$$

Matrix \mathbf{G} can be written as follows:

$$\mathbf{G} = \mathbf{U}_G \text{diag} [\lambda_1^G \lambda_2^G \dots \lambda_{N-1}^G] \mathbf{U}_G^\dagger \quad (3.48)$$

where \mathbf{U}_G the matrix of eigenvectors and λ_i^G ($i = 1, \dots, N - 1$) the eigenvalues of matrix \mathbf{G} . Using (3.48) it is:

$$\begin{aligned} (\kappa \mathbf{I}_{N-1} - \mathbf{G})^{-1} &= ((\kappa \mathbf{I}_{N-1} - \mathbf{G})^{-1})^\dagger = \left(\kappa \mathbf{U}_G \mathbf{U}_G^\dagger - \mathbf{U}_G \text{diag} [\lambda_1^G \lambda_2^G \dots \lambda_{N-1}^G] \mathbf{U}_G^\dagger \right)^{-1} = \\ &= \mathbf{U}_G \text{diag} \left[\frac{1}{\kappa - \lambda_1^G} \frac{1}{\kappa - \lambda_2^G} \dots \frac{1}{\kappa - \lambda_{N-1}^G} \right] \mathbf{U}_G^\dagger \quad (3.49) \end{aligned}$$

Using (3.48) and (3.49), (3.47) can be written as follows:

$$\begin{aligned}
\sigma_{\mathbf{p}} &= \cos^2 \theta \sum_{i=1}^{N-1} \frac{\lambda_i^G |\mathbf{Zg}_i|^2}{(\kappa - \lambda_i^G)^2} + 2 \cos^2 \theta \sum_{i=1}^{N-1} \frac{|\mathbf{Zg}_i|^2}{\kappa - \lambda_i^G} + \cos^2 \theta \mathbf{K}_{11} = \\
&\quad \cos^2 \theta \sum_{i=1}^{N-1} \left[\frac{\lambda_i^G |\mathbf{Zg}_i|^2}{(\kappa - \lambda_i^G)^2} + \frac{2|\mathbf{Zg}_i|^2}{\kappa - \lambda_i^G} \right] + \cos^2 \theta \mathbf{K}_{11} \Leftrightarrow \\
\sigma_{\mathbf{p}} &= \cos^2 \theta \sum_{i=1}^{N-1} \frac{|\mathbf{Zg}_i|^2 (2\kappa - \lambda_i^G)}{(\kappa - \lambda_i^G)^2} + \cos^2 \theta \mathbf{K}_{11} \Leftrightarrow \\
\sigma_{\mathbf{p}} &= 2\kappa \cos^2 \theta \sum_{i=1}^{N-1} \frac{|\mathbf{Zg}_i|^2}{(\kappa - \lambda_i^G)^2} - \cos^2 \theta \sum_{i=1}^{N-1} \frac{\lambda_i^G |\mathbf{Zg}_i|^2}{(\kappa - \lambda_i^G)^2} + \cos^2 \theta \mathbf{K}_{11} \tag{3.50}
\end{aligned}$$

where $\mathbf{g}_i \in \mathbb{C}^{(N-1) \times 1}$ is the i^{th} eigenvector of \mathbf{G} .

Substituting (3.46) into (3.42), it is:

$$\mathbf{p}\mathbf{p}^\dagger = \cos^2 \theta \sum_{i=1}^{N-1} \frac{|\mathbf{Zg}_i|^2}{(\kappa - \lambda_i^G)^2} = \sin^2 \theta \tag{3.51}$$

From (3.50) and (3.51) it is finally:

$$\sigma_{\mathbf{p}} = 2\kappa \sin^2 \theta - \cos^2 \theta \sum_{i=1}^{N-1} \frac{\lambda_i^G |\mathbf{Zg}_i|^2}{(\kappa - \lambda_i^G)^2} + \cos^2 \theta \mathbf{K}_{11} \tag{3.52}$$

Moreover, from (3.51) it is:

$$\Omega(\kappa; \theta) = \|\mathbf{p}\|_2^2 - \sin^2 \theta = Y(\kappa; \theta) - \sin^2 \theta = 0 \tag{3.53}$$

with

$$Y(\kappa; \theta) = \cos^2 \theta \frac{\sum_{i=1}^{N-1} |\mathbf{Zg}_i|^2 \left[\prod_{\substack{j=1 \\ j \neq i}}^{N-1} (\kappa - \lambda_j(\mathbf{G}))^2 \right]}{\prod_{i=1}^{N-1} (\kappa - \lambda_i(\mathbf{G}))^2} \tag{3.54}$$

From (3.54) it can be shown that:

$$\lim_{\kappa \rightarrow \pm\infty} Y(\kappa; \theta) = 0 \tag{3.55}$$

$$\lim_{\kappa \rightarrow \lambda_i(\mathbf{G})} Y(\kappa; \theta) = +\infty \tag{3.56}$$

From (3.55) and (3.56) it can be concluded that (3.53) has at least two real roots that

satisfy (3.45): one below $\lambda_{N-1}(\mathbf{G})$ and one above $\lambda_1(\mathbf{G})$.

Observing (3.52), it can be easily concluded that it is maximized for the maximum real root of (3.53) or, equivalently, of the $2(N-1)$ -degree polynomial equation $P(\kappa; \theta) = 0$ (where $P(\kappa; \theta)$ is expressed by (3.27)). This root will be denoted as r_θ and \mathbf{p}_θ (the solution of the optimization problem (3.37)) is obtained from (3.46) for $\kappa = r_\theta$:

$$\mathbf{p}_\theta = \cos \theta \mathbf{Z} (r_\theta \mathbf{I}_{N-1} - \mathbf{G})^{-1} \quad (3.57)$$

Substituting in (3.34) $\mathbf{p} = \mathbf{p}_\theta$, the solution of the optimization problem (3.30) is:

$$\mathbf{x}_\theta = \cos \theta [1 \ \mathbf{Z} (r_\theta \mathbf{I}_{N-1} - \mathbf{G})^{-1}] \mathbf{W}^T \quad (3.58)$$

Substituting (3.58) into (3.29), the solution of the initial optimization problem (3.28) is:

$$\mathbf{v}_\theta = \cos \theta [1 \ \mathbf{Z} (r_\theta \mathbf{I}_{N-1} - \mathbf{G})^{-1}] \mathbf{W}^T \mathbf{U}^\dagger \quad (3.59)$$

Note that any phase shift of \mathbf{v}_θ is also a solution of (3.28).

For $\theta = 0$ or $\theta = \phi$ it is not necessary to follow the above methodology. From the constraints of (3.28), it results that \mathbf{v}_0 must be along the channel mean, i.e. $\mathbf{v}_0 = \mathbf{m}$. Moreover, \mathbf{v}_ϕ coincides with the dominant eigenvector of \mathbf{R} , i.e. $\mathbf{v}_\phi = \mathbf{U}_{\bullet 1}^\dagger$, (see (3.17)).

■

It can be observed from (3.23) that \mathbf{v}_θ (and hence, $\mathcal{I}_{\text{bf,avg}}(\text{SNR}, \mathbf{v})$ in (3.21)), can be expressed in closed-form (with respect to θ) when the order of $P(x; \theta)$ is ≤ 4 , i.e. for MISO system with $N = 2$ or $N = 3$ transmit antenna elements, since, in this case, all roots of $P(x; \theta)$ - and hence r_θ - can be expressed analytically. For $N > 3$, r_θ must be calculated numerically using a root-finding algorithm and restricting the search area to $x > \lambda_1(\mathbf{G})$, (where $P(x; \theta)$ has its maximum real root).

Theorem 3.2 below provides an alternative geometrically-based approach, especially for MISO systems with $N = 2$ transmit antenna elements. Moreover, as it is mentioned in [78], Theorem 3.2 is also mathematically valid for the following special cases, with $N > 2$:

a. When $\boldsymbol{\mu}$ is a point in the hyperplane defined by $\mathbf{U}_{\bullet 1}^\dagger$ and $\mathbf{U}_{\bullet 2}^\dagger$.

b. When the channel covariance matrix has two eigenvalues, $\lambda_1(\mathbf{R})$ and $\lambda_2(\mathbf{R})$ ($\lambda_1(\mathbf{R}) \geq \lambda_2(\mathbf{R})$) with algebraic multiplicity one and $N - 1$, respectively, or it is rank deficient, with $\text{rank}\{\mathbf{R}\} \leq 2$.

Theorem 3.2 ([74]) For MISO systems with $N = 2$, \mathbf{v}_θ can be expressed by the following (closed-form) equation:

$$\mathbf{v}_\theta = \cos \theta \frac{\mathbf{U}_{\bullet 1}^\dagger \mathbf{m}^\dagger \mathbf{m}}{\|\mathbf{U}_{\bullet 1}^\dagger \mathbf{m}^\dagger \mathbf{m}\|_2} + \sin \theta \frac{\mathbf{m}^* (\mathbf{m}^T \mathbf{U}_{\bullet 1}^\dagger - \mathbf{U}_{\bullet 1}^* \mathbf{m})}{\|\mathbf{m}^* (\mathbf{m}^T \mathbf{U}_{\bullet 1}^\dagger - \mathbf{U}_{\bullet 1}^* \mathbf{m})\|_2} \quad (3.60)$$

Proof: A geometrical approach is employed for proving this Theorem: First the hyperplane formed by vectors $\mathbf{U}_{\bullet 1}^\dagger$ and $\mathbf{m} = \boldsymbol{\mu} \|\boldsymbol{\mu}\|_2^{-1}$ is defined, using the cross product tensor for N -dimensional complex vector spaces. Then it is shown that the optimum beamformer is a point in this hyperplane.

The cross product between $\mathbf{U}_{\bullet 1}^\dagger$ and \mathbf{m} can be represented by an antisymmetric $N \times N$ second-rank tensor, denoted as $\underline{\mathbf{N}}$ [82]:

$$\underline{\mathbf{N}} = \left[(\mathbf{U}_{\bullet 1}^* \boldsymbol{\mu})^T - \mathbf{U}_{\bullet 1}^* \boldsymbol{\mu} \right] \|\boldsymbol{\mu}\|_2^{-1} \quad (3.61)$$

Proposition 3.3 Any vector $\mathbf{U}_{\bullet 1}^\dagger$ can be decomposed into a perpendicular and a parallel vector with respect to \mathbf{m} :

$$\mathbf{U}_{\bullet 1}^\dagger = \mathbf{u}_\perp + \mathbf{u}_\parallel \quad (3.62)$$

where

$$\mathbf{u}_\perp = \boldsymbol{\mu} \underline{\mathbf{N}} \|\boldsymbol{\mu}\|_2^{-1} = \boldsymbol{\mu}^* \left[(\mathbf{U}_{\bullet 1}^* \boldsymbol{\mu})^T - \mathbf{U}_{\bullet 1}^* \boldsymbol{\mu} \right] \|\boldsymbol{\mu}\|_2^{-2} \quad (3.63)$$

$$\mathbf{u}_\parallel = \mathbf{U}_{\bullet 1}^\dagger \mathbf{m}^\dagger \mathbf{m} = \mathbf{U}_{\bullet 1}^\dagger \boldsymbol{\mu}^\dagger \boldsymbol{\mu} \|\boldsymbol{\mu}\|_2^{-2} \quad (3.64)$$

Proof: First it is proven that \mathbf{u}_\perp is perpendicular to $\boldsymbol{\mu}$:

$$\langle \mathbf{u}_\perp, \boldsymbol{\mu} \rangle = \mathbf{u}_\perp \boldsymbol{\mu}^\dagger = \boldsymbol{\mu}^* \left[(\mathbf{U}_{\bullet 1}^* \boldsymbol{\mu})^T - \mathbf{U}_{\bullet 1}^* \boldsymbol{\mu} \right] \|\boldsymbol{\mu}\|_2^{-2} \boldsymbol{\mu}^\dagger \Rightarrow$$

$$\langle \mathbf{u}_\perp, \boldsymbol{\mu} \rangle = \left[\boldsymbol{\mu}^* \boldsymbol{\mu}^T \mathbf{U}_{\bullet 1}^\dagger \boldsymbol{\mu}^\dagger - \boldsymbol{\mu}^* \mathbf{U}_{\bullet 1}^* \boldsymbol{\mu} \boldsymbol{\mu}^\dagger \right] \|\boldsymbol{\mu}\|_2^{-2} = 0$$

Then we prove that \mathbf{u}_\perp has an angle $\xi = \pi/2 - \phi$ with respect to $\mathbf{U}_{\bullet 1}^\dagger$, where ϕ is the angle between $\boldsymbol{\mu}$ and $\mathbf{U}_{\bullet 1}^\dagger$:

The angle ξ between \mathbf{u}_\perp and $\mathbf{U}_{\bullet 1}^\dagger$ is defined as

$$\begin{aligned} \cos \xi &= |\mathbf{u}_\perp \mathbf{U}_{\bullet 1}| \|\mathbf{u}_\perp\|_2^{-1} \Rightarrow \\ \cos \xi &= |\boldsymbol{\mu}^* \left[(\mathbf{U}_{\bullet 1}^* \boldsymbol{\mu})^T - \mathbf{U}_{\bullet 1}^* \boldsymbol{\mu} \right] \mathbf{U}_{\bullet 1} \|\boldsymbol{\mu}\|_2^{-2}| \|\mathbf{u}_\perp\|_2^{-1} \Rightarrow \\ \cos \xi &= |(|\boldsymbol{\mu} \mathbf{U}_{\bullet 1}^*|^2 - \|\boldsymbol{\mu}\|_2^2) \|\boldsymbol{\mu}\|_2^{-2}| \|\mathbf{u}_\perp\|_2^{-1} \Rightarrow \\ \cos \xi &= |(\|\boldsymbol{\mu}\|_2^2 \cos^2 \phi - \|\boldsymbol{\mu}\|_2^2) \|\boldsymbol{\mu}\|_2^{-2}| \|\mathbf{u}_\perp\|_2^{-1} \Rightarrow \\ \cos \xi &= \sin^2 \phi \|\mathbf{u}_\perp\|_2^{-1} \end{aligned}$$

From the definition of \mathbf{u}_\perp in (3.58) it can be proven that $\|\mathbf{u}_\perp\|_2 = \sin \phi$ and hence:

$$\cos \xi = \sin^2 \phi \|\mathbf{u}_\perp\|_2^{-1} = \sin \phi \Rightarrow \xi = \pi/2 - \phi$$

Now, starting from the right-hand side of (3.57) and using (3.58) and (3.59) we have:

$$\begin{aligned} \mathbf{u}_\perp + \mathbf{u}_\parallel &= \boldsymbol{\mu}^* \left[(\mathbf{U}_{\bullet 1}^* \boldsymbol{\mu})^T - \mathbf{U}_{\bullet 1}^* \boldsymbol{\mu} \right] \|\boldsymbol{\mu}\|_2^{-2} + \mathbf{U}_{\bullet 1}^\dagger \boldsymbol{\mu}^\dagger \boldsymbol{\mu} \|\boldsymbol{\mu}\|_2^{-2} \Rightarrow \\ \mathbf{u}_\perp + \mathbf{u}_\parallel &= \boldsymbol{\mu}^* \left[(\mathbf{U}_{\bullet 1}^* \boldsymbol{\mu})^T - \mathbf{U}_{\bullet 1}^* \boldsymbol{\mu} \right] \|\boldsymbol{\mu}\|_2^{-2} + \mathbf{U}_{\bullet 1}^\dagger \boldsymbol{\mu}^\dagger \boldsymbol{\mu} \|\boldsymbol{\mu}\|_2^{-2} \Rightarrow \\ \mathbf{u}_\perp + \mathbf{u}_\parallel &= \boldsymbol{\mu}^* (\mathbf{U}_{\bullet 1}^* \boldsymbol{\mu})^T \|\boldsymbol{\mu}\|_2^{-2} - \boldsymbol{\mu}^* \mathbf{U}_{\bullet 1}^* \boldsymbol{\mu} \|\boldsymbol{\mu}\|_2^{-2} + \mathbf{U}_{\bullet 1}^\dagger \boldsymbol{\mu}^\dagger \boldsymbol{\mu} \|\boldsymbol{\mu}\|_2^{-2} \Rightarrow \\ \mathbf{u}_\perp + \mathbf{u}_\parallel &= \boldsymbol{\mu}^* (\mathbf{U}_{\bullet 1}^* \boldsymbol{\mu})^T \|\boldsymbol{\mu}\|_2^{-2} \Rightarrow \\ \mathbf{u}_\perp + \mathbf{u}_\parallel &= \mathbf{U}_{\bullet 1}^\dagger \end{aligned}$$

■

The normalized \mathbf{u}_\perp and \mathbf{u}_\parallel are defined as:

$$\mathbf{w}_\perp = \mathbf{u}_\perp \|\mathbf{u}_\perp\|_2^{-1} \tag{3.65}$$

$$\mathbf{w}_{\parallel} = \mathbf{u}_{\parallel} \|\mathbf{u}_{\parallel}\|_2^{-1} \quad (3.66)$$

In the following, we set $\mathbf{w}_1 = \mathbf{w}_{\parallel}$ and $\mathbf{w}_2 = \mathbf{w}_{\perp}$ and we choose $N - 1$ vectors $\mathbf{w}_i \in \mathbb{C}^{1 \times N}$, $i = 3, \dots, N$, arbitrarily, with the restriction that the basis $\mathcal{B}_W = [\mathbf{w}_1 \mathbf{w}_2 \dots \mathbf{w}_N]$ is orthonormal in $\mathbb{C}^{1 \times N}$. The set S_{θ} of unit norm vectors that have with $\boldsymbol{\mu}$ an angle θ in the interval $[0, \phi]$ (ϕ is the angle between $\mathbf{U}_{\bullet,1}^{\dagger}$ and \mathbf{m}) can be expressed as:

$$\begin{aligned} S_{\theta} = \{ \mathbf{v} = [e^{ju_1} \cos \theta \mathbf{w}_1 \ a_2 \mathbf{w}_2 \ a_3 \mathbf{w}_3 \ \dots \ a_N \mathbf{w}_N] ; \\ a_i \in \mathbb{C} \ (i = 2, \dots, N), \sum_{i=2}^N |a_i|^2 = \sin^2 \theta, u_1 \in [0, 2\pi] \} \end{aligned} \quad (3.67)$$

The set S'_{θ} of unit-norm vectors that have with $\boldsymbol{\mu}$ an angle θ in the interval $[0, \phi]$ and belong (at the same time) to the hyperplane defined by \mathbf{w}_1 and \mathbf{w}_2 , (i.e. they can be written as a linear combination of \mathbf{w}_1 and \mathbf{w}_2) is expressed as:

$$S'_{\theta} = \{ \mathbf{v} = e^{ju_1} \cos \theta \mathbf{w}_1 + e^{ju_2} \sin \theta \mathbf{w}_2; u_1, u_2 \in [0, 2\pi] \} \quad (3.68)$$

Obviously, S'_{θ} is a subset of S_{θ} .

Proposition 3.4 If ω is the angle between a vector $\mathbf{v} \in S_{\theta}$ and $\mathbf{U}_{\bullet,1}^{\dagger}$, it then holds that $\omega \geq \phi - \theta$, where ϕ is the angle between $\mathbf{U}_{\bullet,1}^{\dagger}$ and \mathbf{m} , as defined by (3.15). Furthermore, ω takes the minimum value in S_{θ} (i.e. $\omega_{min} = \phi - \theta$) if and only if $\mathbf{v} \in S'_{\theta}$ with $u_1 = u_2$.

Proof: The angle ω between $\mathbf{v} \in S_{\theta}$ and $\mathbf{U}_{\bullet,1}^{\dagger}$ is defined as:

$$\cos \omega = |\mathbf{v} \mathbf{U}_{\bullet,1}| \quad (3.69)$$

As shown in the proof of Proposition 3.3:

$$\|\mathbf{u}_{\perp}\|_2 = \sin \phi \quad (3.70)$$

Writing \mathbf{v} as in (3.67), using (3.62), (3.65), (3.70) and after some simple mathematical manipulations, equation (3.69) can be written as:

$$\cos \omega = |e^{ju} \cos \theta \cos \phi + |a_2| \sin \phi| \quad (3.71)$$

where $u = u_1 - \angle a_2$ and $\angle a_2$ is the phase of a_2 . Since $\sum_{i=2}^N |a_i|^2 = \sin^2 \theta \Rightarrow |a_2| \leq \sin \theta$, and hence, from (3.71) it can be concluded that:

$$\cos \omega \leq |\cos(\phi - \theta)| \Rightarrow \omega \geq \phi - \theta \quad (3.72)$$

Moreover, if $\mathbf{v} \in \mathbf{S}'_\theta$ and $u_1 = u_2$, then in (3.71) it is $u = 0$, $|a_2| = \sin \theta$ and hence, (3.72) becomes a strict equality. ■

For MISO systems with $N = 2$ transmit antenna elements it is $\mathbf{S}'_\theta \equiv \mathbf{S}_\theta$ and for an arbitrary $\mathbf{v} \in \mathbf{S}'_\theta$, equation (3.10) becomes:

$$\begin{aligned} \sigma_{\mathbf{v}} = \mathbf{v} \mathbf{R} \mathbf{v}^\dagger &= \sum_{i=1}^N \lambda_i(\mathbf{R}) |\mathbf{v} \mathbf{U}_{\bullet i}|^2 = \lambda_1(\mathbf{R}) |\mathbf{v} \mathbf{U}_{\bullet 1}|^2 + \lambda_2(\mathbf{R}) |\mathbf{v} \mathbf{U}_{\bullet 2}|^2 \Rightarrow \\ \sigma_{\mathbf{v}} &= \lambda_1(\mathbf{R}) \cos^2 \omega + \lambda_2(\mathbf{R}) \sin^2 \omega \end{aligned} \quad (3.73)$$

where ω is the angle between \mathbf{v} and $\mathbf{U}_{\bullet 1}^\dagger$, as defined in (3.69).

It can be observed that (3.73) is maximized if and only if ω is minimized. According to Proposition 3.4, this is achieved when $u_1 = u_2$. Hence, the solution of (3.12) is:

$$\begin{aligned} \mathbf{v}_\theta &= \cos \theta \mathbf{w}_1 + \sin \theta \mathbf{w}_2 \Rightarrow \\ \mathbf{v}_\theta &= \cos \theta \mathbf{w}_\parallel + \sin \theta \mathbf{w}_\perp \end{aligned} \quad (3.74)$$

Substituting (3.63)-(3.66) into (3.74), then (3.60) is obtained. Note also that any phase shift of \mathbf{v}_θ (given by (3.60)) is also a solution of (3.12). ■

The process that is proposed by Theorem 3.1 for the calculation of \mathbf{v}_θ is summarized and visualized for convenience in Figure 3.3. Observe that \mathbf{W} , \mathbf{U} , \mathbf{G} , \mathbf{Z} , $\lambda_i(\mathbf{R})$ do not depend on θ and as a result, the only numerical calculation involved with \mathbf{v}_θ is the calculation r_θ .

Some further useful remarks for the above theorems are provided below:

Remark 1. For $\theta = 0$ and $\theta = \phi$, (3.23) becomes $\mathbf{v}_0 = \mathbf{m}$ and $\mathbf{v}_\phi = \mathbf{U}_{\bullet 1}^\dagger$, respectively.

Remark 2. As stated in Theorem 3.1, the optimization problem expressed by (3.21) is

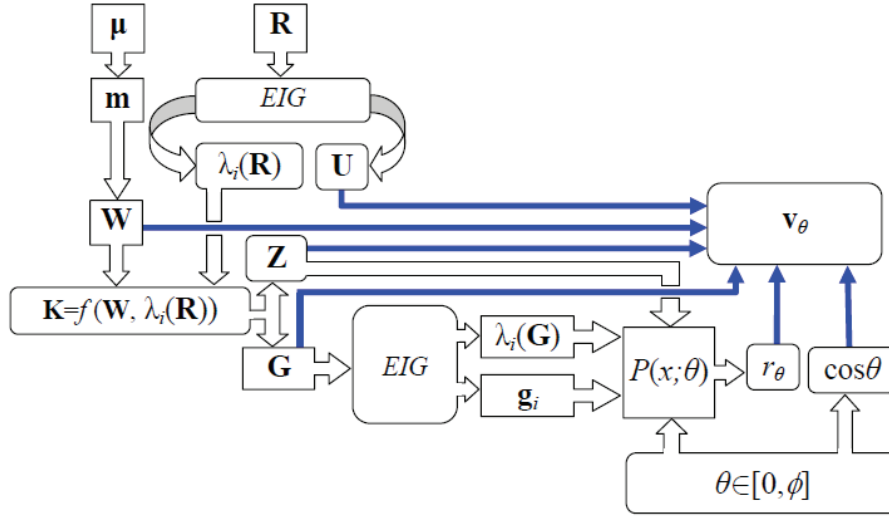


Figure 3-3: Diagrammatic representation of the calculation of \mathbf{v}_θ (equation (3.23)) for Theorem 3.1 (EIG stands for eigen-decomposition).

1-D with respect to θ . Practically, since $\mathbf{v}_{\text{opt}} \in \mathcal{S}_o$, the (1-D) objective function that has to be maximized with respect to θ is obtained by substituting (3.23) (or (3.60) for the cases of Theorem 3.2) into (3.3):

$$\mathcal{I}_{\text{bf,avg}}(\theta) = \mathcal{I}_{\text{bf,avg}}(\text{SNR}, \mathbf{v}_\theta) \quad (3.75)$$

$$\theta_{\text{opt}} = \arg \max_{\theta \in [0, \phi]} \mathcal{I}_{\text{bf,avg}}(\theta) \quad (3.76)$$

Solving (3.76), θ_{opt} is determined simultaneously with the optimum beamformer. Vector $\mathbf{v}_{\text{opt}} = \mathbf{v}_{\theta_{\text{opt}}}$. $\mathcal{I}_{\text{bf,avg}}(\theta)$ is continuously differentiable, regardless of the values of the channel parameters $(\boldsymbol{\mu}, \mathbf{R})$ and the SNR, due to the continuity and differentiability of \mathbf{v}_θ ⁶. Hence, gradient based or direct search programming algorithms [76] can be employed for the solution of (3.76), which generally can be solved very fast, (see results in Section 3.4).

For the solution of the optimization problem (3.21), the evaluation of $\mathcal{I}_{\text{bf,avg}}(\theta)$ is required in each iteration of the employed 1-D search algorithm. $\mathcal{I}_{\text{bf,avg}}(\theta)$ can be evaluated using Monte-Carlo integration or alternatively, by the following infinite series:

⁶In (3.23), r_θ (and hence, \mathbf{v}_θ) is a continuous and differentiable function of θ , due to the continuity and differentiability of the coefficients of the polynomial $P(x; \theta)$ with respect to θ . The continuity of \mathbf{v}_θ also ensures the continuity of the trajectory expressed by the set \mathcal{S}_o on the Euclidean ball, (see discussion in Section 3.2 and Figure 3.2).

Proposition 3.5

$$\mathcal{I}_{\text{bf,avg}}(\theta) = \mathcal{I}_{\text{bf,avg}}(\text{SNR}, \mathbf{v}_\theta) = (\ln 2)^{-1} \exp\left(\frac{1 - \text{SNR} m_{\mathbf{v}}^2}{\text{SNR} \sigma_{\mathbf{v}}}\right) \sum_{n=0}^{\infty} \left[\frac{1}{n!} \left(\frac{m_{\mathbf{v}}^2}{\sigma_{\mathbf{v}}}\right)^n \sum_{k=0}^n \left(\frac{1}{\text{SNR} \sigma_{\mathbf{v}}}\right)^k \Gamma\left(-k, \frac{1}{\text{SNR} \sigma_{\mathbf{v}}}\right) \right] \Bigg|_{\mathbf{v}=\mathbf{v}_\theta} \quad (3.77)$$

where $\Gamma(\cdot, \cdot)$ is the upper incomplete Gamma function [74], [78].

Proof: Setting $x = |z|$ in equation (3.7), $\mathcal{I}_{\text{bf,avg}}(\text{SNR}, \mathbf{v})$ can be expressed with the help of (3.8) by the following integral:

$$\mathcal{I}_{\text{bf,avg}}(\text{SNR}, \mathbf{v}) = \int_0^{\infty} \log_2(1 + \text{SNR}x^2) \frac{2x}{\sigma_{\mathbf{v}}} I_0\left(\frac{2m_{\mathbf{v}}x}{\sigma_{\mathbf{v}}}\right) \exp\left(-\frac{x^2 + m_{\mathbf{v}}^2}{\sigma_{\mathbf{v}}}\right) dx \quad (3.78)$$

where $I_0(\cdot)$ is the zero-order modified Bessel function of the first kind, and $m_{\mathbf{v}}$ and $\sigma_{\mathbf{v}}$ are given by (3.9) and (3.10), respectively. Setting $y = x^2$, (3.78) is written as:

$$\mathcal{I}_{\text{bf,avg}}(\text{SNR}, \mathbf{v}) = \frac{1}{\sigma_{\mathbf{v}}} \int_0^{\infty} \log_2(1 + \text{SNR}y) I_0\left(\frac{2m_{\mathbf{v}}y^{1/2}}{\sigma_{\mathbf{v}}}\right) \exp\left(-\frac{y + m_{\mathbf{v}}^2}{\sigma_{\mathbf{v}}}\right) dy \quad (3.79)$$

Then, using the infinite-series representation $I_0(\xi) = \sum_{n=0}^{\infty} \frac{\xi^{2n}}{2^{2n}(n!)^2}$ from [83], (3.79) becomes:

$$\begin{aligned} \mathcal{I}_{\text{bf,avg}}(\text{SNR}, \mathbf{v}) &= \frac{1}{\sigma_{\mathbf{v}}} \sum_{n=0}^{\infty} \left[\frac{1}{2^{2n}(n!)^2} \int_0^{\infty} \log_2(1 + \text{SNR}y) \left(\frac{2m_{\mathbf{v}}y^{1/2}}{\sigma_{\mathbf{v}}}\right)^{2n} \exp\left(-\frac{y + m_{\mathbf{v}}^2}{\sigma_{\mathbf{v}}}\right) dy \right] \Rightarrow \\ \mathcal{I}_{\text{bf,avg}}(\text{SNR}, \mathbf{v}) &= \frac{1}{(\ln 2) \sigma_{\mathbf{v}}} \exp\left(-\frac{m_{\mathbf{v}}^2}{\sigma_{\mathbf{v}}}\right) \sum_{n=0}^{\infty} \left[\frac{1}{(n!)^2} \left(\frac{m_{\mathbf{v}}}{\sigma_{\mathbf{v}}}\right)^{2n} \int_0^{\infty} \ln(1 + \text{SNR}y) y^n \exp\left(-\frac{y}{\sigma_{\mathbf{v}}}\right) dy \right] \end{aligned} \quad (3.80)$$

Using the following identity from [84]:

$$\int_0^{\infty} \ln(1 + ax) x^n e^{-bx} dx = n! e^{b/a} \frac{1}{b^{n+1}} \sum_{k=0}^n \left(\frac{b}{a}\right)^k \Gamma\left(-k, \frac{b}{a}\right) \quad (3.81)$$

and considering that $a = \text{SNR}$ and $b = \frac{1}{\sigma_v}$, (3.80) is finally written as follows:

$$\mathcal{I}_{\text{bf,avg}}(\text{SNR}, \mathbf{v}) = (\ln 2)^{-1} \exp\left(\frac{1 - \text{SNR}m_v^2}{\text{SNR}\sigma_v}\right) \sum_{n=0}^{\infty} \left[\frac{1}{n!} \left(\frac{m_v^2}{\sigma_v}\right)^n \sum_{k=0}^n \left(\frac{1}{\text{SNR}\sigma_v}\right)^k \Gamma\left(-k, \frac{1}{\text{SNR}\sigma_v}\right) \right] \quad (3.82)$$

Setting in (3.82) $\mathbf{v} = \mathbf{v}_\theta$, the infinite-series (3.77) is proven.

The convergence of (3.77) can be proven by truncating the series at the $n = I - 1$ term and then showing that the remainder R_I , defined as:

$$R_I = (\ln 2)^{-1} \exp\left(\frac{1 - \text{SNR}m_v^2}{\text{SNR}\sigma_v}\right) \sum_{n=I}^{\infty} \left[\frac{1}{n!} \left(\frac{m_v^2}{\sigma_v}\right)^n \sum_{k=0}^n \left(\frac{1}{\text{SNR}\sigma_v}\right)^k \Gamma\left(-k, \frac{1}{\text{SNR}\sigma_v}\right) \right] \Bigg|_{\mathbf{v}=\mathbf{v}_\theta} \quad (3.83)$$

converges to zero for $I \rightarrow +\infty$ (i.e. $\lim_{I \rightarrow +\infty} R_I = 0$).

In (3.83), it follows from [85] that:

$$\lim_{n \rightarrow +\infty} \frac{1}{n!} \left(\frac{m_v^2}{\sigma_v}\right)^n = 0 \quad (3.84)$$

Hence, in order to show that $\lim_{I \rightarrow +\infty} R_I = 0$, it suffices to show that the following series converges:

$$A = \sum_{k=0}^{\infty} \left(\frac{1}{\text{SNR}\sigma_v}\right)^k \Gamma\left(-k, \frac{1}{\text{SNR}\sigma_v}\right) = \sum_{k=0}^{\infty} \int_{\frac{1}{\text{SNR}\sigma_v}}^{\infty} \left(\frac{1}{\text{SNR}\sigma_v}\right)^k \frac{1}{t^{k+1}} e^{-t} dt \quad (3.85)$$

In the same manner, A will converge if its remainder R_i , after truncation of A at the $k = i - 1$ term, converges to zero for $i \rightarrow +\infty$, i.e.:

$$\lim_{i \rightarrow +\infty} R_i = \lim_{i \rightarrow +\infty} \sum_{k=i}^{\infty} \int_{\frac{1}{\text{SNR}\sigma_v}}^{\infty} \left(\frac{1}{\text{SNR}\sigma_v}\right)^k \frac{1}{t^{k+1}} e^{-t} dt = 0 \quad (3.86)$$

But (3.86) holds, since for $t \geq \frac{1}{\text{SNR}\sigma_v}$:

$$\lim_{k \rightarrow +\infty} \left(\frac{1}{\text{SNR}\sigma_v} \right)^k \frac{1}{t^{k+1}} = 0 \quad (3.87)$$

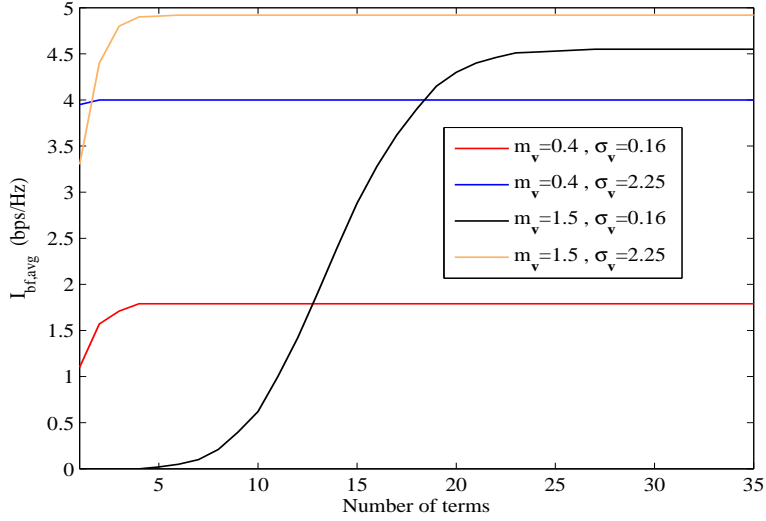


Figure 3.4: Convergence of the infinite-series (3.77), for different $\{m_v, \sigma_v\}$ values and a MISO 4×1 system with $\text{SNR} = 10\text{dB}$.

Figure 3.4 demonstrates that (3.77) converges relatively fast (a few tens of terms are required) to the capacity value calculated by the Monte-Carlo method with 10^4 channel samples. Observe that the lower the m_v and the higher the σ_v , the faster convergence is achieved. ■

3.4 Simulation results

3.4.1 Simulation model

In the following, a spatially correlated MISO Rician fading channel with $N = 4$ transmit antenna elements is produced and subsequently used in simulations in order to validate the theoretical analysis. The produced channel is for uniform (i.e. equi-spaced) linear array (ULA) transmit antennas. The channel transmit covariance matrix \mathbf{R} is produced by

the *two-path delay spread* model proposed in [86] and has the following Toeplitz form:

$$\mathbf{R} = \beta \begin{pmatrix} 1 & \rho_{12} & \rho_{13} & \rho_{14} \\ \rho_{12}^* & 1 & \rho_{12} & \rho_{13} \\ \rho_{13}^* & \rho_{12}^* & 1 & \rho_{12} \\ \rho_{14}^* & \rho_{13}^* & \rho_{12}^* & 1 \end{pmatrix} \quad (3.88)$$

where β is the channel variance and ρ_{kl} , $k, l = 1, \dots, 4$, is the correlation coefficient between the k^{th} and the l^{th} transmit antenna element. According to [86] the correlation coefficient is a function of the transmit antenna inter-element distance D (in wavelengths), the angular spread Δ of multipath at the transmit antenna location, and the azimuth ψ of the receive antenna location with respect to the boresight of the transmit antenna, (see Figure 3.5). The simulations presented in the following are for $\Delta = 10^\circ$ (typical mean value for urban macro-cellular environments, according to [87]) and $\psi = 0^\circ$. In this case, ρ_{kl} are positive real numbers, (this is due to $\psi = 0^\circ$ [86]), and depend only on D , (since Δ and ψ are assumed to be fixed). Hence, \mathbf{R} is completely characterized by β and D , or, equivalently, by β and the transmit antenna correlation coefficient (between two successive elements of the transmit array antenna) $\rho = \rho_{12}$. Note that ρ_{13} and ρ_{14} are uniquely defined once ρ_{12} is determined for a value of D .

Based on the analysis presented in [86], the relation between ρ and D (expressed in wavelengths λ), when $\Delta = 10^\circ$ and $\psi = 0^\circ$, is shown in Table 3.1:

Table 3.1: Relation between correlation coefficient ρ and interelement distance D

ρ	0.1	0.2	0.3	0.4	0.5	0.6	0.7	0.8	0.9
D	2.6	2.37	2.15	1.94	1.73	1.51	1.3	1.04	0.72

The channel distribution parameters that affect optimum beamforming are β , ρ and μ , for the aforementioned model. The simulations that follow are with respect to these parameters and the SNR.

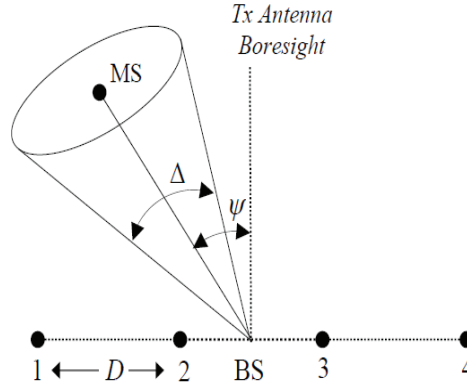


Figure 3-5: MISO 4×1 system, where the multipath from a user (MS), at an angle ψ with respect to the transmit antenna boresight, arrives at the base station (BS) with an angular spread Δ .

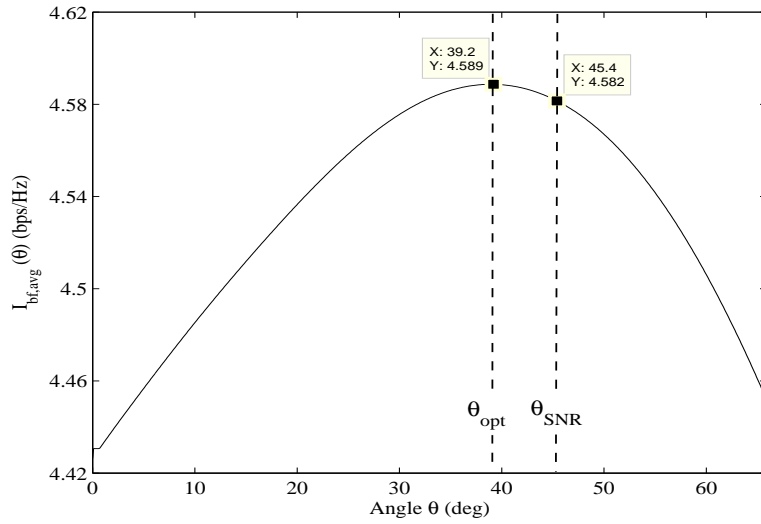
3.4.2 Calculation of the optimum beamformer

Under the channel simulation model described above, for most of the β , ρ , μ and SNR values, the function $\mathcal{I}_{\text{bf,avg}}(\theta)$ (defined in (3.75)) is unimodal⁷ in $[0, \phi]$, as shown in the example in Figure 3.6(a). For these cases, if a starting point is required by the algorithm employed for solving the 1-D optimization problem (3.71), it can be chosen arbitrarily in $[0, \phi]$. However, a starting point/angle that ensures fast convergence is the angle $\theta_o = \theta_{\text{SNR}}$, which is defined as the angle of the max SNR beamformer (see Section 3.4.4) with μ . The example in Figure 3.6(a) demonstrates that θ_{opt} is close to θ_{SNR} .

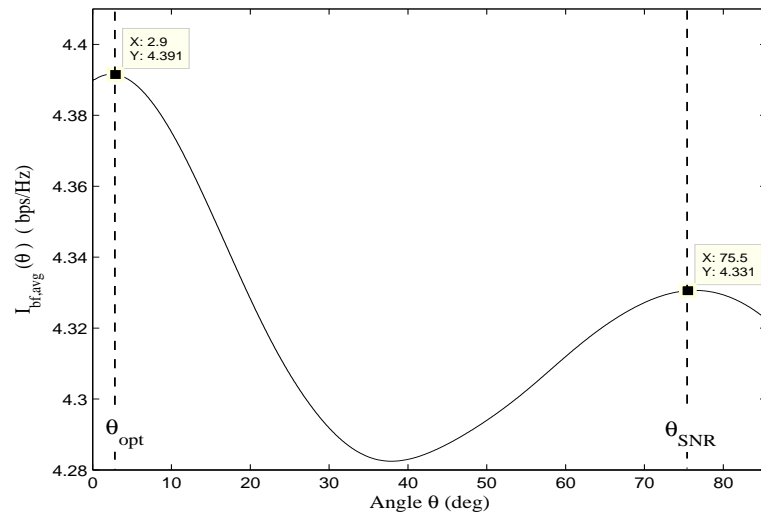
Nevertheless, $\mathcal{I}_{\text{bf,avg}}(\theta)$ is not always unimodal. For some (limited) ρ , μ values⁸, $\mathcal{I}_{\text{bf,avg}}(\theta)$ appears to have two local maxima in $[0, \phi]$, as it is demonstrated in Figure 3.6(b). In these cases, starting with $\theta_o = \theta_{\text{SNR}}$, the convergence to the overall maximum is not always successful, (as shown in Figure 3.6(b), the 1-D algorithm will possibly converge to the lower local maximum, if $\theta_o = \theta_{\text{SNR}}$). Hence, the convergence to θ_{opt} is ensured, if

⁷The unimodality of $\mathcal{I}_{\text{bf,avg}}(\theta)$ implies that this function has a unique maximum, θ_{opt} , and that $\forall \theta_1, \theta_2$ with $\theta_1 \leq \theta_2 \leq \theta_{\text{opt}}$ or $\theta_{\text{opt}} \leq \theta_2 \leq \theta_1$, it is: $\mathcal{I}_{\text{bf,avg}}(\theta_1) \leq \mathcal{I}_{\text{bf,avg}}(\theta_2) \leq \mathcal{I}_{\text{bf,avg}}(\theta_{\text{opt}})$.

⁸e.g. for ULAs and the two-path delay spread correlation model used in these simulations, this range of values is $\rho \geq 0.7$ and all μ with $1.1 \leq \|\mu\|_2 \leq 1.4$. that result in $\phi \geq 75^\circ$.



(a)



(b)

Figure 3-6: Unimodal (a), and non unimodal (b) cases of $\mathcal{I}_{bf,avg}(\theta)$.

the algorithm runs twice, from two different starting points⁹, e.g. $\theta_{o,1} \approx 0$ and $\theta_{o,2} \approx \phi$. Algorithms that do not require a starting point (e.g. direct search methods [76]) must run for multiple intervals in $[0, \phi]$, where unique (local) maxima exist. Nevertheless, it has been observed from extensive simulations that the two local maxima never appear together below or above $\phi/2$ and hence, $[0, \phi]$ can be split into just two intervals, $([0, \phi/2]$ and $[\phi/2, \phi])$.

Moreover, extensive simulations with thousands of random transmit covariance matrices \mathbf{R} show that the aforementioned behavior of the $\mathcal{I}_{\text{bf,avg}}(\theta)$ is also valid for random array antenna geometries and correlation models.

3.4.3 Computational complexity assessment

The optimization problem (3.76) is solved using Theorem 3.1 with an 1-D direct search algorithm, (a combination of parabolic interpolation and golden section search methods), and its computational complexity is compared with algorithms which can be also employed to solve the same (optimum beamforming) problem, such as:

a. An interior-point multi-dimensional algorithm (with a logarithmic barrier function), using as a starting point the max SNR beamformer. An interior-point method was also employed in [49] for the calculation of the optimum transmit covariance matrix in spatially correlated MIMO/MISO Rician fading channels.

b. The iterative algorithm proposed in [50]. As mentioned in Section 3.1, this algorithm¹⁰ is an asymptotic approach that is used to calculate the overall optimum transmit covariance matrix without rank constraints in spatially correlated MIMO/MISO Rician fading channels and hence, it is not dedicated to solving the optimum beamforming problem, generally. Nevertheless, this algorithm can calculate the optimum beamformer when the necessary and sufficient optimality condition (2.34) is satisfied.

⁹Parallel processing is recommended in this case, for reduction of the computational time.

¹⁰The algorithm proposed in [50] was shown to have significantly lower computational complexity than the algorithm presented in [49], and it almost achieves ergodic capacity (for the same number of steps).

The three algorithms are evaluated using the channel scenarios presented in Table 3.2. The first scenario does not satisfy the optimality condition (2.34)¹¹, whereas the second and third scenarios satisfy (2.34). The algorithms are restricted to perform 10 iterations (enough for convergence to the C_{bf}) using Matlab on the same computer (1.8GHz processor). In Tables 3.3 and 3.4 we present the parameters of the 1-D and the multidimensional (interior-point) algorithm, respectively, which have been used in the simulations for the calculation of the optimum beamformer. Table 3.5 presents the parameters of the algorithm employed for the solution of the 2×2 non-linear system of equations, which is required in each iteration of the asymptotic approach [50].

Table 3.2: Simulation scenarios

	β	ρ	$\ \boldsymbol{\mu}\ _2$	ϕ	SNR	K	Condition (2.34)
Scenario #1	~ 0.1250	0.9	~ 0.7	$\sim 85^\circ$	10dB	1	Not satisfied
Scenario #2	~ 0.1250	0.5	~ 0.7	$\sim 85^\circ$	10dB	1	Satisfied
Scenario #3	~ 0.2273	0.9	~ 0.3	$\sim 85^\circ$	10dB	0.1	Satisfied

Table 3.3: Parameters of the 1-D algorithm for the calculation of the optimum beamformer

Parameter	Description or Value
Matlab Function	fminbnd
Algorithm	Golden section and parabolic interpolation
MaxIter	10
MaxFunEvals	200
TolFun	10^{-40}
TolX	10^{-40}

¹¹In this case the asymptotic approach in [50] does not calculate the optimum beamformer, but it calculates the optimum transmit covariance matrix Σ_{opt} , with $rank\{\Sigma_{opt}\} > 1$.

Table 3.4: Parameters of the multidimensional algorithm for the calculation of the optimum beamformer

Parameter	Description or Value
Matlab Function	fmincon
Algorithm	Interior-point with logarithmic barrier function
Starting vector	max SNR beamformer
MaxIter	10
MaxFunEvals	200
TolFun	10^{-40}
TolX	10^{-40}

Table 3.5: Parameters for the solution of the 2×2 (non-linear) system of equations in [50]

Parameter	Description or Value
Matlab Function	fsolve
Algorithm	Trust-region-dogleg
Starting point	[1, 1]
MaxIter	10
MaxFunEvals	200
TolFun	10^{-5}
TolX	10^{-5}

For reasons of consistency, the same complexity assessment analysis that was performed for the algorithms presented in [49]-[50], was also carried out here. The computational complexity is shown in terms of program runtime per iteration versus:

- a. The number of channel samples in Figure 3.7(a).
- b. The number of transmit antenna elements¹² N for 2×10^4 channel samples, in Figure 3.7(b).

¹²Note that scenarios #2 and #3 satisfy the condition (2.34) when $N = 4$. If $N \neq 4$ this may not be the case and hence, the asymptotic approach may not calculate the optimum beamformer. Nevertheless, the runtime with respect to N is indicative of the computational complexity of this algorithm.

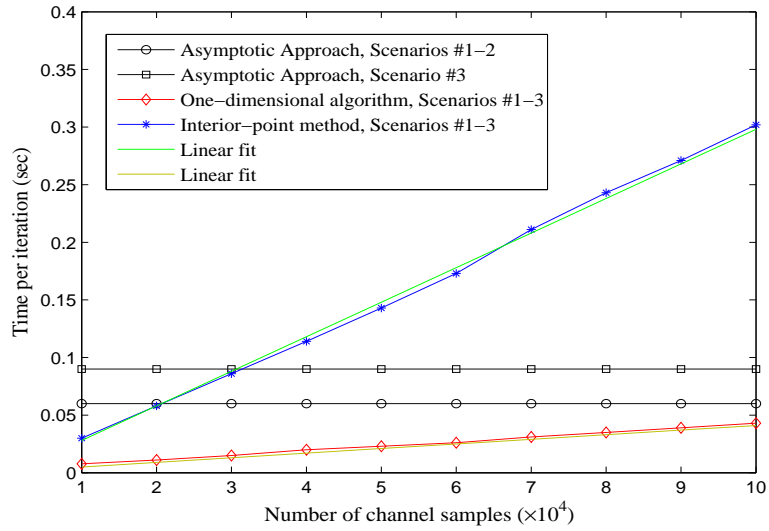
In Figure 3.7(a), the runtime scales almost linearly with the number of channel samples for both the interior-point method and the 1-D algorithm, while it is constant for the asymptotic approach¹³. Nevertheless, the runtime of the 1-D algorithm increases very slowly, it is on average ~ 3.6 to 7.3 times faster than the interior-point method, and ~ 1.4 to 18 times faster than the asymptotic approach, (observe also that for a number of channel samples $\leq 3 \times 10^4$ in scenarios #1 or #2 and $\leq 2 \times 10^4$ in scenario #3, the interior-point method is faster than the asymptotic approach). The same trends can be noticed not only with the employed simulation model but also with any random antenna array geometry and correlation model. This relative processing gain can be exploited to either reduce cost by using devices with lower processing power or in order to:

- a. Operate in environments with smaller coherence time (e.g. 3.6 to 7.3 times), and hence, support operational scenarios with higher mobility (3.6 to 7.3 times higher speed).
- b. Increase the available processing power required by the system for other supplementary techniques.

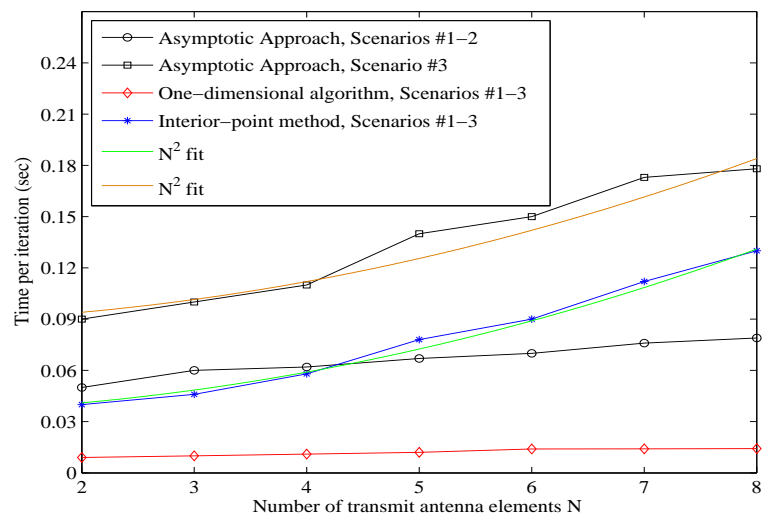
In Figure 3.7(b), the runtime scales as N^2 for the interior-point method, whereas for the 1-D algorithm scales linearly and with a low rate, (for $N = 4/8$ the 1-D algorithm is approximately $5.2/9.3$ times faster than the interior-point method, respectively). Moreover, the asymptotic approach appears to scale almost as N^2 for the scenarios with higher Rician factor (Table 3.2, scenarios #1 and #2) and almost linearly for the scenario with the smaller Rician factor (Table 3.2, scenario #3). For $N = 4/8$ the 1-D algorithm is approximately:

- $5.63/5.64$ times faster than the asymptotic approach for scenarios #1 and #2.
- $10/12.7$ times faster than the asymptotic approach for scenario #3.

¹³The asymptotic approach does not require Monte Carlo integration and hence, it is not affected by the number the channel samples. However, it can be observed that the runtime of the asymptotic approach is affected by the Rician factor K : compare in Figure 3.7(a) the curves for scenario #1 or #2 ($K = 1$) with scenario #3 ($K = 0.1$). Moreover, the complexity of the algorithm is not affected by (2.34), e.g. the runtime in scenario #1 ((2.34) is not satisfied) is the same with scenario #2 ((2.34) is satisfied).



(a)



(b)

Figure 3-7: Runtime vs. the number of channel samples for a MISO 4×1 system (a), and the number of transmit antenna elements N (MISO $N \times 1$) with 2×10^4 channel samples (b).

3.4.4 Simulation results for the ergodic beamforming capacity

Comparison with the max SNR beamformer

The ergodic beamforming capacity achieved by the optimum beamformer (calculated by Theorem 3.1) can be compared with the average mutual information achieved by the max SNR beamformer, denoted as $\mathbf{v}_{\max\text{SNR}} \in \mathbb{C}^{1 \times N}$. The max SNR beamformer is the beamforming transmission along the complex conjugate transpose dominant eigenvector of the channel transmit correlation matrix $\mathcal{E}_h[\mathbf{h}^\dagger \mathbf{h}]$, [75]. The max SNR beamformer is currently the prevalent real-time beamforming transmission scheme [75].

In the following, results are produced for the mean information rate gain, which is defined as:

$$\mathcal{E}[\Delta \mathcal{I}_{\text{bf,avg}}] = \mathcal{E}[\mathcal{I}_{\text{bf,avg}}(\text{SNR}, \mathbf{v}_{\text{opt}}) - \mathcal{I}_{\text{bf,avg}}(\text{SNR}, \mathbf{v}_{\max\text{SNR}})] \quad (3.89)$$

(note that $\mathcal{I}_{\text{bf,avg}}(\text{SNR}, \mathbf{v}_{\text{opt}}) = C_{\text{bf}}$).

$\mathcal{E}[\Delta \mathcal{I}_{\text{bf,avg}}]$ is calculated for 10^4 samples¹⁴ of $\boldsymbol{\mu}$ and fixed ρ, β, SNR and $\|\boldsymbol{\mu}\|_2, \phi$, (i.e. all samples of $\boldsymbol{\mu}$ have fixed norm and angle with respect to $\mathbf{U}_{\bullet 1}^\dagger$). In this manner, since $\boldsymbol{\mu}$ is averaged out, it is $\mathcal{E}[\Delta \mathcal{I}_{\text{bf,avg}}] = f(\|\boldsymbol{\mu}\|_2, \rho, \beta, \phi, \text{SNR})$. Figure 3.8 shows an example where $\mathcal{E}[\Delta \mathcal{I}_{\text{bf,avg}}]$ is plotted versus $\|\boldsymbol{\mu}\|_2$ and ρ , for $\beta = 1, \phi = 85^\circ$ and $\text{SNR} = 10\text{dB}$. Similar simulations, performed over a wide range of $\|\boldsymbol{\mu}\|_2, \rho, \beta, \phi$ and SNR values, lead to the following conclusions:

a. The optimum beamformer is always better than or asymptotically equal to the max SNR beamformer. The mean relative information rate gain of the optimum beamformer with respect to the max SNR beamformer, which is defined as $\left(\mathcal{E} \left[\frac{\Delta \mathcal{I}_{\text{bf,avg}}}{\mathcal{I}_{\text{bf,avg}}(\text{SNR}, \mathbf{v}_{\max\text{SNR}})} \right] \right)$, is less than 5% in most cases. However, there are operational scenarios where the optimum beamformer achieves higher mean relative information rate gain: e.g. the peak value in Figure 3.8 ($\sim 0.39\text{bps/Hz}$ for $\|\boldsymbol{\mu}\|_2 = 1.67, \rho = 0.9, \phi = 85^\circ, \text{SNR} = 10$), corresponds to a mean relative information rate gain $\sim 8.5\%$. Generally, the mean or the instantaneous

¹⁴The elements of $\boldsymbol{\mu}$ are produced by independent, zero-mean, unit variance complex Gaussian distributions.

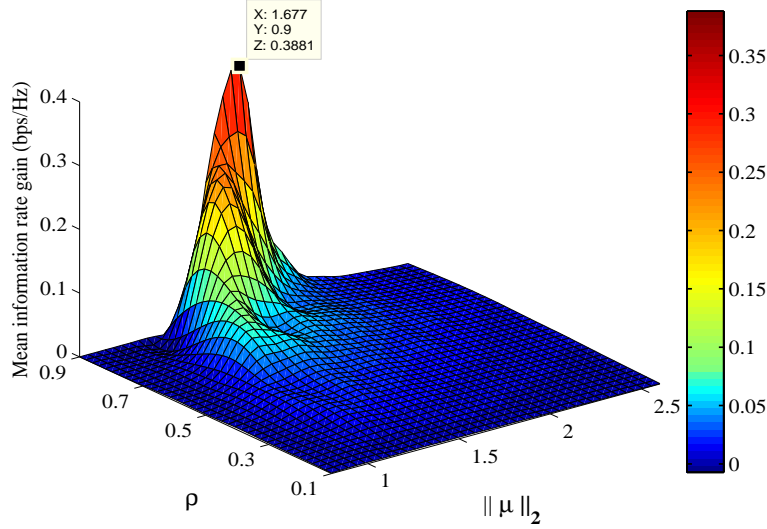


Figure 3-8: $\mathcal{E}[\Delta\mathcal{I}_{\text{bf,avg}}]$ vs. $\|\boldsymbol{\mu}\|_2$ and ρ , for a MISO 4×1 system with $\{N = 4, \beta = 1, \phi = 85^\circ, \text{SNR} = 10\text{dB}\}$.

relative information rate gain can reach 10%, but it can rarely exceed this value.

b. The mean information rate gain $\mathcal{E}[\Delta\mathcal{I}_{\text{bf,avg}}]$ increases with the SNR, following a concave curve, as shown in Figure 3.9. For high SNR values the gain converges asymptotically to a maximum value which depends on ρ , β , $\|\boldsymbol{\mu}\|_2$ and ϕ . The same figure shows the mean relative information rate gain (with respect to the max SNR beamformer). It can be observed that the best performance for the optimum beamformer in this operational scenario is achieved for $\text{SNR} = 6\text{dB}$, which is $\sim 8.8\%$ better than the $\mathcal{I}_{\text{bf,avg}}(\text{SNR}, \mathbf{v}_{\text{maxSNR}})$, (note that the best mean relative information rate gain does not correspond to the highest mean information rate gain).

Comparison with the ergodic capacity

The ergodic beamforming capacity achieved by optimum beamformer is compared with the ergodic capacity achieved by the asymptotic approach from [50] for different SNR values and operational scenarios¹⁵. In [50] it was shown that the therein proposed algorithm achieves the same ergodic capacity with the algorithm in [49], (and hence, results

¹⁵These results are for a random $\boldsymbol{\mu}$, $\rho = 0.5$, $\phi = 85^\circ$ and different values of the Rician factor K ($K = 0.5/0.1$).

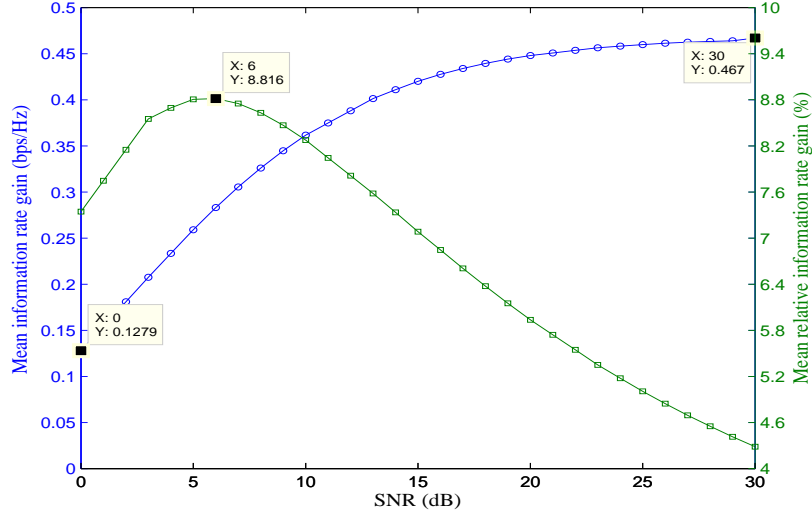


Figure 3-9: $\mathcal{E}[\Delta\mathcal{I}_{\text{bf,avg}}]$ and $\mathcal{E}\left[\frac{\Delta\mathcal{I}_{\text{bf,avg}}}{\mathcal{I}_{\text{bf,avg}}(\text{SNR}, \mathbf{v}_{\text{maxSNR}})}\right]$ vs. the SNR, for a MISO 4×1 system with $\{\|\boldsymbol{\mu}\|_2 = 1.6, \rho = 0.9, \phi = 85^\circ, \beta = 1\}$.

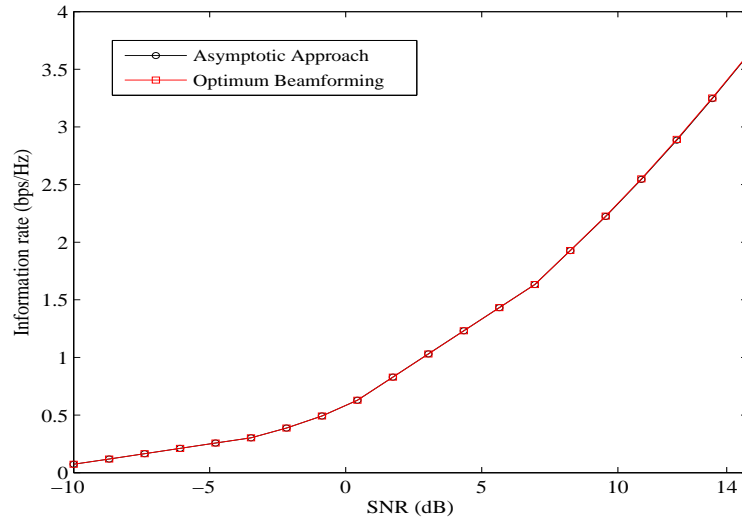
with respect to the algorithm from [49] are omitted). In the scenario of Figure 3.10(a), condition (2.34) is satisfied for $\text{SNR} \leq 20\text{dB}$ and hence, in this SNR region, the optimum beamformer coincides with the asymptotic approach. For $\text{SNR} > 20\text{dB}$ condition (2.34) is not satisfied, however, the asymptotic approach does not show practical advantage over the optimum beamformer. In the scenario of Figure 3.10(b), (2.34) is never satisfied and hence, the asymptotic approach shows a gap (i.e. higher rate) with respect to the optimum beamformer, especially for high SNR values (in the low SNR region the gap is extremely small). However, this gap corresponds to $< 4\%$ relative information rate gain, (defined as $\left(\frac{C_{\text{erg}} - C_{\text{bf}}}{C_{\text{bf}}}\right)$). The same behavior was also observed for other similar simulation scenarios.

In Figure 3.11 are presented results using a channel sample from the channel distribution that was used in the simulations of [49] and [50]¹⁶. The channel transmit covariance matrix used in this simulation example corresponds to a random array antenna geometry/configuration. The results are for Rician factors $K = 0.1$ and $K = 1$, and demonstrate that the optimum beamformer has near-optimum performance in both cases, (practically,

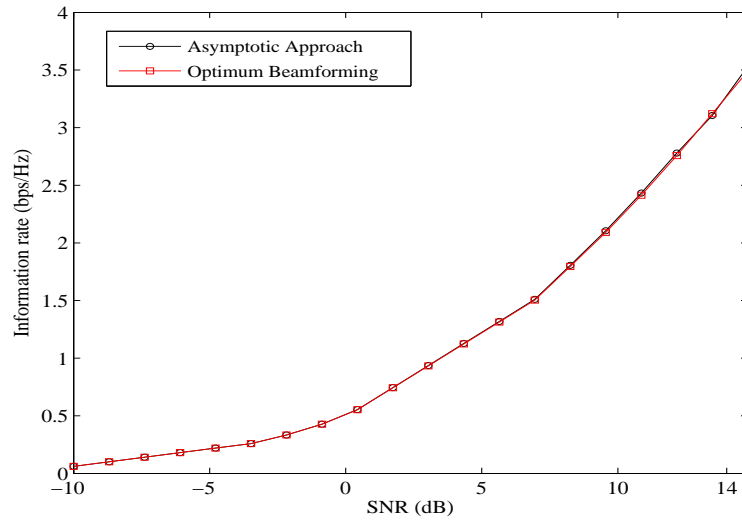
¹⁶More precisely, the same transmit covariance matrix (\mathbf{R}_t) along with the first row of the channel mean matrix (\mathbf{H}_m) have been used, (see Appendix of [49]).

it achieves slightly better rate than the asymptotic approach (i.e. $C_{\text{bf}} \geq C_{\text{erg}}$), for the same number of algorithmic steps).

Figures 3.10 and 3.11 indicate that there are channels where the optimum beamformer may have near-optimum performance, i.e. $C_{\text{bf}} \approx C_{\text{erg}}$.



(a)



(b)

Figure 3-10: Ergodic capacity C_{erg} and ergodic beamforming capacity C_{bf} achieved by the asymptotic approach from [50] and the optimum beamformer, respectively, versus the SNR, for a MISO 4×1 system and different fading scenarios: (a) $\{K = 0.5, \rho = 0.9, \phi = 85^\circ\}$, (b) $\{K = 0.1, \rho = 0.5, \phi = 85^\circ\}$.

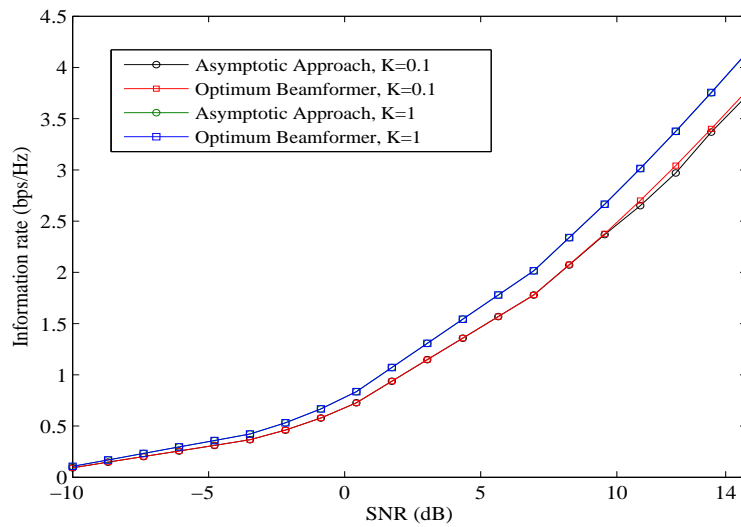


Figure 3.11: Ergodic capacity C_{erg} and ergodic beamforming capacity C_{bf} achieved by the asymptotic approach from [50] and by the optimum beamformer, respectively, vs. the SNR, for a MISO 4×1 system, the transmit antenna array configuration used in [49] and different fading scenarios: $K = 0.1$ and $K = 1$.

Chapter 4

RATE-OPTIMUM BEAMFORMING TRANSMISSION AND RESULTS FOR THE OPTIMALITY OF BEAMFORMING CONDITION FOR MIMO RICIAN FADING CHANNELS

4.1 Introduction

It was proven in the previous chapter for MISO systems, that the calculation of the optimum beamformer for the combined CMI-CCI model is an 1-D optimization problem which can be solved very fast and efficiently.

The present chapter extends the work presented in Chapter 3 to MIMO Rician fading channels, and shows that a similar simple 1-D scheme can also be employed for the calculation of the optimum beamformer. Furthermore, it demonstrates via simulations that there are cases where the optimum beamformer has significant rate gains (e.g. approximately 0.83bps/Hz for a MIMO 4×4 channel at $\text{SNR} = 10\text{dB}$), compared to the max SNR beamformer [75]. Finally, it shows that the proposed 1-D scheme has significantly better computational complexity than other currently employed multi-dimensional algorithms (e.g. interior-point methods), and hence, real time applications are feasible even when devices use moderate processing power.

This chapter is organized as follows: In Section 4.2 the channel model and the optimum beamforming problem are introduced. The solution of the optimum beamforming problem is presented in Section 4.3. In Section 4.4 simulations are provided that support the theoretical analysis and Section 4.5 concludes the chapter.

4.2 System model and problem statement

Assume a MIMO system in a flat fading channel, with N transmit and M receive antenna elements. The received signal $\mathbf{y} \in \mathbb{C}^{1 \times M}$ is expressed by (2.1) and the channel

matrix \mathbf{H} follows the model expressed by (2.25). Equations (2.1) and (2.5) are repeated here for convenience:

$$\mathbf{y} = \mathbf{H}\mathbf{x}^T + \mathbf{n}^T \quad (4.1)$$

$$\mathbf{H} = \mathbf{H}_m + \mathbf{R}_r^{1/2}\mathbf{H}_w\mathbf{R}_t^{1/2} \quad (4.2)$$

Throughout this chapter it is assumed that the channel mean matrix $\mathbf{H}_m \in \mathbb{C}^{M \times N}$ in (4.2) represents the specular, i.e. the Line of Sight, component between the transmitter and the receiver.

At this point it must be noted that $rank\{\mathbf{H}_m\} = 1$, as referred to in [47] and explained in the following: When the mobile station has a fixed position with respect to the base station, \mathbf{H}_m is the LOS component, which is expressed as $\mathbf{H}_m = \mathbf{a}_r^\dagger \mathbf{a}_t$, where $\mathbf{a}_r/\mathbf{a}_t$ are the (row) vectors of the receive/transmit incident plane wave, respectively [47]. In this case, since \mathbf{a}_r and \mathbf{a}_t do not change in time, \mathbf{H}_m is deterministic and *rank*-1. When the mobile station moves around the base station, then \mathbf{a}_r and \mathbf{a}_t change in time and \mathbf{H}_m is the mean LOS component, expressed as $\mathbf{H}_m = \mathcal{E}[c(t)\mathbf{a}_r^\dagger(t)\mathbf{a}_t(t)]$, where $c(t)$ is a scalar (function of time) related to Doppler, (see also the model of 3GPP in [87]). Even in this case, \mathbf{H}_m is a *rank*-1 matrix, since $\mathbf{a}_r(t)$ and $\mathbf{a}_t(t)$ are practically independent variables, (the orientation of the MS antenna is assumed to be random).

Since \mathbf{H}_m represents the LOS component, the combined CMI-CCI model assumed in this chapter is a long-term model, (see discussion in Chapter 2). However, in MIMO systems, even in the long-term combined CMI-CCI model it is possible to have a non *rank*-1 LOS (mean) matrix. This is possible in short-range communications (i.e. when the distance between the transmit and receive antennas is comparable to the antenna size), where the LOS component cannot be considered as a plane wave but as a spherical wave [88]-[92]. In this case, as in the case of the short-term combined CMI-CCI model for MIMO systems, the beamforming optimization problem is multi-dimensional, (and the method presented hereafter cannot be employed for its solution).

In the context of our analysis it is assumed that the receiver has perfect CSI, whereas

the transmitter is only aware of the channel long-term statistics \mathbf{H}_m , \mathbf{R}_t and \mathbf{R}_r , which are calculated by the receiver and fed back to the transmitter via a low-rate control channel.

The covariance matrix Σ of the transmitted signal \mathbf{x} is restricted to be *rank-1* when beamforming is considered, and hence:

$$\Sigma = P\mathbf{v}\mathbf{v}^\dagger \quad (4.3)$$

with P the transmitted power and $\mathbf{v} \in \mathbb{C}^{1 \times N}$ the unit-norm beamforming vector. In this case the ergodic beamforming capacity is expressed by (2.29):

$$\begin{aligned} C_{\text{bf}} &= \max_{\|\mathbf{v}\|_2=1} \mathcal{E}_{\mathbf{H}} [\mathcal{I}_{\text{bf}}(\text{SNR}, \mathbf{v}, \mathbf{H})] = \max_{\|\mathbf{v}\|_2=1} \mathcal{I}_{\text{bf,avg}}(\text{SNR}, \mathbf{v}) = \\ &= \max_{\|\mathbf{v}\|_2=1} \mathcal{E}_{\mathbf{H}} [\log_2 \det (\mathbf{I}_M + \text{SNR}\mathbf{H}\mathbf{v}\mathbf{v}^\dagger\mathbf{v}\mathbf{H}^\dagger)] \quad (4.4) \end{aligned}$$

The beamforming vector that maximizes (4.4) is the solution of the following optimization problem:

$$\mathbf{v}_{\text{opt}} = \arg \max_{\mathbf{v} \in \mathbf{S}} \mathcal{I}_{\text{bf,avg}}(\text{SNR}, \mathbf{v}) \quad (4.5)$$

$$\mathbf{S} = \{\mathbf{v}; \mathbf{v} \in \mathbb{C}^{1 \times N}, \|\mathbf{v}\|_2 = 1\} \quad (4.6)$$

Generally, (4.5) is a complex N -dimensional optimization problem. In the next section, Theorem 4.1 proves that (4.5) can be transformed into a simple 1-D optimization problem, which can be subsequently solved using any standard 1-D search algorithm.

4.3 Optimum beamforming transmission in MIMO Rician fading channels

Theorem 4.1 ([93]) Consider a flat fading Rician MIMO channel expressed by (4.2). The optimum beamformer is the solution of the following 1-D optimization problem:

$$\mathbf{v}_{\text{opt}} = \arg \max_{\mathbf{v} \in \mathbf{S}_o} \mathcal{I}_{\text{bf,avg}}(\text{SNR}, \mathbf{v}) \quad (4.7)$$

$$\mathbf{S}_o = \{\mathbf{v}_\theta; \theta \in [0, \phi]\} \quad (4.8)$$

where $\phi \in [0, \pi/2]$ is defined as:

$$\phi = \cos^{-1}(|\mathbf{q}\mathbf{u}_1|) \quad (4.9)$$

with $\mathbf{q}^\dagger \in \mathbb{C}^{1 \times N}$ the right singular vector of \mathbf{H}_m and $\mathbf{u}_1 \in \mathbb{C}^{N \times 1}$ the dominant eigenvector of \mathbf{R}_t . Moreover, \mathbf{v}_θ in (4.8) is defined as:

$$\mathbf{v}_\theta = \cos \theta [1 \ \mathbf{Z}(r_\theta \mathbf{I}_{N-1} - \mathbf{G})^{-1}] \mathbf{W}^T \mathbf{U}^\dagger \quad (4.10)$$

where:

a. \mathbf{U} is the eigenvector matrix of \mathbf{R}_t and \mathbf{W} is a complex $N \times N$ matrix with its first column defined as $\mathbf{W}_{\bullet 1} = \mathbf{U}^T \mathbf{q}^\dagger$, whereas the rest of its columns ($\mathbf{W}_{\bullet i}$, $i = 2, \dots, N$) are arbitrarily chosen with the restriction that $\mathbf{W}^\dagger \mathbf{W} = \mathbf{I}_N$. Moreover, it is:

$$\mathbf{G} = \begin{pmatrix} \mathbf{K}_{22} & \cdots & \mathbf{K}_{2N} \\ \vdots & \ddots & \vdots \\ \mathbf{K}_{N2} & \cdots & \mathbf{K}_{NN} \end{pmatrix} \quad (4.11)$$

$$\mathbf{Z} = [\mathbf{K}_{12} \ \mathbf{K}_{13} \ \cdots \ \mathbf{K}_{1N}] \quad (4.12)$$

where \mathbf{K}_{lm} is the l^{th} row and m^{th} column element of matrix \mathbf{K} , which is defined as:

$$\mathbf{K} = \sum_{i=1}^N \lambda_i(\mathbf{R}_t) \mathbf{W}_{i\bullet}^T \mathbf{W}_{i\bullet}^* \quad (4.13)$$

b. r_θ is the maximum real root of the $2(N-1)$ -degree polynomial:

$$P(x; \theta) = \cos^2 \theta \sum_{i=1}^{N-1} |\mathbf{Z}\mathbf{g}_i|^2 \left[\prod_{\substack{j=1 \\ j \neq i}}^{N-1} (x - \lambda_j(\mathbf{G}))^2 \right] - \sin^2 \theta \prod_{i=1}^{N-1} (x - \lambda_i(\mathbf{G}))^2 \quad (4.14)$$

where $\mathbf{g}_i \in \mathbb{C}^{(N-1) \times 1}$ is the i^{th} eigenvector of matrix \mathbf{G} .

Proof: Using the identity $|\mathbf{I}_M + \mathbf{A}\mathbf{B}| = |\mathbf{I}_N + \mathbf{B}\mathbf{A}|$ with $A \in \mathbb{C}^{M \times N} / B \in \mathbb{C}^{N \times M}$ and setting

$\mathbf{z} = \mathbf{H}\mathbf{v}^\dagger$, it is:

$$\mathcal{I}_{\text{bf,avg}}(\text{SNR}, \mathbf{v}) = \mathcal{E}_{\mathbf{z}}[\log_2(1 + \text{SNR} \sum_{i=1}^M |\mathbf{z}_i|^2)] \quad (4.15)$$

where \mathbf{z}_i is the i^{th} element of vector \mathbf{z} . Using the channel model (4.2), \mathbf{z} is expressed as follows:

$$\mathbf{z} = \mathbf{H}_m \mathbf{v}^\dagger + \mathbf{R}_r^{1/2} \mathbf{H}_w \mathbf{R}_t^{1/2} \mathbf{v}^\dagger \quad (4.16)$$

Hence, the mean and covariance of \mathbf{z} can be calculated as:

$$\mathbf{m}_{\mathbf{z}} = \mathcal{E}[\mathbf{z}] = \mathbf{H}_m \mathbf{v}^\dagger \quad (4.17)$$

$$\Sigma_{\mathbf{z}} = \mathcal{E}[(\mathbf{z} - \mathbf{m}_{\mathbf{z}})(\mathbf{z} - \mathbf{m}_{\mathbf{z}})^\dagger] = (\mathbf{v} \mathbf{R}_t \mathbf{v}^\dagger) \mathbf{R}_r \quad (4.18)$$

Using (4.17), (4.18), and setting $\sigma_{\mathbf{z}}^2 = \mathbf{v} \mathbf{R}_t \mathbf{v}^\dagger$, (4.16) can be written equivalently:

$$\mathbf{z} = \mathbf{m}_{\mathbf{z}} + \sigma_{\mathbf{z}} \mathbf{R}_r^{1/2} \mathbf{h}_w^T \quad (4.19)$$

where $\mathbf{h}_w \in \mathbb{C}^{1 \times M}$ is a vector of i.i.d zero-mean and unit variance complex Gaussian elements. Equation (4.19) is equivalent to (4.16) since both have exactly the same distribution and hence, using them in (4.15) they produce the same ergodic capacity.

Using singular value decomposition (SVD) for the \mathbf{H}_m , (4.17) can be written as:

$$\mathbf{m}_{\mathbf{z}} = (\mu \mathbf{q} \mathbf{v}^\dagger) \mathbf{p}^T \quad (4.20)$$

where $\mathbf{p}^T \in \mathbb{C}^{M \times 1}$ and $\mathbf{q}^\dagger \in \mathbb{C}^{N \times 1}$ are the left and right singular vectors of \mathbf{H}_m , respectively, and μ is its (unique) singular value, (\mathbf{H}_m is *rank*-1 and hence is modeled as $\mathbf{H}_m = \mu \mathbf{p}^T \mathbf{q}$).

In the following it is proven that (3.15) is an increasing function of the parameters $\sigma_{\mathbf{z}}^2$ and $|\mathbf{m}_{\mathbf{z},i}|$ ($i = 1, \dots, M$), ($\mathbf{m}_{\mathbf{z},i}$ is the i^{th} element of vector $\mathbf{m}_{\mathbf{z}}$):

First we define

$$\mathbf{R}_r^{1/2} = \begin{pmatrix} r_{11} & \cdots & r_{1M} \\ \vdots & \ddots & \vdots \\ r_{M1} & \cdots & r_{MM} \end{pmatrix} \quad (4.21)$$

$$\mathbf{h}_w = [h_1 \ h_2 \ \cdots \ h_M]^T \quad (4.22)$$

From (4.19) and (4.21)-(4.22), the random variables \mathbf{z}_i , can be written as ([75]):

$$\mathbf{z}_i = |\mathbf{m}_{\mathbf{z},i}| + \sigma_{\mathbf{z}} w_{1i} + j\sigma_{\mathbf{z}} w_{2i} \quad (4.23)$$

where

$$w_{1i} = \sum_{l=1}^M \Re\{r_{il}\}\Re\{h_l\} - \Im\{r_{il}\}\Im\{h_l\} \quad (4.24)$$

$$w_{2i} = \sum_{l=1}^M \Re\{r_{il}\}\Im\{h_l\} - \Im\{r_{il}\}\Re\{h_l\} \quad (4.25)$$

($\Re\{\cdot\}$ and $\Im\{\cdot\}$ denote the real and imaginary parts). Substituting (4.23) into (4.15) and:

a. Differentiating (4.15) with respect to $|\mathbf{m}_{\mathbf{z},i}|$, $i = 1, \dots, M$:

$$\frac{\partial \mathcal{I}_{\text{bf,avg}}}{\partial |\mathbf{m}_{\mathbf{z},i}|} = \mathcal{E}_{\mathbf{z}} \left[2\text{SNR} \frac{|\mathbf{m}_{\mathbf{z},i}| + \sigma_{\mathbf{z}} w_{1i}}{1 + \text{SNR} \sum_{i=1}^M \left[(|\mathbf{m}_{\mathbf{z},i}| + \sigma_{\mathbf{z}} w_{1i})^2 + (\sigma_{\mathbf{z}} w_{2i})^2 \right]} \right] \quad (4.26)$$

Using the fact that w_{1i} is symmetrically distributed around 0, from (4.26) it can be observed that:

$$\frac{\partial \mathcal{I}_{\text{bf,avg}}}{\partial |\mathbf{m}_{\mathbf{z},i}|} \geq 0 \quad (4.27)$$

b. Differentiating (4.15) with respect to $\sigma_{\mathbf{z}}$:

$$\frac{\partial \mathcal{I}_{\text{bf,avg}}}{\partial \sigma_{\mathbf{z}}} = \mathcal{E}_{\mathbf{z}} \left[2\text{SNR} \frac{\sum_{i=1}^M \left[w_{1i} (|\mathbf{m}_{\mathbf{z},i}| + \sigma_{\mathbf{z}} w_{1i}) + \sigma_{\mathbf{z}} w_{2i}^2 \right]}{1 + \text{SNR} \sum_{i=1}^M \left[(|\mathbf{m}_{\mathbf{z},i}| + \sigma_{\mathbf{z}} w_{1i})^2 + (\sigma_{\mathbf{z}} w_{2i})^2 \right]} \right] \quad (4.28)$$

Using the fact that w_{1i} and w_{2i} are i.i.d zero-mean Gaussian distributed (real) random variables, from (4.28) it can be observed that:

$$\frac{\partial \mathcal{I}_{\text{bf,avg}}}{\partial \sigma_{\mathbf{z}}} \geq 0 \quad (4.29)$$

Hence, from (4.27) and (4.29) it becomes clear that $\mathcal{I}_{\text{bf,avg}}$ increases monotonically with $|\mathbf{m}_{\mathbf{z},i}|$ and $\sigma_{\mathbf{z}}$. Equivalently, it can be concluded that $\mathcal{I}_{\text{bf,avg}}$ increases monotonically with

the parameters σ_z^2 and $|\mathbf{q}\mathbf{v}^\dagger|$, since the quantity $|\mathbf{q}\mathbf{v}^\dagger|$ is common for all $|\mathbf{m}_{z,i}|$ (see (4.20)). This is also demonstrated graphically in Figure 4.1. As a result, \mathbf{v}_{opt} can be determined by maximizing (4.15) with respect to $\mathbf{v}\mathbf{R}_t\mathbf{v}^\dagger$ and $|\mathbf{q}\mathbf{v}^\dagger|$. This optimization problem can be solved now using a similar method with that presented in Chapter 3 for MISO systems, with the following modification: the normalized channel mean vector in the MISO case (which was denoted in Chapter 3 as $\mathbf{m} \in \mathbb{C}^{1 \times N}$) is replaced by \mathbf{q} , in the MIMO case. ■

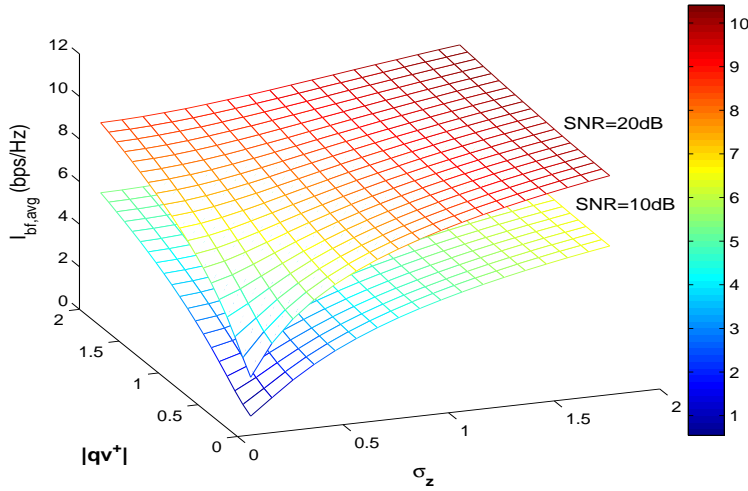


Figure 4.1: $\mathcal{I}_{\text{bf,avg}}$ vs. σ_z and $|\mathbf{q}\mathbf{v}^\dagger|$, for $\{\mathbf{R}_r = \mathbf{I}_M, \mu = 1\}$.

For MIMO $2 \times M$ systems and some special cases of $N \times M$ systems, equation (4.10) of Theorem 4.1 can be further simplified, as shown with Theorem 4.2 below.

Theorem 4.2 ([93]) For MIMO systems with $N = 2$ or $N \geq 3$ and $\text{rank}\{\mathbf{R}_t\} \leq 2$, \mathbf{v}_θ can be expressed by the following (closed-form) equation:

$$\mathbf{v}_\theta = \cos \theta \frac{\mathbf{u}_1^\dagger \mathbf{q}^\dagger \mathbf{q}}{\|\mathbf{u}_1^\dagger \mathbf{q}^\dagger \mathbf{q}\|_2} + \sin \theta \frac{\mathbf{q}^* (\mathbf{q}^T \mathbf{u}_1^\dagger - \mathbf{u}_1^* \mathbf{q})}{\|\mathbf{q}^* (\mathbf{q}^T \mathbf{u}_1^\dagger - \mathbf{u}_1^* \mathbf{q})\|_2} \quad (4.30)$$

Proof: The proof of this Theorem is similar to the proof of Theorem 3.2. ■

The 1-D function with respect to θ , $f(\theta) = \mathcal{I}_{\text{bf,avg}}(\text{SNR}, \mathbf{v}_\theta)$ (see (4.7)-(4.8)), is continuously differentiable (see Chapter 3) and hence, gradient-based or direct search algorithms can be employed to solve the optimization problem (4.7). The optimum value θ_{opt} that

maximizes $f(\theta)$, also determines the optimum beamformer through (4.10): $\mathbf{v}_{\text{opt}} = \mathbf{v}_{\theta_{\text{opt}}}$.

4.4 Simulation results for the optimum beamformer

4.4.1 Simulation model

A spatially correlated MIMO 4×4 Rician channel (see (4.2)) is produced and used in the simulations in order to demonstrate the theoretical analysis. The simulations are for linear, equi-spaced Tx/Rx array antennas (i.e. ULAs). \mathbf{R}_t is produced using the *two-path delay spread* correlation model [86] and has the following Toeplitz form¹:

$$\mathbf{R}_t = \beta_t \begin{pmatrix} 1 & \rho_{12}^t & \rho_{13}^t & \rho_{14}^t \\ (\rho_{12}^t)^* & 1 & \rho_{12}^t & \rho_{13}^t \\ (\rho_{13}^t)^* & (\rho_{12}^t)^* & 1 & \rho_{12}^t \\ (\rho_{14}^t)^* & (\rho_{13}^t)^* & (\rho_{12}^t)^* & 1 \end{pmatrix} \quad (4.31)$$

where β_t is the channel transmit variance and ρ_{ll}^t , $l = 2, 3, 4$, is a function of the transmit antenna array inter-element distance D_t and angular spread Δ_t , as well as of the azimuth ψ_t of the receive array antenna with respect to the boresight of the transmit array antenna. In the same manner the parameters β_r , ρ_{ll}^r , D_r , Δ_r , ψ_r are defined for the receiver. These parameters are shown in Figure 4.2.

The simulations presented in the following are for $\Delta_t = 10^\circ$ (typical mean value for urban macrocellular environments [87]) and for Tx/Rx antennas with aligned boresights, i.e. $\psi_t = \psi_r = 0^\circ$. In this case, ρ_{kl} are positive real numbers and \mathbf{R}_t is completely characterized by β_t and the transmit antenna correlation coefficient $\rho_t = \rho_{12}^t = f(D_t)$, (ρ_{13} and ρ_{14} are uniquely defined once ρ_{12}^t is determined for a value of D_t , since Δ_t and ψ_t are fixed). From [86], for $D_r = 0.5\lambda$ (Rx antenna inter-element distance), $\Delta_r = 68^\circ$ (typical mean angular spread value at the receiver/mobile station for many operational environments [87]) and $\psi_r = 0^\circ$, the Rx antenna correlation coefficient ρ_r has a fixed value $\rho_r = -0.08$. Moreover it is assumed that $\beta_r = \beta_t = \beta$. Finally, the channel mean is

¹ \mathbf{R}_r is defined exactly in the same manner.

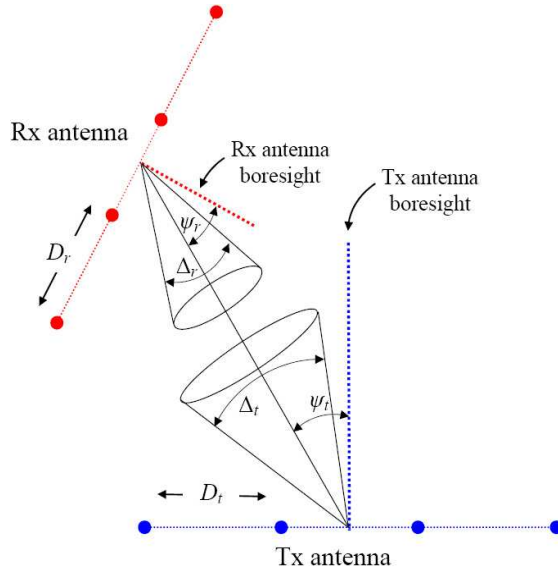


Figure 4.2: MIMO 4×4 system.

modeled as $\mathbf{H}_m = \mu \mathbf{q}^\dagger \mathbf{q}$ (i.e. $\mathbf{q}^\dagger = \mathbf{p}^T$, since $N = M$). Therefore, the channel distribution parameters that affect the optimum beamformer are $\mu, \beta, \rho_t, \mathbf{q}$ and obviously the SNR.

4.4.2 Computational complexity assessment

Setting $\mu = 1, \beta = 1, \rho_t = 0.9, \text{SNR} = 10\text{dB}$ and choosing a random² \mathbf{q} , the optimization problem (4.7) is solved using Theorem 4.1 along with an 1-D algorithm, (a combination of parabolic interpolation and golden section search methods). The parameters of the 1-D algorithm are described in Table 4.1.

Table 4.1: Parameters of the 1-D algorithm for the calculation of the optimum beamformer

Parameter	Description or Value
Matlab Function	fminbnd
Algorithm	Golden section and parabolic interpolation
MaxIter	10
MaxFunEvals	10^3
TolFun	10^{-40}
TolX	10^{-40}

² $\mathbf{q} = [0.1947 + 0.0655j \ 0.2898 - 0.6247j \ -0.0521 + 0.6856j \ 0.1041 + 0.0023j]$. This \mathbf{q} results in $\phi = 85^\circ$ (see (9)), which is a computationally demanding case for the algorithm of Theorem 4.1, since it requires a very wide search area.

The same optimization problem is then solved using an interior-point (multi-dimensional) algorithm, with starting point the max SNR beamformer (see subsection 4.4.3). The parameters of the multidimensional algorithm are described in Table 4.2.

Table 4.2: Parameters of the multidimensional algorithm for the calculation of the optimum beamformer

Parameter	Description or Value
Matlab Function	fmincon
Algorithm	Interior-point with logarithmic barrier function
Starting vector	max SNR beamformer
MaxIter	10
MaxFunEvals	10^3
TolFun	10^{-40}
TolX	10^{-40}

Both algorithms are limited to perform 10 iterations (enough for convergence to C_{bf} with an error tolerance of 10^{-4}) with the same computer (1.8GHz processor) using Matlab. Figures 4.3 and 4.4 show the computational complexity in terms of program runtime per iteration versus:

- a. The number of channel samples, for $N = M = 4$ (Figures 4.3).
- b. The number of Tx antenna elements³ N , with $M = 4$ and 2×10^4 channel samples (Figures 4.4).

Similar plots are shown in [49]-[50] for the complexity assessment of the algorithms presented therein.

The runtime scales almost linearly with the number of channel samples for both algorithms (Figure 4.3), however the increase rate of the 1-D algorithm is significantly lower, (it is approximately 8.5 times faster than the interior-point method). Also, for $N \leq 8$ the runtime scales as N^2 for the interior-point method, whereas for the 1-D algorithm scales

³When $N \neq M$, \mathbf{H}_m is modeled as $\mathbf{H}_m = \mu \mathbf{p}^T \mathbf{q}$ (see Theorem 4.1). For these simulations, random \mathbf{p} , \mathbf{q} vectors have been used.

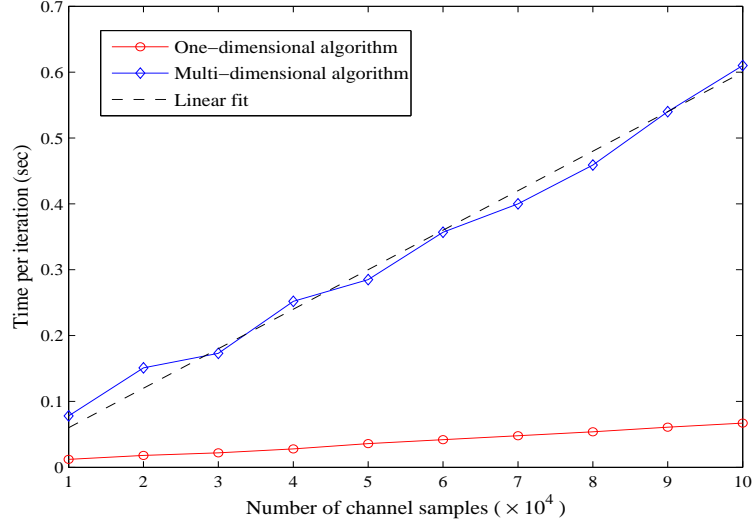


Figure 4.3: Runtime vs. the number of channel samples.

almost linearly, which is faster than the order of N^3 predicted by theory (a similar deviation between theory and practice has also been observed in [49]), and with a low rate (Figure 4.4), (for $N = 4/8$ the 1-D algorithm is $\sim 8.3/13$ times faster than the interior-point method, respectively). Generally, from Figures 4.3 and 4.4, it can be concluded (as a rule of thumb) that the 1-D algorithm is approximately an order of magnitude faster than the interior-point method.

The theoretical computational complexity of the 1-D algorithm in Theorem 4.1 is proven in the following proposition.

Proposition 4.1 The computational complexity of the 1-D algorithm for the calculation of the optimum beamformer is $\mathcal{O}(N^3 + M!)$.

Proof:

The following assumptions are made:

a. The number of digits of all real parameters is fixed, e.g. n digits. This means that the operations of summation, subtraction and multiplication between real/complex scalars (and as a result, the functions \cos, \sin, \log) will not affect the computational complexity of the algorithm, as long as n remains invariant, (e.g. summation and subtraction are $\mathcal{O}(n)$,

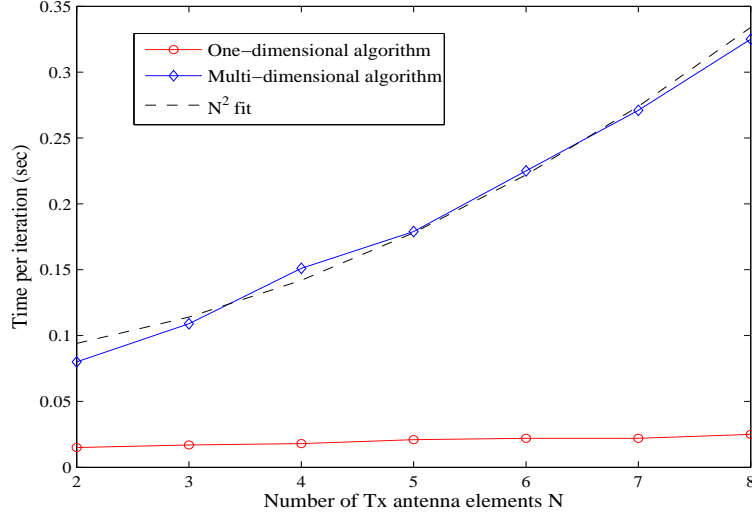


Figure 4-4: Runtime vs. the number of transmit antenna elements (N).

multiplication is $\mathcal{O}(n^2)$, etc.). Hence the only parameters that can affect the computational complexity of the algorithm are the number of transmit (N) and receive (M) antenna elements.

b. The 1-D search method used for the solution of the optimization problem (4.7) is the *golden section search method*, described in [76]. The search is with respect to the parameter θ . According to this method, (which is direct search), the convergence to θ_{opt} is accomplished by successive calculations of $\mathcal{I}_{\text{bf,avg}}(\text{SNR}, \mathbf{v}_\theta)$ (see (4.4) and (4.10)) at the (two) limits of an interval, which changes dynamically and becomes successively smaller at each step of the search, converging to θ_{opt} . Hence, the computational complexity of the proposed 1-D algorithm coincides with the computational complexity of the calculation of $\mathcal{I}_{\text{bf,avg}}(\text{SNR}, \mathbf{v}_\theta)$.

c. It is assumed that the number of steps of the golden section search for convergence to θ_{opt} is not affected by N and M , as long as the search interval $[0, \phi]$ remains invariant.

Complexity of \mathbf{v}_θ :

- The complexity of the root r_θ is $\mathcal{O}(N)$: r_θ is the maximum real root of the polynomial $P(x; \theta)$ and in Chapter 3 it was shown that this root is restricted in the interval $x > \lambda_1(\mathbf{G})$. Hence, the Newton-Raphson method can be employed in this interval for the calculation

of r_θ (i.e. there is no need to employ the Horner method). The computational complexity of the Newton-Raphson method depends on the order of $P(x; \theta)$ and is $\mathcal{O}(N)$.

- The complexity of $r_\theta \mathbf{I}_{N-1}$ is $\mathcal{O}(N)$.
- The complexity of $r_\theta \mathbf{I}_{N-1} - \mathbf{G}$ is $\mathcal{O}(N)$.
- The complexity of $(r_\theta \mathbf{I}_{N-1} - \mathbf{G})^{-1}$ is $\mathcal{O}(N^3 + N) = \mathcal{O}(N^3)$.
- The complexity of $\cos \theta \mathbf{Z}(r_\theta \mathbf{I}_{N-1} - \mathbf{G})^{-1}$ is $\mathcal{O}(N^3 + N^2 + N) = \mathcal{O}(N^3)$.
- The complexity of $\mathbf{v}_\theta = \cos \theta [1 \ \mathbf{Z}(r_\theta \mathbf{I}_{N-1} - \mathbf{G})^{-1}] \mathbf{W}^T \mathbf{U}^\dagger$ is $\mathcal{O}(N^3 + NM)$.

Setting (4.10) in (4.4), the complexity of $\mathcal{I}_{\text{bf,avg}}(\text{SNR}, \mathbf{v}_\theta)$ is as follows:

- The complexity of $\sqrt{\text{SNR} \mathbf{v}_\theta^\dagger}$ is $\mathcal{O}(N^3 + NM + N) = \mathcal{O}(N^3 + NM)$.
- The calculation of $\mathbf{H} \sqrt{\text{SNR} \mathbf{v}_\theta^\dagger}$ is $\mathcal{O}(N^3 + NM)$.
- The complexity of $\mathbf{I}_M + \text{SNR} \mathbf{H} \mathbf{v}_\theta^\dagger \mathbf{v}_\theta \mathbf{H}^\dagger$ is $\mathcal{O}(N^3 + M^2 + NM) = \mathcal{O}(N^3 + M^2)$.
- The complexity of $\det(\mathbf{I}_M + \text{SNR} \mathbf{H} \mathbf{v}_\theta^\dagger \mathbf{v}_\theta \mathbf{H}^\dagger)$ is $\mathcal{O}(N^3 + M^2 + M!) = \mathcal{O}(N^3 + M!)$, (since $M! > M^2$ for $M > 3$).

The complexity of $\mathcal{I}_{\text{bf,avg}}(\text{SNR}, \mathbf{v}_\theta)$ is not further affected by $\log_2(\cdot)$ and the Monte Carlo integration that must be employed for the calculation of the average mutual information ($\mathcal{E}_{\mathbf{H}}[\mathcal{I}_{\text{bf}}]$), when a fixed number of channel samples is used.

Hence the complexity of $\mathcal{I}_{\text{bf,avg}}(\text{SNR}, \mathbf{v}_\theta)$ - and hence, of Theorem 4.1 - is finally $\mathcal{O}(N^3 + M!)$. ■

4.4.3 Simulation results for the ergodic beamforming capacity

In the following the ergodic beamforming capacity achieved by the optimum beamformer is compared with the average mutual information achieved by the max SNR beamformer, denoted as $\mathbf{v}_{\text{maxSNR}} \in \mathbb{C}^{1 \times N}$, and calculated as the complex conjugate transpose dominant eigenvector of the channel transmit correlation matrix $\mathcal{E}_{\mathbf{H}}[\mathbf{H}^\dagger \mathbf{H}]$ [75].

In the following, results are produced for the mean information rate gain, which is

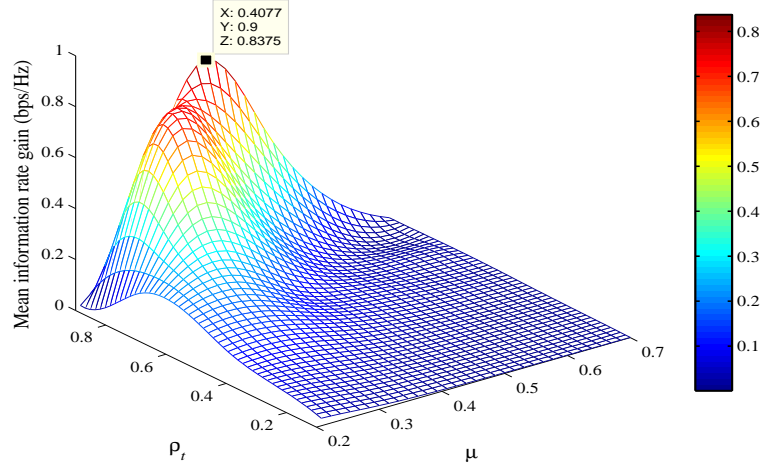


Figure 4.5: $\mathcal{E}[\Delta\mathcal{I}_{\text{bf,avg}}]$ vs. $\|\mu\|_2$ and ρ_t , for a MIMO 4×4 system with $\{\phi = 85^\circ, \beta = 0.2, \text{SNR} = 10\text{dB}\}$.

defined as:

$$\mathcal{E}[\Delta\mathcal{I}_{\text{bf,avg}}] = \mathcal{E}[\mathcal{I}_{\text{bf,avg}}(\text{SNR}, \mathbf{v}_{\text{opt}}) - \mathcal{I}_{\text{bf,avg}}(\text{SNR}, \mathbf{v}_{\text{maxSNR}})] \quad (4.32)$$

Note that $\mathcal{I}_{\text{bf,avg}}(\text{SNR}, \mathbf{v}_{\text{opt}}) = C_{\text{bf}}$, the mean is calculated over a set of 10^4 samples⁴ of \mathbf{q} , holding fixed $\{\mu, \beta, \rho_t, \text{SNR}, \phi\}$ (i.e. all samples are “forced” to have a fixed angle with respect to \mathbf{u}_1 (see (4.9)). In this manner, since \mathbf{q} is averaged out, it is $\mathcal{E}[\Delta\mathcal{I}_{\text{bf,avg}}] = f(\mu, \beta, \rho_t, \phi, \text{SNR})$.

Figure 4.5 demonstrates an example where $\mathcal{E}[\Delta\mathcal{I}_{\text{bf,avg}}]$ is plotted versus $\mu - \rho_t$, for $\{\beta = 0.2, \phi = 85^\circ, \text{SNR} = 10\text{dB}\}$. Observe that the mean capacity gain is high, (0.83bps/Hz for $\{\rho_t = 0.9, \mu = 0.4\}$). Simulations performed for a wide range of $\{\mu, \beta, \rho_t, \phi, \text{SNR}\}$ lead to the following conclusions:

- a. The optimum beamformer shows advantage over the max SNR beamformer (i.e. a high $\mathcal{E}[\Delta\mathcal{I}_{\text{bf,avg}}]$) for relatively small $\beta - \mu$ and high $\rho_t - \phi$ values.
- b. $\mathcal{E}[\Delta\mathcal{I}_{\text{bf,avg}}]$ increases monotonically with the SNR, (e.g. in the example of Figure 4.5, the gain 0.83bps/Hz increases to 1bps/Hz when $\text{SNR} = 15\text{dB}$).

⁴The elements of \mathbf{q} are produced by independent, zero-mean, unit variance complex Gaussian distributions.

4.5 Simulation results for the optimality of beamforming

This section presents simulations and results for ULAs and spatially correlated MIMO Rician fading channels [94].

First, a MIMO 4×4 channel is simulated, with \mathbf{R}_t and \mathbf{R}_r produced by the two-path delay spread correlation model developed in [86]. For ULAs the $\mathbf{R}_t/\mathbf{R}_r$ covariance matrices have a Toeplitz form and are expressed as in (4.31).

Throughout the simulations the following assumptions are made:

a. The transmit/receive array antennas are aligned for maximum directional radiation and reception at boresight, ($\psi_t = \psi_r = 0^\circ$).

b. $D_t = D_r = \lambda/2$.

c. $\Delta_r = 68^\circ$, (typical mean value for many operational scenarios [87]).

d. $\beta = \beta_t\beta_r$ is referred to as “channel variance”.

Under the aforementioned assumptions and exploiting the analysis presented in section 4.3 (see also [74], [93]), the calculation of \mathbf{v}_{opt} (1-D algorithm) is affected by the SNR, the channel variance β , the transmit antenna correlation coefficient $\rho_t = \rho_{12}^t = f(\Delta_t)$, the singular value μ of \mathbf{H}_m , the dominant eigenvector \mathbf{q} of \mathbf{H}_m (when $N = M = 4$, \mathbf{H}_m is modeled as $\mathbf{H}_m = \mu\mathbf{q}^\dagger\mathbf{q}$, i.e. $\mathbf{p}^T = \mathbf{q}^\dagger$, where \mathbf{p} and \mathbf{q} were defined in Theorem 4.1) and the angle $\phi = \cos^{-1}|\mathbf{q}\mathbf{u}_1|$, where $\mathbf{u}_1 \in \mathbb{C}^{N \times 1}$ is the dominant eigenvector of \mathbf{R}_t . Note that these parameters are all scalars except from \mathbf{q} , which is a complex vector. In order to show the effect of \mathbf{q} on (2.34), the scalar parameters are fixed to different sets of values, the validity of (2.34) is checked for 10^4 random \mathbf{q} vectors (the elements of \mathbf{q} are produced by i.i.d zero-mean complex Gaussian distributions with unit variance), and the following probability is calculated:

$$\Pr_{\text{bf}} = \frac{\text{Number of times (2.34) is true}}{\text{Number of times (2.34) is tested}} \quad (4.33)$$

High \Pr_{bf} for a set of values for the scalar parameters indicates that (2.34) has a high prob-

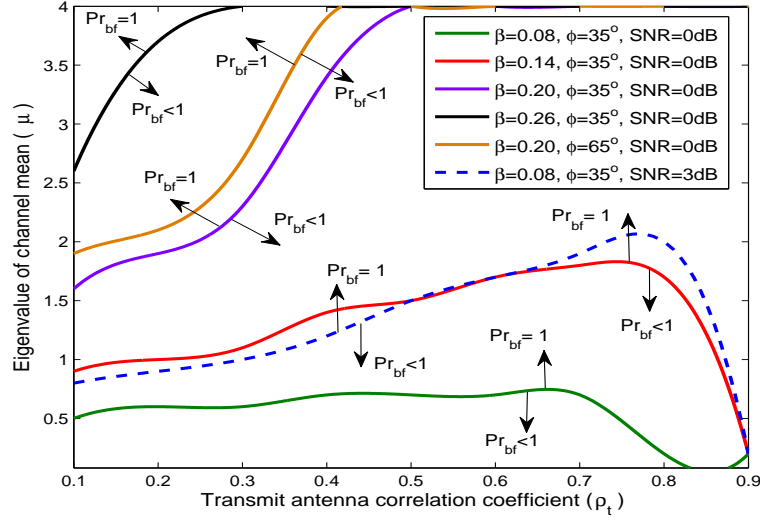


Figure 4.6: Optimality region $\mu - \rho_t$, for a MIMO 4×4 system and $\{\text{SNR} = 0/3\text{dB}, \phi = 35^\circ/65^\circ, \Delta_r = 68^\circ\}$.

ability to be satisfied in this operational scenario and hence, that \mathbf{v}_{opt} has a high probability to achieve ergodic capacity. Obviously, this is a very important piece of information, which can be taken into account during a system design/deployment phase.

Subsequently, the most representative results are shown, produced from extensive simulations. It must be mentioned here that the observations made from the presented results were always confirmed by several complementary simulations with different values for the considered set of parameters.

Figure 4.6 shows a set of curves on the $\mu - \rho_t$ plane ($\mu \leq 4$, since $\mu = 4$ is the highest possible value for MIMO 4×4), for different β values and $\{\phi = 35^\circ/65^\circ, \text{SNR} = 0/3\text{dB}, \Delta_r = 68^\circ\}$.

As explained previously, each curve represents a bound: Any $\{\mu, \rho_t\}$ point above this bound corresponds to an operational scenario where the optimum beamformer achieves ergodic capacity, i.e. (2.34) is always satisfied ($\text{Pr}_{\text{bf}} = 1$). On the other hand, any $\{\mu, \rho_t\}$ point below this bound represents an operational scenario where $\text{Pr}_{\text{bf}} < 1$. The $\mu - \rho_t$ region where $\text{Pr}_{\text{bf}} = 1$ is referred to as “optimality region”. From Figure 4.6 Observations 1-5 can be made:

Observation 1. Beamforming becomes the optimum strategy as μ (the singular value of \mathbf{H}_m) increases.

Observation 2. Beamforming becomes the optimum strategy as β (the channel variance) decreases.

Observation 3. Beamforming becomes the optimum strategy as the SNR decreases.

From (4.31) and given that $\mathbf{H}_m = \mu \mathbf{p}^T \mathbf{q}$, (4.2) can be re-written as follows:

$$\mathbf{H} = \sqrt{\beta} \left(\frac{\mu}{\sqrt{\beta}} \mathbf{p}^T \mathbf{q} + \left(\mathbf{R}'_r \right)^{1/2} \mathbf{H}_w \left(\mathbf{R}'_t \right)^{1/2} \right) = \sqrt{\beta} \mathbf{H}_{eq} \quad (4.34)$$

Substituting (4.34) into (2.7), the ergodic capacity is expressed equivalently as:

$$C_{\text{erg}} = \max_{\text{tr}\{\mathbf{Q}\} \leq 1, \mathbf{Q} \succeq 0} \mathcal{E}_{\mathbf{H}} \left[\log_2 \det(\mathbf{I}_M + \text{SNR}_{eq} \mathbf{H}_{eq} \mathbf{Q} \mathbf{H}_{eq}^\dagger) \right] \quad (4.35)$$

where

$$\text{SNR}_{eq} = \text{SNR} \beta \quad (4.36)$$

The Rician factor of the channel distribution is:

$$K = \frac{\|\mathbf{H}_m\|_F^2}{\text{tr}(\mathbf{R})} = \frac{\mu^2}{MN\beta^2} \quad (4.37)$$

where $\mathbf{R} = \mathbf{R}_t^T \otimes \mathbf{R}_r$ (see (2.14)).

From (4.36) and (4.37) it can be seen that: An increase in μ causes an increase in the Rician factor K of the channel distribution and consequently, an increase in the disparity between the singular values of any channel matrix realization. Moreover a decrease in β causes an increase in K but also a decrease in the SNR_{eq} .

Observation 1 is consistent with results presented in [47] for spatially uncorrelated MIMO Rician channels, while Observations 2 and 3 are consistent with results presented in [47] for MIMO Rayleigh and spatially uncorrelated MIMO Rician channels. All three observations are consistent with the notion of water-filling⁵ over the channel eigenvalues:

⁵The widely known water-filling iterative algorithm [66] cannot be employed for CDIT models. The eigenvalues of the optimum input covariance are calculated numerically using methods of non-linear program-

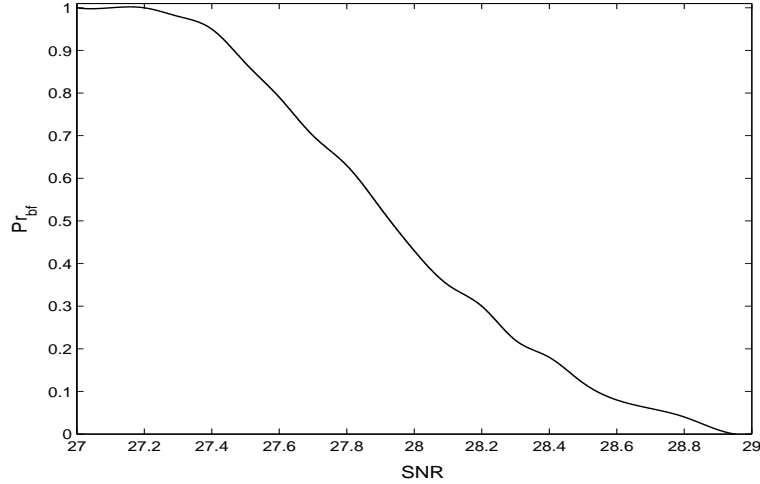


Figure 4-7: Pr_{bf} vs. SNR, for a MIMO 4×4 system and $\{\beta = 0.01, \phi = 45^\circ, \mu = 1.4, \rho_t = 0.1, \Delta_r = 68^\circ\}$.

The lower the SNR and/or the higher disparity between the channel singular values (i.e. high Rician factor K) the more power must be allocated to the dominant channel modes and the transmission converges to beamforming. Figures 4.7 and 4.8 show how Pr_{bf} varies with the SNR for $\{\beta = 0.01, \phi = 45^\circ, \mu = 1.4, \rho = 0.1\}$ and $\{\beta = 0.01, \phi = 45^\circ, \mu = 1.4, \rho = 0.1\}$, respectively.

Comparing the corresponding curve in Figure 4.6 for $\{\beta = 0.2, \phi = 65^\circ, \text{SNR} = 0\text{dB}\}$ with the corresponding curve for $\{\beta = 0.2, \phi = 35^\circ, \text{SNR} = 0\text{dB}\}$, it can be seen that:

Observation 4. Beamforming becomes the optimum strategy as ϕ decreases.

The angle ϕ between \mathbf{q} and the dominant eigenvector \mathbf{u}_1 of \mathbf{R}_t is a parameter presented here for the first time in simulations related to the optimality condition (2.34) and appears only in MIMO Rician channels, (it does not exist in MIMO Rayleigh channels). Figures 4.9 and 4.10 show again the effect of the decrease of ϕ on the optimality region, for $\text{SNR} = 0\text{dB}$ and different set of values β, ϕ than those used in Figure 4.6.

Practically, a decrease in ϕ causes an effect similar to an increase in the disparity of the two largest eigenvalues of \mathbf{R}_t , which favors the optimum beamformer and increases

ming [76]. However it seems that the general “rules” of water-filling are also valid for the complex Gaussian CDIT models studied in this thesis.

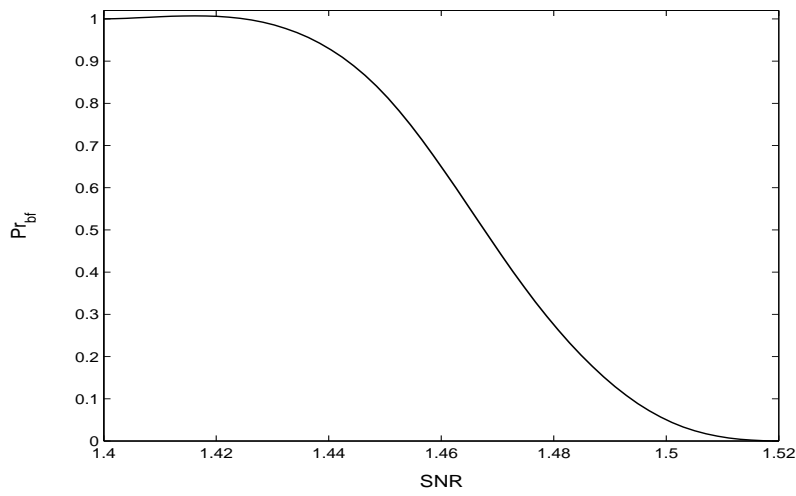


Figure 4-8: Pr_{bf} vs. SNR, for a MIMO 4×4 system and $\{\beta = 0.14, \phi = 45^\circ, \mu = 1.4, \rho_t = 0.1, \Delta_r = 68^\circ\}$.

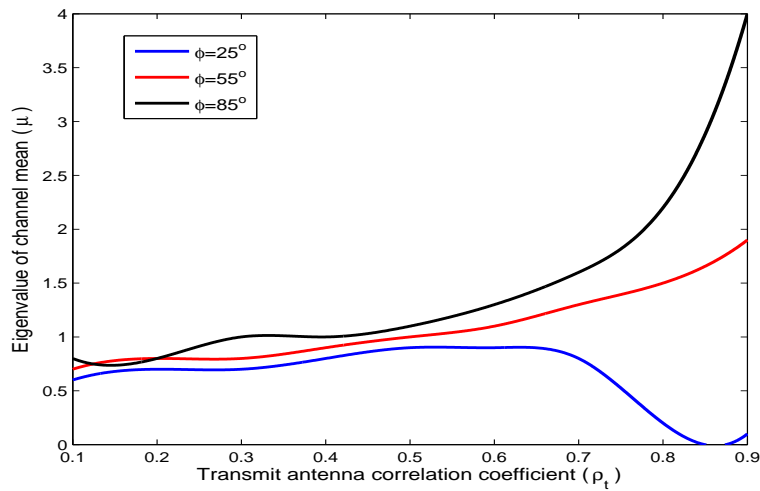


Figure 4-9: Optimality region $\mu - \rho_t$, for a MIMO 4×4 system and $\{\text{SNR} = 0\text{dB}, \beta = 0.1, \Delta_r = 68^\circ\}$.

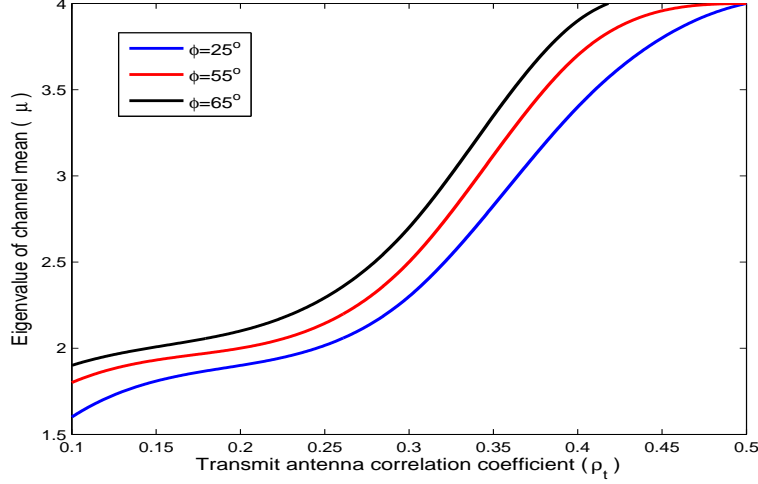


Figure 4-10: Optimality region $\mu - \rho_t$, for a MIMO 4×4 system and $\{\text{SNR} = 0\text{dB}, \beta = 0.2, \Delta_r = 68^\circ\}$.

the optimality region, as it was shown in [47] for MIMO Rayleigh channels:

Assuming for simplicity and without any loss of the generality that $N = M$, the *rank-1* channel mean \mathbf{H}_m can be written as:

$$\mathbf{H}_m = \mu \mathbf{q}^\dagger \mathbf{q} \quad (4.38)$$

Using eigen-decomposition, \mathbf{R}_t can be written as:

$$\mathbf{R}_t = \sum_{i=1}^N \lambda_i \mathbf{u}_i \mathbf{u}_i^\dagger \quad (4.39)$$

where λ_i/\mathbf{u}_i are the eigenvalues/eigenvectors of \mathbf{R}_t , (note that $\mathbf{u}_i \in \mathbb{C}^{N \times 1}$).

If $\phi = \phi_1$ is the angle between \mathbf{q}^\dagger and \mathbf{u}_1 , then \mathbf{q}^\dagger can be expressed as:

$$\mathbf{q}^\dagger = \sum_{i=1}^N e^{j\omega_i} \cos \phi_i \mathbf{u}_i \quad (4.40)$$

with $\sum_{i=1}^N \cos^2 \phi_i = 1$, (since $\|\mathbf{q}^\dagger\|_2 = \|\mathbf{u}_i\|_2 = 1$).

From (4.2), (4.38), (4.39), (4.40), eigen-decomposition of \mathbf{H}_w and assuming that $\mathbf{R}_r = \mathbf{I}_M$, it can be proven (after some simple mathematical manipulations) that any channel

realization \mathbf{H} can also be expressed as:

$$\mathbf{H} = \sum_{i=1}^N \left[\sum_{j=1}^N \left(\mu \cos^2 \phi_i + \lambda_i^{1/2} \lambda_j^w \right) \mathbf{v}_j \mathbf{v}_j^\dagger \right] \mathbf{u}_i \mathbf{u}_i^\dagger \quad (4.41)$$

where λ_j^w/\mathbf{v}_j are the eigenvalues/eigenvectors of \mathbf{H}_w , (with $\mathbf{v}_j \in \mathbb{C}^{N \times 1}$).

Setting $a_{ij} = \mu \cos^2 \phi_i + \lambda_i^{1/2} \lambda_j^w$, the following can be observed:

- In MIMO Rayleigh channels the first summand in a_{ij} does not exist, i.e. it is $a_{ij} = \lambda_i^{1/2} \lambda_j^w$. In these channels, an increase in the disparity between λ_1 and λ_2 causes, equivalently, an increase in the disparity of a_{1j} and a_{2j} ($\forall j$), which leads the channel distribution in the beamforming optimality region, as it was also shown in [47].

- In spatially correlated MIMO Rician channels a decrease in $\phi = \phi_1$ (i.e. increase of $\cos \phi_1$) causes a similar increase in the disparity of a_{1j} and a_{2j} (note that when ϕ_1 decreases, ϕ_2 increases) and leads the channel distribution in the optimality region, as in MIMO Rayleigh channels.

Observation 5. Relatively low channel variance leads to abrupt increase of the optimality region for relatively high ρ_t values, (i.e. high disparity for the eigenvalues of \mathbf{R}_t). This can be seen in Figure 4.6 from the curves for $\beta = \{0.14, 0.08\}$. This also agrees with results for MIMO Rayleigh fading channels from [47]. However, this effect seems to vanish for higher β and/or ϕ values (see curves for $\beta = \{0.2, 0.26\}$), which “resist” to the optimality of beamforming, as explained in Observations 2 and 4. Moreover, in the low- ρ_t regime, the optimality region seems to be rather “insensitive” to an increase of the SNR, β and ϕ .

In Figure 4.11, Pr_{bf} is plotted versus M for three sets of values for $\{\beta, \phi, \mu, \rho\}$ and $\{N = 4, \text{SNR} = 0\text{dB}, \Delta_r = 68^\circ\}$.

It can be observed that Pr_{bf} decreases with M . From (4.38), a decrease in M causes an increase in the Rician factor K of the channel distribution.

Observation 6. Beamforming becomes the optimum strategy as the number of receive antenna elements (M) decreases.

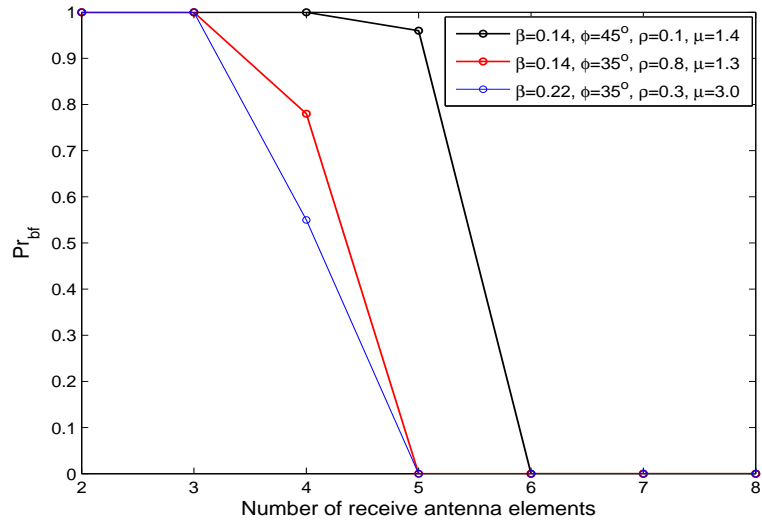


Figure 4.11: Pr_{bf} vs. M , for $\{N = 4, \text{SNR} = 0\text{dB}, \Delta_r = 68^\circ\}$.

This observation also agrees with results in [47], for MIMO Rayleigh and spatially uncorrelated MIMO Rician channels, and is consistent with the notion of water-pouring over the channel modes. As a consequence, the optimality regions presented in Figure 4.6 ($\forall \beta, \phi$ and SNR value) will further increase for $M < 4$.

Chapter 5

CAPACITY AND OPTIMALITY OF BEAMFORMING FOR DIFFERENT OPERATIONAL ENVIRONMENTS

5.1 Introduction

The nature of the wireless channel (e.g. statistical properties, correlation) plays a key role to the study of its capacity. As a result, attention has turned to the development of realistic channel models that will provide the basis for accurate capacity analysis. In this chapter, a MIMO channel simulation model is developed, which is based on the Technical Report [87] of the 3rd Generation Partnership Project (3GPP). This simulation model is used to produce (thousands of) channel samples which simulate different operational environments and then these samples are used to study the capacity performance and the “probability of beamforming” achieved by different channel feedback information models.

5.2 MIMO channel simulation model

As explained in the preceding chapters, the impulse response of a MIMO channel is an $N \times M$ matrix $\mathbf{H}(t)$. Sample of the MIMO channel matrix $\mathbf{H}(t)$ can be generated according to the Technical Report of 3GPP [87], for the following operational environments:

- a. Suburban macrocell,
- b. Urban macrocell with mean angular spread $\mathcal{E}[\sigma_{AS}] = 8^\circ$ or $\mathcal{E}[\sigma_{AS}] = 15^\circ$,
- c. Urban microcell.

Moreover the following optional features can be simulated:

- a. Antenna Polarization (valid in all environments),
- b. Far Scatterer Clusters (valid only in urban macrocell environments),

- c. Urban canyon (valid only in urban environments),
- d. Line Of Sight multipath component (valid only in urban microcell environments),
- e. Intercell interference (3-sector or 6-sector cellular systems can be simulated).

In order to generate many channel samples (i.e. realizations of matrix $\mathbf{H}(t)$), the time axis is divided into N_{drops} drops and each drop into N_{frames} frames. During a drop, the location and the orientation parameters of the Mobile Station (MS), the Angular Spread (σ_{AS}), the Delay Spread (σ_{DS}) (at both the BS and MS) and the Shadow Fading (σ_{SF}) do not change. All these parameters change per drop and their values are chosen randomly from distributions described in [87, page 17, Table 5.1], (these distributions are different in each operational environment).

The Angles of Departure (AoD) (from the BS), the Angles of Arrival (AoA) (to the MS), the path delays and the path powers of the F dominant multipath components between the BS and the MS change from frame to frame randomly, according to distributions described in the Technical Report [87], (these distributions are different in each operational environment). Each one of the F multipath components is comprised of S sub-paths: in [87] it is recommended, $F = 6$ and $S = 20$. In each frame a three-dimensional ($M \times N \times F$) MIMO Channel Matrix $\mathbf{H}(t)$ (3-D impulse response) is generated. The elements of this matrix, denoted as $\mathbf{H}_{m,n,f}$ (f^{th} multipath component between the m^{th} receive and the n^{th} transmit array antenna element), are expressed by the following equation:

$$\begin{aligned} \mathbf{H}_{m,n,f}(t) = & \sqrt{\frac{P_f \sigma_{SF}}{M}} \sum_{s=1}^S \left(\sqrt{G_{MS}(\theta_{f,s,AoA}) G_{BS}(\theta_{f,s,AoD})} \right. \\ & \times \exp\left(\sqrt{-1} [kd_n \sin(\theta_{f,s,AoD}) + \Phi_{f,s}]\right) \times \exp\left(jkd_m \sin(\theta_{f,s,AoD})\right) \\ & \left. \times \exp\left(\sqrt{-1} k \|v\|_2 \cos((\theta_{f,s,AoA} - \theta_v)t)\right) \right) \end{aligned} \quad (5.1)$$

where: P_f is the power of the f^{th} multipath component, σ_{SF} is the shadowing (bulk parameter, applied to all paths), $\theta_{f,s,AoD}$ and $\theta_{f,s,AoA}$ is the AoD and AoA, respectively, for the s^{th} subpath of the f^{th} multipath component, $G_{BS}(\theta_{f,s,AoD})$ is the gain of each element

of the BS array antennas along the azimuth angle $\theta_{f,s,AoD}$ and $G_{MS}(\theta_{f,s,AoA})$ is the gain of each element of the MS array antenna along the azimuth angle $\theta_{f,s,AoA}$. All elements of the BS/MS array antenna are assumed to have the same antenna pattern, $k = 2\pi/\lambda$, d_n is the distance of the n^{th} transmit array antenna element with respect to the reference antenna element, d_m is the distance of the m^{th} receive array antenna element with respect to the reference antenna element, $\Phi_{f,s}$ is the phase of the s^{th} subpath of the f^{th} multipath component and $\|v\|_2$ and θ_v is the norm and angle of the MS velocity vector, respectively.

If only one path can be resolved in each frame, the 3-D channel matrix is degenerated into a two-dimensional matrix:

$$\begin{aligned} \mathbf{H}_{m,n}(t) = & \sum_{f=1}^F \left(\sqrt{\frac{P_f \sigma_{SF}}{M}} \sum_{s=1}^S \left(\sqrt{G_{MS}(\theta_{f,s,AoA}) G_{BS}(\theta_{f,s,AoD})} \right. \right. \\ & \times \exp\left(\sqrt{-1} [kd_n \sin(\theta_{f,s,AoD}) + \Phi_{f,s}]\right) \times \exp\left(jkd_m \sin(\theta_{f,s,AoD})\right) \\ & \left. \left. \times \exp\left(\sqrt{-1} k \|v\|_2 \cos((\theta_{f,s,AoA} - \theta_v)t)\right) \right) \right) \end{aligned} \quad (5.2)$$

The channel matrix calculated above is the with respect to the serving BS in a 2-tier cellular system (i.e. 19 cells), as shown in Figure 5.1. The serving BS is characterized by the highest received power, based on pathloss (according to the COST231 Hata model for suburban/urban macrocell environments or the COST231 Walfish-Ikegami NLOS/street canyon model for the urban microcell environment [87]), shadowing (σ_{SF}) and BS antenna gain (for the simulations it is assumed that the BS array antenna has the pattern described in [87, page 18]).

Practically, for the simulations the time parameter t is multiples of the frame duration T_{frame} , (i.e. $t = (jN_{frames} + i)T_{frame}$, $j = 1, \dots, N_{drops}$, $i = 1, \dots, N_{frames}$) and the elements of the channel matrix at the i^{th} frame and j^{th} simulation drop are denoted as $\mathbf{H}_{m,n}^{ij}$. In MISO systems, for simplicity, $\mathbf{H}_{m,n}^{ij}$ is denoted as \mathbf{h}_n^{ij} . An overview of the channel simulation process is presented in Table 5.1 (at the end of this Chapter).

In the following, using $N_{drops} = 10^4$ and $N_{frames} = 10, 10^5$ MISO 2×1 channels are pro-

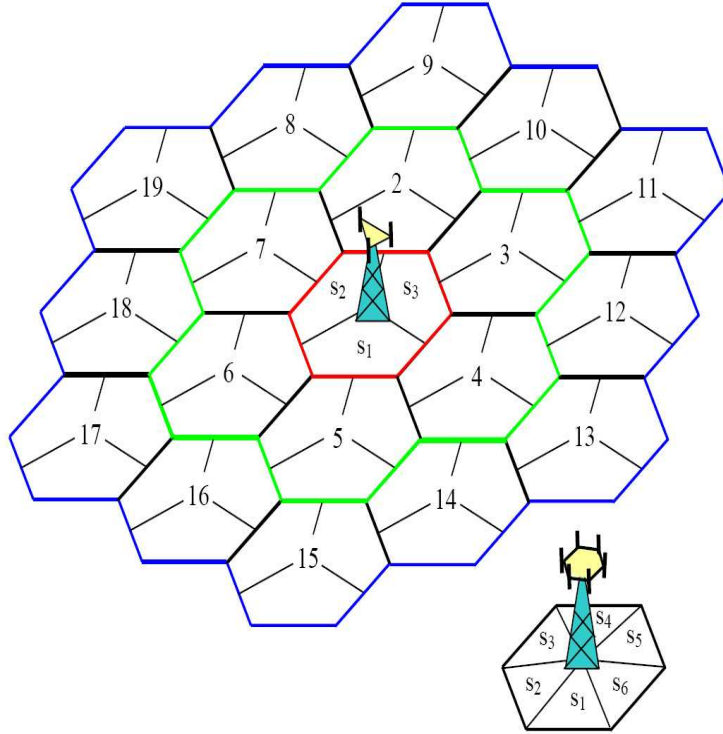


Figure 5-1: Two tier cellular structure. s_i is the sector numbering, with $i = 1, \dots, 3$ for the 3-sector scenario or $i = 1, \dots, 6$ for the 6-sector scenario.

duced ($N = 2, M = 1$) for different operational environments (without optional simulation features). Moreover, the following assumptions have been made: $G_{BS}(\theta) = G_{MS}(\theta) = 1$ ($\forall \theta \in [0, 2\pi]$), the inter-element distance at the transmit antenna is $\lambda/2$, the carrier frequency is $f_c = 2\text{GHz}$ and the frame duration is $T_{frame} = 10\text{msec}$ (power control period for UMTS). In all environments it is $T_{frame} \gg \mathcal{E}[\sigma_{DS}]$ ($\mathcal{E}[\sigma_{DS}] = 0.17/0.65/0.251\text{microsec}$ for suburban/urban macro/urban micro), a fact that justifies the initial assumption for the existence of only one resolvable path in each frame (and hence, the use of (5.2) instead of (5.1) in the simulations).

Using the aforementioned 10^5 channels, Figure 5.2 demonstrates the Rayleigh distribution that best fits to the $|\mathbf{H}_{1,n}|$ (for $n = 1, 2$). The distribution of the $\text{arg}(\mathbf{H}_{1,n})$ can be approximated by the uniform distribution $U(-\pi, \pi)$ (in all environments). In Figure 5.2 it can be observed that the Rayleigh distribution of $|\mathbf{H}_{1,n}|$ in an urban micro environment presents the highest variance, followed by the variance of the urban macro $\mathcal{E}[\sigma_{AS}] = 15^\circ$

environment and the suburban macro/urban macro $\mathcal{E}[\sigma_{AS}] = 8^\circ$ environment, (note that the curves for the suburban macro and urban macro $\mathcal{E}[\sigma_{AS}] = 8^\circ$ environments are very close).

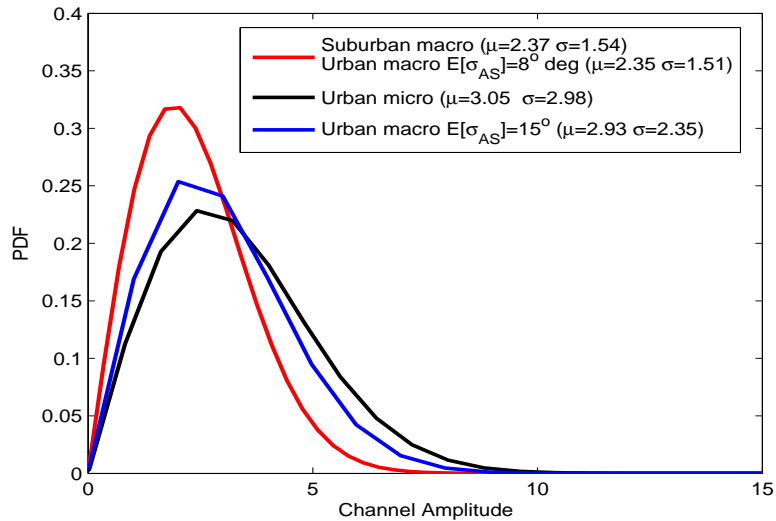


Figure 5-2: Rayleigh distribution of $|\mathbf{H}_{1,n}|$.

Table 5.2 presents the calculated mean and standard deviation (std) of the correlation coefficient (which is assumed to be a random variable¹) between the two transmit antenna elements in all environments.

Table 5.2: Correlation coefficient statistics

Environment	mean	std
Suburban macro	0.96	0.02
Urban macro $\mathcal{E}[\sigma_{AS}] = 8^\circ$	0.92	0.11
Urban macro $\mathcal{E}[\sigma_{AS}] = 15^\circ$	0.79	0.17
Urban micro	0.59	0.17

¹In each drop the correlation coefficient is calculated along all frames ($N_{frames} = 10$) of the drop. Hence, 10^4 values for the correlation coefficient random variable are produced (since $N_{drops} = 10^4$) and then used to calculate its statistics.

From this table it can be observed that the correlation is inversely proportional to $\mathcal{E}[\sigma_{AS}]$ (as also predicted by theory [66]): a high correlation is observed in suburban/urban macro environments with $\mathcal{E}[\sigma_{AS}] = 5^\circ/8^\circ$, while the urban macro/micro environments with $\mathcal{E}[\sigma_{AS}] = 15^\circ/19^\circ$ follow with lower correlations.

5.3 Simulations for MISO 2×1 Rayleigh fading channels

In this section we present simulation results for the maximum ergodic capacity and the the optimality of beamforming in different operational environments (suburban macro, urban macro, urban micro) - using the simulation model described in the previous section - and for the following channel feedback information models [95]:

- a. perfect CSI at the transmitter,
- b. unknown channel to the transmitter,
- c. Channel Mean Information model,
- d. Channel Covariance Information model.

For the ergodic capacity simulations the following are considered:

- 3-sector cellular system,
- $N_{drops} = 10^2$,
- $N_{frames} = 10$,
- $T_{frame} = 10\text{msec}$,
- $F = 6, S = 20$,
- $N = 2, M = 1$ (i.e. a MISO 2×1 system),
- $f_c = 2\text{GHz}$,
- inter-element distance $\lambda/2$ and
- velocity of the mobile station $\|v\|_2 = 5\text{km/h}$.

For the optimality of beamforming simulations the same values have been consid-

ered, except from the following: $N_{drops} = 10^4$. Moreover, it must be noted that in these simulations, the optimality of beamforming is not studied with the condition (2.34), but statistically, as discussed in the following subsection 5.3.2.

Moreover, the generated channel samples simulate Raleigh fading channels without additional simulation features (e.g. LOS component, urban canyon, etc.).

For the simulations of the CMI and CCI models, the following issues must be discussed:

(1) CMI model

In the context of this model, the ergodic capacity achieved for every channel sample that is fed back to the transmitter by the receiver is calculated, i.e. for each of the $N_{drops} \times N_{frames} = 10^3$ channels. The CMI model, as it appears in the open literature and discussed in Chapter 2, is a short-term model that achieves ergodic capacity based on an estimation of the “real” channel (used as the “channel mean” information) and on the assumption of a white error covariance matrix (with equal diagonal elements). If correlation effects are also taken into account, then the channel error covariance matrix is not white and the feedback information model in this case is not a “pure” CMI model but a short-term combined CMI-CCI model.

However, in the 3GPP model, there is no temporal correlation between successive channel realizations/samples (that simulate fast fading) in the context of the same drop, (i.e. $\mathbf{R}_s = \mathbf{0}$ (see (2.17))). Assuming a delay in the control channel equal to one frame duration T_{frame} , the best estimation (made by the transmitter) for the $(i + 1)^{th}$ (channel) frame (i.e. the “real” channel), based on the i^{th} frame (feedback information), is the channel mean $\tilde{\mathbf{h}}^j$, [44], which is calculated over all frames of the j^{th} drop:

$$\tilde{\mathbf{h}}^j = \frac{1}{N_{frames}} \sum_{i=1}^{N_{frames}} \mathbf{h}^{ij} \quad (5.3)$$

Moreover, the channel error covariance ($\mathbf{R}_{e,s}$, (see (2.19))) coincides with the channel

covariance matrix Σ_j , which is also calculated over all frames of the j^{th} drop:

$$\Sigma_j = \frac{1}{N_{frames}} \sum_{i=1}^{N_{frames}} (\mathbf{h}^{ij} - \bar{\mathbf{h}}^j)^\dagger (\mathbf{h}^{ij} - \bar{\mathbf{h}}^j) \quad (5.4)$$

Practically, we have a long-term feedback model where the long-term channel statistics² $\bar{\mathbf{h}}^j$ and Σ_j are used in order to achieve ergodic capacity. Therefore, it is not necessary to feed back to the transmitter the frames of the j^{th} drop, one by one. The channel distribution during the j^{th} drop is $\mathbf{h}^j \sim (\bar{\mathbf{h}}^j, \Sigma_j)$, where \mathbf{h}^j denotes any channel sample/realization in the j^{th} drop. For this long-term model, the following cases can be separated:

a. The channel mean is $\bar{\mathbf{h}}^j \neq \mathbf{0}$ and Σ_j is a diagonal matrix with equal diagonal elements. In this case the standard solution of the long-term CMI model (see Chapter 2) can be employed, as also described in [46].

b. The channel mean is $\bar{\mathbf{h}}^j \neq \mathbf{0}$ and Σ_j is not a diagonal matrix or it is a diagonal matrix with unequal diagonal elements. This is a long-term combined CMI-CCI model and must be solved numerically using the methods discussed in [49] or [50].

c. The channel mean is $\bar{\mathbf{h}}^j = \mathbf{0}$. In this case, regardless of the value of Σ_j , we have a (long-term) CCI model (see also discussion below). However, in the context of the simulation model proposed by 3GPP, assuming a finite and small number of frames, it is really rare (practically impossible) to have a zero channel mean, even in environments that simulate pure Rayleigh fading channels, (e.g suburban or urban macro).

Using the parameters described in the first paragraph of this section, simulations have shown that case (b) described above (i.e. the long-term combined CMI-CCI model) dominates in all drops.

However, in the context of the simulations presented hereafter, the following assumptions have been made:

²These are calculated at the beginning of each drop, in the context of a training period, by the receiver and then are fed back to the transmitter. These statistics are valid during the whole drop.

- a. In each drop, the channel frames are fed back to the transmitter, one by one.
- b. The feedback control channel has a time delay equal to the duration of one frame (T_{frame}). This means that when the i^{th} frame of the j^{th} simulation drop, denoted as $\mathbf{h}^{ij} = [\mathbf{h}_1^{ij}, \mathbf{h}_2^{ij}, \dots, \mathbf{h}_n^{ij}]$, arrives at the transmitter, the “real” channel is the $\mathbf{h}^{(i+1)j}$, i.e. in the next frame.
- c. Based on the channel feedback information \mathbf{h}^{ij} , the transmitter’s estimation for the “real” channel ($\mathbf{h}^{(i+1)j}$) is expressed as follows:

$$\widehat{\mathbf{h}}^{(i+1)j} = \mathbf{h}^{ij} + \overline{\mathbf{h}}_e^j \quad (5.5)$$

where $\overline{\mathbf{h}}_e^j$ is the mean channel error calculated in each simulation drop as:

$$\overline{\mathbf{h}}_e^j = \mathcal{E}_i[\mathbf{h}^{(i+1)j} - \mathbf{h}^{ij}] \quad (5.6)$$

where the mean is calculated with respect to i (i.e. with respect to all frames of the j^{th} drop). Obviously, the statistics of the channel error in the j^{th} drop, namely its mean $\overline{\mathbf{h}}_e^j$ and its covariance matrix $\mathbf{R}_e^j = cov_i[\mathbf{h}^{(i+1)j} - \mathbf{h}^{ij}]$, are long-term statistics, calculated by the receiver at the beginning of each drop³ and fed back to the transmitter.

- d. After the feedback of the i^{th} frame (in the j^{th} drop) the channel distribution assumed by the transmitter for the solution of the CMI model is $\mathbf{h} \sim \mathcal{N}(\widehat{\mathbf{h}}^{(i+1)j}, a\mathbf{I}_N)$, with a referred to as “channel error variance”. Observe that in the CMI model a white channel error covariance matrix is assumed⁴.

(2) CCI model

In this long-term model the ergodic capacity is achieved by the transmitter, exploiting only the feedback information of the channel covariance, which is calculated by the receiver at the beginning of each simulation drop. The transmission strategy that achieves

³e.g. in the context of a training period

⁴Practically, the channel error covariance matrix is not white. However, for the simulations, the off-diagonal elements of the channel error covariance matrix are ignored (i.e. set to zero) and its maximum diagonal element is considered to be the channel error variance a .

ergodic capacity is applied to all frames of a drop. For MISO Rayleigh fading channels, the channel transmit covariance matrix Σ_j (in the j^{th} drop coincides with the channel transmit correlation matrix C_j , since it is $\bar{\mathbf{h}}^j = \mathbf{0}$, i.e.

$$\Sigma_j = C_j = \mathcal{E}_i[(\mathbf{h}^{ij})^\dagger \mathbf{h}^{ij}] \quad (5.7)$$

For the reason discussed in the previous paragraph (CMI model) the model of 3GPP provides a non zero channel mean in each drop, i.e. $\bar{\mathbf{h}}^j \neq \mathbf{0}$, even though a Rayleigh fading channel is simulated. However, in the simulations presented in the following it is assumed that $\bar{\mathbf{h}}^j = \mathbf{0} \forall j$ (i.e. the channel mean is ignored) and the channel correlation matrix C_j is considered by the transmitter as a covariance matrix, which is subsequently used to employ the standard solution of the CCI model [46].

5.3.1 Simulation results for the ergodic capacity

Figures 5.3-5.6 show the ergodic capacity vs. the SNR, for different channel feedback information models. In all channel feedback information models the ergodic capacity is calculated over all simulation drops and frames. In all figures (i.e. in all simulated environments) it can be observed that the “perfect CSI at the transmitter” (Perfect CSIT) and the “unknown channel to the transmitter” (Unknown Channel) models are the upper and the lower bounds, respectively, while the CCI and CMI models are between these bounds. The results show that the CCI model outperforms the CMI model in all environments. The CCI model is easier to employ than the CMI model, since it is a long-term model and the transmission strategy is calculated once, at the beginning of each drop. On the other hand, the CMI model is a short-term model and the transmission strategy changes at each frame, (despite the fact that the mean and variance of the channel error are calculated as long-term statistics). Moreover, the performance of the CMI model (according to the way that it is simulated herein) will further deteriorate if we assume very large delays in the feedback control channel, equal to or greater than the drop duration T_{drop} ($T_{drop} = N_{frames} \times T_{frame}$). In the latter case, the channel error mean and variance,

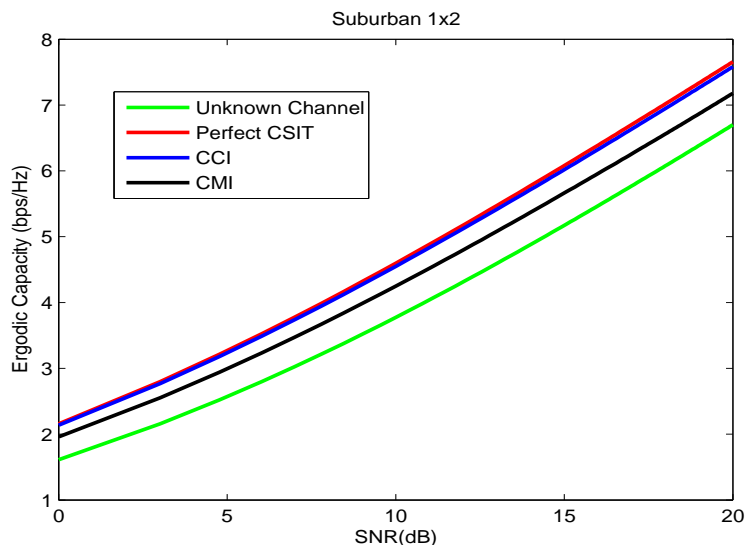


Figure 5.3: Ergodic capacity vs. SNR, in a suburban environment.

that will be used by the CMI algorithm, are related to a previous drop and the transmission scheme that we will be finally used does not achieve ergodic capacity.

Furthermore, in Figures 5.3 and 5.4 it can be observed that the CCI model achieves high capacity, very close to the the capacity of the Perfect CSIT model, despite the fact that a zero channel mean has been assumed. These results indicate that in suburban or urban macro $\mathcal{E}[\sigma_{AS}] = 8^\circ$ environments it is practically meaningless to solve the combined CMI-CCI model, that is valid if we do not assume a zero channel mean. The latter model is more complex ([49], [50]) and its relative capacity gain with respect to the CCI model under the zero channel mean assumption is very small.

Finally, in all figures (Figures 5.3-5.6), it can be observed that the lower the correlation between the transmit antenna elements (see Table 5.2) the lower is the capacity performance of both the CMI and CCI models with respect to the Perfect CSIT model.

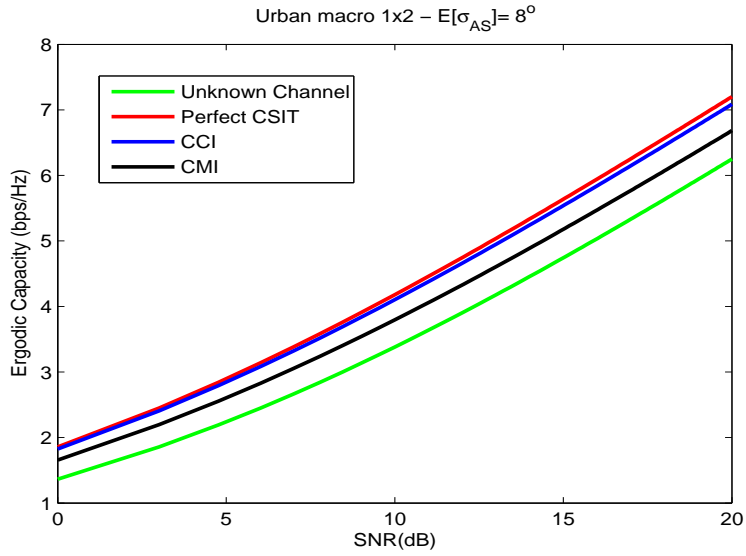


Figure 5-4: Ergodic capacity vs. SNR, in an urban macro environment with $\mathcal{E}[\sigma_{AS}] = 8^\circ$.

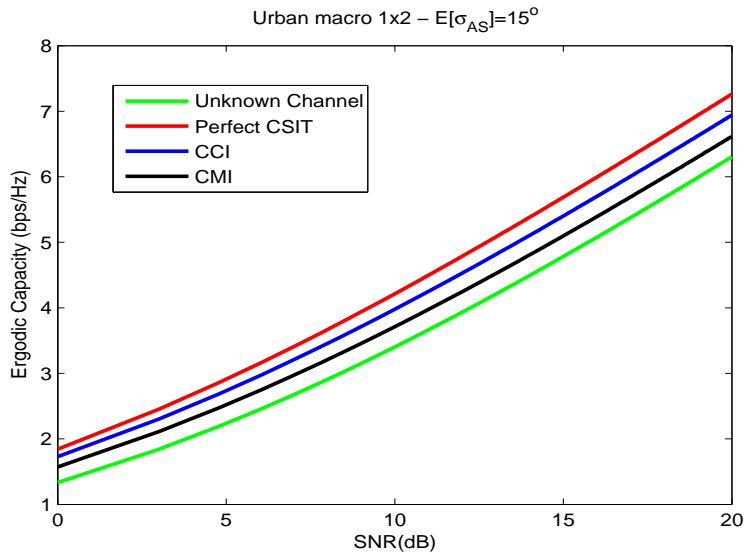


Figure 5-5: Ergodic capacity vs. SNR, in an urban macro environment with $\mathcal{E}[\sigma_{AS}] = 15^\circ$.

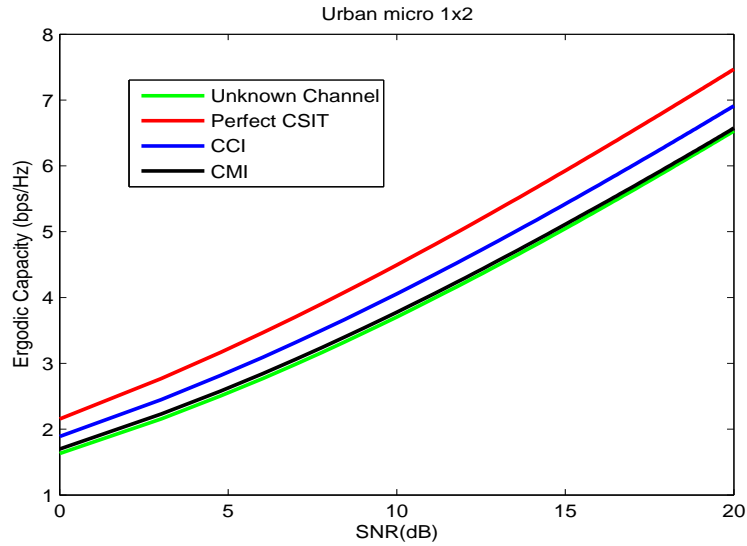


Figure 5.6: Ergodic capacity vs. SNR, in an urban micro environment.

5.3.2 Simulation results for the optimality of beamforming

In the following, the optimality of beamforming is studied statistically, by introducing the following probability \Pr_{bf} :

$$\Pr_{bf} = \frac{\text{Number of times that power is allocated to only one beam}}{\text{Number of times that power is allocated to more than one beams}} \quad (5.8)$$

The probability defined with (5.8) is generally similar to the probability defined with equation (4.33) in Chapter 4, but with the following main difference: in (4.33), condition (2.34) is used and tested in order to calculate \Pr_{bf} , whereas in (5.8) a more practical method is employed.

Figures 5.7 and 5.8 present results for the \Pr_{bf} vs. the SNR for the CMI and CCI models, respectively, and different operational environments.

It can be observed that \Pr_{bf} decreases as the SNR increases in both models. This result coincides with results reported in [46] and [96], for the CMI and the CCI model, respectively. Moreover, \Pr_{bf} depends on the operational environment as follows:

(1) CMI model simulation results

In Figure 5.7 \Pr_{bf} is plotted versus the SNR for the CMI model and different opera-

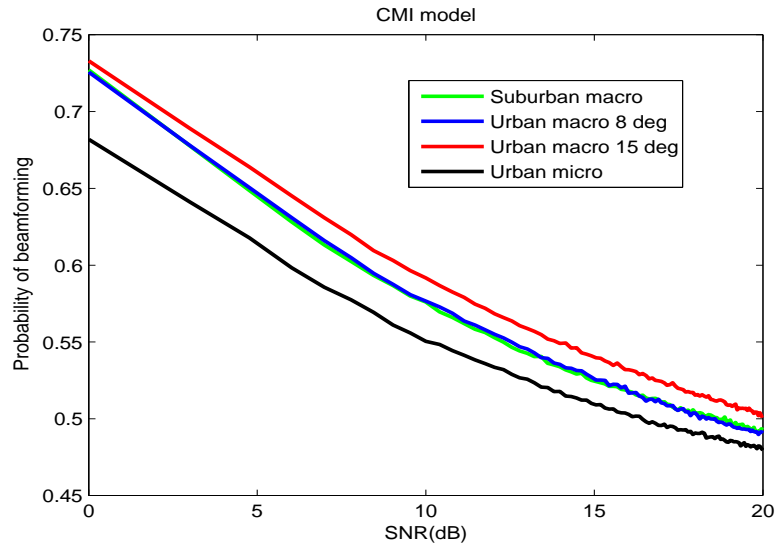


Figure 5-7: Propability of beamforming vs. SNR, for the CMI model.

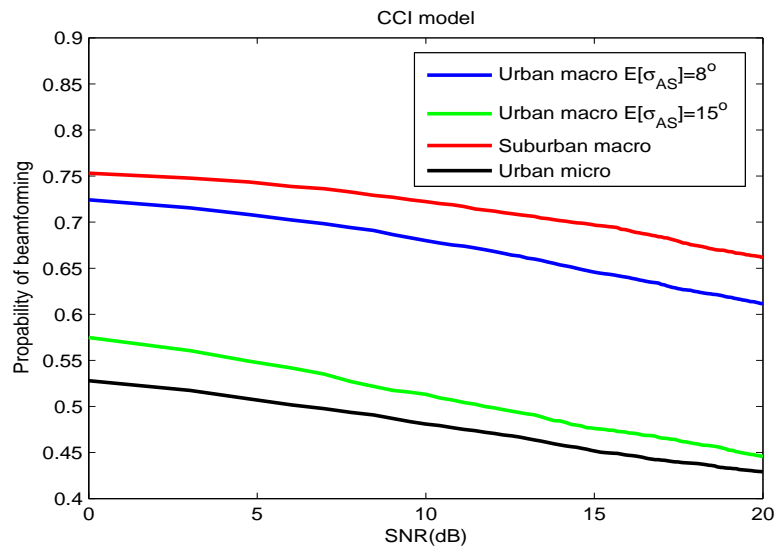


Figure 5-8: Propability of beamforming vs. SNR, for the CCI model.

tional channels. In this figure it can be observed that the curves for the suburban and urban macro $\mathcal{E}[\sigma_{AS}] = 8^\circ$ environments almost coincide. The urban macro $\mathcal{E}[\sigma_{AS}] = 15^\circ$ environment presents the highest and the urban micro environment the lowest Pr_{bf} , respectively. In [96] it is shown that the optimality of beamforming condition, for a given SNR, is a function of the channel error variance a and the parameter $\frac{\|\hat{\mathbf{h}}^{(i+1)j}\|_2}{a}$, referred to as “feedback quality”⁵. In Table 5.3 we calculate the mean and standard deviation (std) of the channel error variance a and the feedback quality $\frac{\|\hat{\mathbf{h}}^{(i+1)j}\|_2}{a}$, (these statistics have been calculated over all simulation drops for the parameter a and over all simulation drops and frames for the parameter $\frac{\|\hat{\mathbf{h}}^{(i+1)j}\|_2}{a}$). We observe that the statistics (mean and variance) of the feedback quality $\frac{\|\hat{\mathbf{h}}^{(i+1)j}\|_2}{a}$ are almost the same in all environments, and hence, these statistics cannot be associated with the results in Figure 5.7. However, in Table 5.3 it is clear that both the mean and the std of a increase as $\mathcal{E}[\sigma_{AS}]$ increases. Hence, the statistics of the channel error variance a can be associated with the results presented in Figure 5.7: In the macro environments and for any fixed SNR value, Pr_{bf} increases as the std of a increases (the mean of a remains almost the same in all macro environments) or, equivalently, as the $\mathcal{E}[\sigma_{AS}]$ increases. However, in the urban micro environment, Pr_{bf} seems to deteriorate, due to the very high mean and std of a (compared to the macro environments).

Table 5.3: Statistics of channel error variance and feedback quality

Environment	a		$\frac{\ \hat{\mathbf{h}}^{(i+1)j}\ _2}{a}$	
	mean	std	mean	std
Suburban macro	9.2	31.6	1.7	1.6
Urban macro $\mathcal{E}[\sigma_{AS}] = 8^\circ$	9.8	46.2	1.7	1.6
Urban macro $\mathcal{E}[\sigma_{AS}] = 15^\circ$	10.7	50.6	1.7	1.6
Urban micro	16.9	141.7	1.7	1.5

⁵The higher this parameter is, the better “knowledge” the transmitter has for the channel.

(2) CCI model simulation results

In Figure 5.8 Pr_{bf} is plotted versus the SNR for the CCI model and different operational channels. In this model, for any fixed SNR value, Pr_{bf} is inversely proportional to the statistics of a or, equivalently, to the $\mathcal{E}[\sigma_{AS}]$, (practically, Pr_{bf} decreases with the following order, with respect to the operational environment: suburban macro, urban macro $\mathcal{E}[\sigma_{AS}] = 8^\circ$, urban macro $\mathcal{E}[\sigma_{AS}] = 15^\circ$, urban micro). This result can also be explained as follows: the correlation between the transmit antenna elements is inversely proportional to the $\mathcal{E}[\sigma_{AS}]$, as shown in Table 5.2. A high correlation, and hence, a small $\mathcal{E}[\sigma_{AS}]$, increases the disparity between the eigenvalues of Σ_j , a fact that causes an increase in Pr_{bf} . This result agrees with the results presented in [47] for the CCI model and is consistent with the notion of water-filling along the channel modes⁶.

5.4 Simulations for MISO 4×1 Rician fading channels

In the previous section Rayleigh fading MIMO channels were simulated and studied. The combined CMI-CCI model can occur even with spatially correlated MIMO channels with a Rayleigh long-term pdf, when a short-term feedback model is employed, (i.e. when $\mathbf{R}_s \neq 0$, see discussion for the CMI model in Chapter 2). The fact that the combined CMI-CCI model can also occur in spatially correlated MIMO Rayleigh fading channels when a long-term feedback model is employed (i.e. when $\mathbf{R}_s = 0$) is just a weakness of the 3GPP model and of the limited number of simulation drops and frames, (see discussion for the CCI model in the previous section). However, in the simulations presented in the previous section, the combined CMI-CCI model was totally “ignored” and the “conventional” CMI/CCI were used as short/long-term models, respectively.

Spatially correlated or uncorrelated with non-unit covariance matrix MIMO Rician fading channels and represented by the combined CMI-CCI model, both as a short and

⁶A stochastic water-filling algorithm is used to allocate the available power to the eigenvectors of Σ_j [69]. The higher the disparity between $\lambda_1(\Sigma_j)$ and $\lambda_2(\Sigma_j)$ the more power is allocated to the dominant eigenvector of Σ_j . Statistically, in some drops all power is allocated to the dominant eigenvector of Σ_j and hence, beamforming achieves ergodic capacity in these drops. The more often this happens (i.e. in environments with higher correlation), the higher Pr_{bf} is.

long-term feedback model, when $\mathbf{R}_s \neq \mathbf{0}$ and $\mathbf{R}_s = \mathbf{0}$, respectively. According to the spatial channel model of 3GPP, the operational environment that can simulate a Rician channel and hence, fit to the combined CMI-CCI model, is the urban micro environment. This is due to the fact that in urban micro environments there is a probability of existence of a Line of Sight (LOS) component, (in suburban or urban macro environments this probability is zero). Especially for the long-term combined CMI-CCI feedback model, the LOS component is the channel mean information.

In the following, using the MIMO channel simulation model of [87] (described in the previous sections of this chapter), the ergodic beamforming capacity achieved by the optimum beamformer and the optimality of beamforming condition are tested for the urban micro environment with a LOS component (which is an optional simulation feature of the 3GPP model) and for the following simulation parameters [97]:

- 3-sector cellular system,
- $N_{drops} = 10^2$,
- $N_{frames} = 10^2$,
- $F = 6, S = 20$,
- $N = 4, M = 1$ (i.e. MISO 4×1),
- $f_c = 2.4\text{GHz}$,
- inter-element distance at the transmit array antenna $\lambda/2$,
- velocity of the mobile station $\|v\|_2 = 20\text{km/h}$
- $T_{frame} = 9.2\text{ms}$, (this frame duration is equal to the channel coherence time T_c , which results from the system operating frequency $f_c = 2.4\text{GHz}$ and the MS velocity $\|v\|_2 = 20\text{km/h}$, [98]).

Moreover, the MS is assumed to move around the main⁷ BS within a distance⁸ $d < 300\text{m}$ and is forced⁹ to have LOS communication with the (main) BS.

The elements of the channel vector at the i^{th} frame and j^{th} drop are expressed by the following equation ([87]):

$$\begin{aligned}
\mathbf{h}_n^{ij} = & \sigma_{SF} \sqrt{\frac{13 - 0.03d}{14 - 0.03d}} \left(\sqrt{G_{MS}(\theta_{MS})G_{BS}(\theta_{BS})} \right. \\
& \times \exp\left(\sqrt{-1}[(n-1)\pi \sin(\theta_{BS}) + \Phi_{LOS}]\right) \\
& \times \exp\left(\sqrt{-1}k\|v\|_2 \cos((\theta_{MS} - \theta_v)t)\right) \\
& + \sqrt{\frac{1}{14 - 0.03d}} \sum_{f=1}^F \left(\sqrt{\frac{P_f \sigma_{SF}}{S}} \sum_{s=1}^S \left(\sqrt{G_{MS}(\theta_{f,s,AoA})G_{BS}(\theta_{f,s,AoD})} \right. \right. \\
& \times \exp\left(\sqrt{-1}[(n-1)\pi \sin(\theta_{f,s,AoD}) + \Phi_{f,s}]\right) \\
& \left. \left. \times \exp\left(\sqrt{-1}k\|v\|_2 \cos((\theta_{f,s,AoA} - \theta_v)t)\right) \right) \right) - m_n^j \tag{5.9}
\end{aligned}$$

where $n = 1, \dots, 4$, θ_{BS}/θ_{MS} are the AoD/AoA of the LOS component, respectively, and Φ_{LOS} is the phase of the LOS component. Again it is assumed that all transmit/receive antenna elements are omnidirectional in azimuth, with $G_{BS} = G_{MS} = 1$. Moreover, m_n^j is the mean of the second summand in (5.9), calculated over all frames of the j^{th} drop¹⁰.

5.4.1 Simulation results for the ergodic beamforming capacity

The ergodic beamforming capacity achieved by the optimum beamformer (see Theorem 3.1 in Chapter 3) is compared with the average mutual information achieved by

⁷As “main” BS is described the BS in which the MS physically exists and moves (practically it is always the first sector of the first cell, as shown in Figure 5.1). The “main” BS is different from the “serving” BS, which is the BS with the strongest signal/power.

⁸According to 3GPP, the probability of existence of a LOS component is zero for distances greater than 300m.

⁹According to the simulation model, a MS with a distance less than 300m away from the main BS does not have necessarily a LOS communication with the main BS. The probability of existence of a LOS component is a function inversely proportional to distance, [87, page 26].

¹⁰This term is used in order to compensate for the non-zero mean of scattering, which is not exactly Rayleigh distributed in each drop: this is due to the limited number of frames, paths and sub-paths, used by the simulation model of 3GPP.

the max SNR beamformer¹¹, in the context of both the short and long-term combined CMI-CCI model:

(1) Short-term feedback model simulation results

In the short-term combined CMI-CCI model, at the j^{th} drop the channel covariance information Σ_j , (which is calculated over all frames of the drop), is expressed by equation (5.4). Moreover, each channel sample \mathbf{h}^{ij} (i^{th} frame, j^{th} drop) that is fed back to the transmitter represents the (dynamic) channel mean information¹² which is used along with Σ_j , which represents the channel error covariance, in Theorem 3.1 (Chapter 3) in order to calculate the optimum beamformer $\mathbf{v}_{\text{opt}}^{ij}$. In this manner the optimum beamformer is dynamically calculated in each frame. The corresponding max SNR beamformer, denoted as $\mathbf{v}_{\text{maxSNR}}^{ij}$, is the dominant eigenvector of the channel correlation matrix:

$$\mathbf{C}_{ij} = \Sigma_j + (\mathbf{h}^{ij})^\dagger \mathbf{h}^{ij} \quad (5.10)$$

The ergodic beamforming capacity, calculated over all drops and frames, achieved by the optimum beamformer in the short-term feedback model is expressed by the following equation:

$$C_{\text{bf}}^{\text{st}}(\text{SNR}) = \frac{1}{N_{\text{drops}} N_{\text{frames}}} \sum_{j=1}^{N_{\text{drops}}} \sum_{i=1}^{N_{\text{frames}}} \log_2 \left(1 + \text{SNR} |(\mathbf{h}^{ij} + \mathbf{h}_w^{ij} \Sigma_j^{1/2})(\mathbf{v}_{\text{opt}}^{ij})^\dagger|^2 \right) \quad (5.11)$$

The average mutual information, calculated over all drops and frames, achieved by the max SNR beamformer in the short-term feedback model is expressed as follows:

$$\mathcal{I}_{\text{maxSNR}}^{\text{st}}(\text{SNR}) = \frac{1}{N_{\text{drops}} N_{\text{frames}}} \sum_{j=1}^{N_{\text{drops}}} \sum_{i=1}^{N_{\text{frames}}} \log_2 \left(1 + \text{SNR} |(\mathbf{h}^{ij} + \mathbf{h}_w^{ij} \Sigma_j^{1/2})(\mathbf{v}_{\text{maxSNR}}^{ij})^\dagger|^2 \right) \quad (5.12)$$

¹¹As shown in [75], the max SNR beamformer is a low-complexity near-optimum beamformer that coincides with the dominant eigenvector of the channel transmit correlation matrix.

¹²In these simulations we use the feedback samples as a channel mean information exactly when they arrive from the receiver and we do not consider any estimation of the real channel (i.e. of the next frame), as we did in the previous section with (5.5).

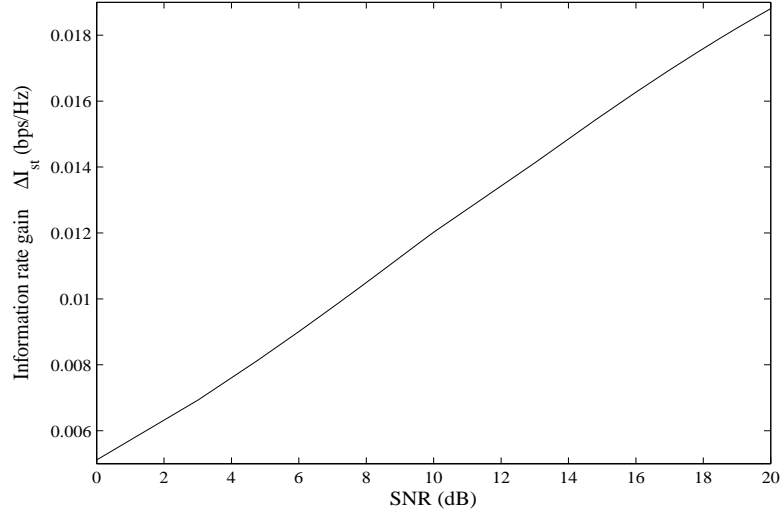


Figure 5.9: $\Delta \mathcal{I}_{st}$ vs. SNR.

In both equations (5.11) and (5.12), $\mathbf{h}_w^{ij} \in \mathbb{C}^{1 \times N}$, $\forall \{i, j\}$, is a zero mean complex Gaussian random vector with unit covariance matrix.

The information rate gain of the optimum beamformer with respect to the max SNR beamformer, defined as $\Delta \mathcal{I}_{st} = C_{bf}^{st} - \mathcal{I}_{\max SNR}^{st}$, is plotted in Figure 5.9. In this figure it can be observed that $\Delta \mathcal{I}_{st}$ increases with the SNR, however, it is very small for all SNR values: 0.0119bps/Hz and 0.0193bps/Hz for SNR = 10dB and 20dB, respectively.

(2) Long-term feedback model simulation results

At the j^{th} drop, the channel mean $\bar{\mathbf{h}}^j$ and covariance Σ_j are expressed by equations (5.3) and (5.4), respectively. Using Σ_j and $\bar{\mathbf{h}}^j$ in Theorem 3.1 the optimum beamformer during the j^{th} drop, $\mathbf{v}_{\text{opt}}^j$, can be calculated. Note that in this model the optimum beamformer is calculated only once in each drop. The corresponding max SNR beamformer, denoted as $\mathbf{v}_{\text{maxSNR}}^j$, is the dominant eigenvector of the channel correlation matrix:

$$\mathbf{C}_j = \Sigma_j + (\bar{\mathbf{h}}^j)^\dagger \bar{\mathbf{h}}^j \quad (5.13)$$

The ergodic beamforming capacity, calculated over all drops and frames, achieved by the optimum beamformer in the long-term feedback model is expressed as follows:

$$C_{\text{bf}}^{\text{lt}}(\text{SNR}) = \frac{1}{N_{\text{drops}}} \sum_{j=1}^{N_{\text{drops}}} \mathcal{E}_{\mathbf{h}_w} \left[\log_2 \left(1 + \text{SNR} |(\bar{\mathbf{h}}^j + \mathbf{h}_w \Sigma_j^{1/2})(\mathbf{v}_{\text{opt}}^j)^\dagger|^2 \right) \right] \quad (5.14)$$

The average mutual information, calculated over all drops and frames, achieved by the max SNR beamformer in the long-term feedback model is expressed as follows:

$$\mathcal{I}_{\text{maxSNR}}^{\text{lt}}(\text{SNR}) = \frac{1}{N_{\text{drops}}} \sum_{j=1}^{N_{\text{drops}}} \mathcal{E}_{\mathbf{h}_w} \left[\log_2 \left(1 + \text{SNR} |(\bar{\mathbf{h}}^j + \mathbf{h}_w \Sigma_j^{1/2})(\mathbf{v}_{\text{maxSNR}}^j)^\dagger|^2 \right) \right] \quad (5.15)$$

In Figure 5.10 the information rate gain $\Delta \mathcal{I}_{\text{lt}} = C_{\text{bf}}^{\text{lt}} - \mathcal{I}_{\text{maxSNR}}^{\text{lt}}$, is plotted versus the SNR. Also for this feedback model the gain is very small for all SNR values (it does not exceed the value 13.5×10^{-8} even for $\text{SNR} = 20\text{dB}$).

(3) Comparison between the short and long-term channel feedback models

In Figure 5.11 $C_{\text{bf}}^{\text{st}}$, $C_{\text{bf}}^{\text{lt}}$ and the relative capacity gain, calculated as $(C_{\text{bf}}^{\text{st}} - C_{\text{bf}}^{\text{lt}})/C_{\text{bf}}^{\text{lt}} \times 100$, are plotted versus the SNR. It can be observed that:

a. The short-term model achieves higher ergodic beamforming capacity than the long-term model for all SNR values.

b. The difference $(C_{\text{bf}}^{\text{st}} - C_{\text{bf}}^{\text{lt}})$ increases with the SNR (for $\text{SNR} = 0\text{dB}$ it is $\simeq 0.337\text{bps/Hz}$ and for $\text{SNR} = 20\text{dB}$ it becomes $\simeq 0.6\text{bps/Hz}$), however, the relative capacity gain de-

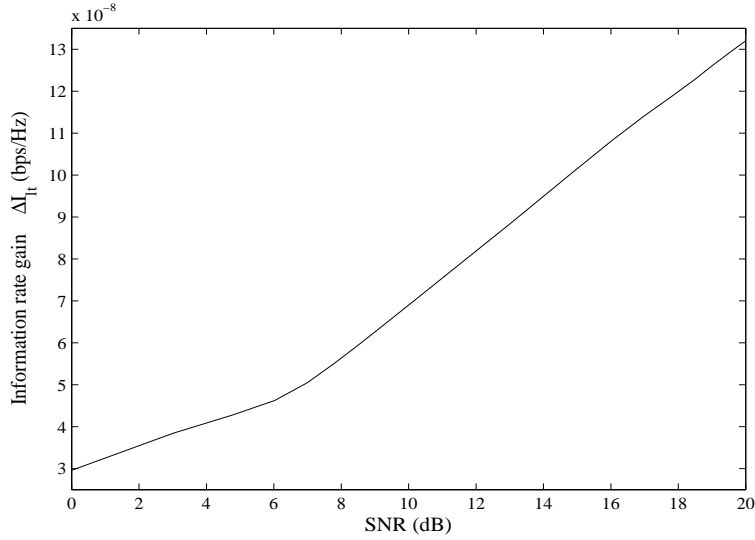


Figure 5.10: $\Delta\mathcal{I}_t$ vs. SNR.

creases with the SNR and does not exceed 16% (for SNR = 0 – 20dB).

5.4.2 Simulation results for the optimality of beamforming

In the following, the optimality of beamforming condition (2.34), is tested for its validity, for the short and long-term feedback models. For the short and long-term models, a probability is defined, denoted as $\text{Pr}_{\text{bf}}^{\text{st}}$ and $\text{Pr}_{\text{bf}}^{\text{lt}}$, respectively, which are calculated with (4.34), (Chapter 4), and are functions of the SNR:

$$\text{Pr}_{\text{bf}}^{\text{st/lt}}(\text{SNR}) = \frac{\text{Number of times condition (2.34) is satisfied}}{\text{Number of times condition (2.34) is tested}} \quad (5.16)$$

For the short-term model the optimality condition (2.34) is tested for $N_{\text{drops}} \times N_{\text{frames}} = 10^4$ times, whereas for the long-term model, condition (2.34) is tested for $N_{\text{drops}} = 10^2$ times.

In the short-term model, it is $\text{Pr}_{\text{bf}}^{\text{st}} \geq 0.99$ for all SNR values (0-20dB), which indicates that the optimum beamformer almost always achieves ergodic capacity, in the context of this feedback model.

In the long-term model, it is $\text{Pr}_{\text{bf}}^{\text{lt}} = 1$ for all SNR values (for SNR = 0 – 20dB), indicating that the optimum beamformer always achieves ergodic capacity.

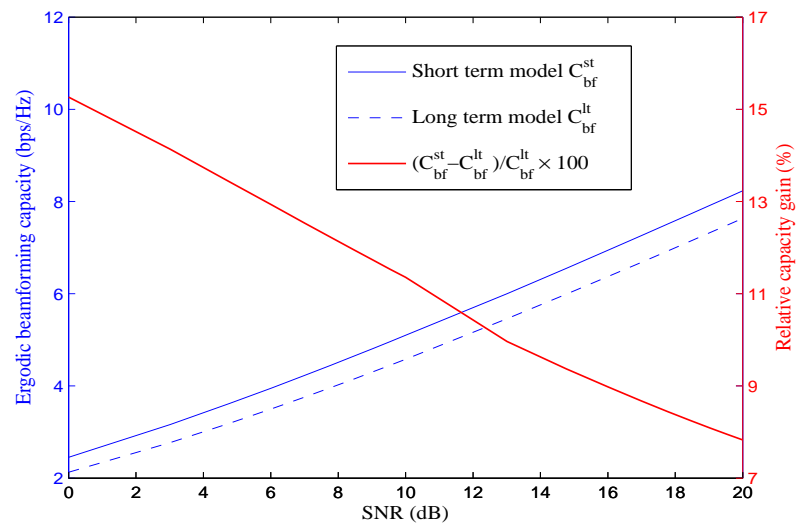
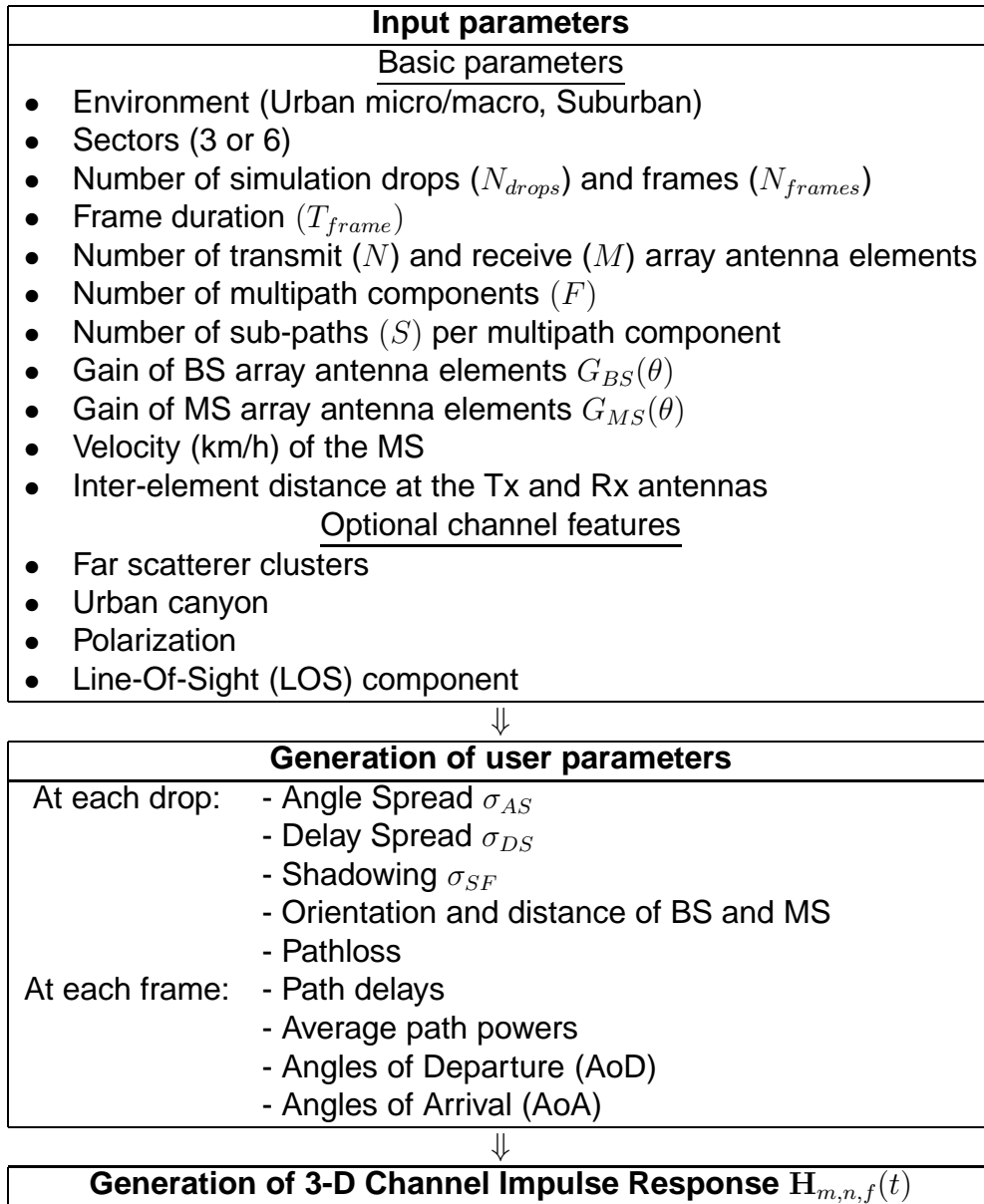


Figure 5.11: C_{bf}^{st} , C_{bf}^{lt} and $\left(\frac{C_{bf}^{st}-C_{bf}^{lt}}{C_{bf}^{lt}} \times 100\right)$ vs. SNR.

Table 5.1: Channel simulation process



Chapter 6

CONCLUSIONS AND FUTURE WORK

6.1 Rate-optimum beamforming transmission in MISO and MIMO Rician fading channels

In Chapters 3 and 4 of this doctoral thesis was studied the solution of the multi-dimensional and hence, computationally complex optimum beamforming problem - i.e. the beamforming transmission that maximizes the average mutual information between transmitter and receiver and achieves ergodic beamforming capacity - in spatially correlated or uncorrelated with non-unit covariance matrix MIMO Rician flat fading channels. The importance of this solution is summarized below:

- a. The optimum beamforming transmission reduces the complexity of the system and as a consequence the overall cost.
- b. The ergodic beamforming capacity achieved by the optimum beamformer is very close to the ergodic capacity (which is achieved by higher rank transmission schemes) for many operational scenarios/channels.
- c. The optimum beamformer achieves ergodic capacity when the necessary and sufficient optimality of beamforming condition is satisfied in a channel.

The aforementioned optimization problem was transformed into a simple 1-D optimization problem which can be subsequently solved using standard 1-D search algorithms, (gradient based or direct search methods). The proof of this transformation was based on geometrical properties, basis transformations and the Karush-Kuhn-Tucker (KKT) conditions. Especially for MIMO $2 \times M$ systems or MIMO $N \times M$ systems with $rank\{\mathbf{R}_t\} \leq 2$, it was proven that the aforementioned 1-D optimization problem can be further simplified. This proof was based on a geometric approach, where the definition of the external

product between vectors in high-dimensional vector spaces was exploited.

The computational complexity of the proposed 1-D scheme (runtime in seconds per iteration) was presented, via simulations, with respect to:

- a. The number of channel samples, which are used for the calculation of the ergodic beamforming capacity (using Monte Carlo integration).
- b. The number of transmit antenna elements N .

The aforementioned complexity was compared with the corresponding complexity of the following multi-dimensional algorithms:

- a. An interior-point algorithm with logarithmic barrier function (the “fmincon” Matlab function was employed), for MIMO and MISO systems.
- b. An iterative asymptotic (and hence, sub-optimum) approach for MISO systems (algorithm developed in [50]).

Results for Uniform Linear Array (ULA) array antennas, demonstrated that the 1-D scheme has significantly lower computational complexity:

- a. For the simulated scenarios related to MISO systems, the runtime of the 1-D algorithm is on average ~ 5 to 7 times faster than the interior-point method and ~ 2 to 10 times faster than the asymptotic approach.
- b. For the simulated scenarios related to MIMO systems, the runtime of the 1-D algorithm it is approximately 8.5 times faster than the interior-point method.

The reduced complexity can be exploited to either reduce cost by using devices with lower processing power or in order to:

- a. Operate in environments with smaller coherence time, proportional to the relative processing gain, and hence, support operational scenarios with higher mobility, (i.e. higher speeds, proportional to the relative processing gain).
- b. Increase the available processing power required by the system for other supplementary techniques.

Furthermore, the ergodic beamforming capacity achieved by the optimum beamformer, for MIMO and MISO systems, was compared with the average mutual information achieved by the max SNR beamformer. Simulations showed that the optimum beamformer always achieves a higher information rate (in bps/Hz) than the max SNR beamformer. For the simulation model and scenarios presented in this work, the (instantaneous) relative information rate gain can be up to 10%, however, the mean relative information rate gain does not exceed 5%. Hence, for the simulation model and scenarios of this work¹, the max SNR beamformer can be used as an alternative beamforming scheme with near-optimum information rate performance.

It is important to note that the solution of the optimum beamforming problem (as presented with Theorems 3.1, 3.2, 4.1 and 4.2) is not only important due to the reasons referred to at the beginning of this section, but also due to the following two reasons:

a. In the context of the solution, an infinite-series expression was derived for the calculation of the ergodic beamforming capacity, which converges very fast to the corresponding Monte Carlo calculation, (a few tens of terms are required).

b. In the context of the solution, a closed-form expression was derived (as a function of a unique parameter) for the vector set where the optimum beamformer belongs. This set defines a continuous trajectory on the unit-radius Euclidean ball. This closed-form expression may be exploited in the context of future work in order to provide an alternative and less complex solution - compared to currently used interior-point and sub-optimum methods - for the calculation of the transmission scheme (spatial precoding) that achieves ergodic capacity, under the combined CMI-CCI model.

As referred to at the beginning of this section, the optimum beamformer achieves ergodic capacity when the necessary and sufficient optimality of beamforming condition is satisfied. This condition was studied in this doctoral thesis, for the long-term combined CMI-CCI model with Kronecker structured covariance (i.e. separable transmit and receive covariance matrices). The parameters that affect the optimality condition and hence, the

¹i.e. for ULAs and the “two-path delay spread” correlation model.

optimality region were studied via simulations, leading to important observations. The results showed that the CDIT model under consideration (long-term combined CMI-CCI) incorporates and combines characteristics from both MIMO Rayleigh and spatially uncorrelated with unit covariance matrix MIMO Rician flat fading channels (i.e. the CCI and CMI model, respectively). Moreover, the model appears to have some new and unique characteristics with respect to ϕ (the angle between the dominant right singular vector of the channel mean matrix and the dominant eigenvector of the channel transmit covariance matrix) and ρ_t (the transmit antenna correlation coefficient, for ULA antennas). The presented analysis for the “production” of the optimality region can be valuable during the system design and deployment phases: if information for the targeted operational scenarios/channels is available, it can be used to produce the optimality regions and hence, decide if optimum beamforming can be employed as the main transmission strategy, which ultimately leads to reducing the system's complexity and cost. The most important observations related to the study of the optimality of beamforming condition for the combined CMI-CCI model are summarized below:

Observation 1. Beamforming becomes the optimum strategy as the singular value of the channel mean increases.

Observation 2. Beamforming becomes the optimum strategy as the channel variance β decreases.

Observation 3. Beamforming becomes the optimum strategy as the SNR decreases.

Observation 4. Beamforming becomes the optimum strategy as ϕ decreases.

Observation 5. Relatively low channel variance leads to abrupt increase of the optimality region for relatively high ρ_t values, (i.e. high disparity for the eigenvalues of the channel transmit covariance matrix). However, this effect seems to vanish for higher β and/or ϕ values, which “resist” to the optimality of beamforming, as referred to Observations 2 and 4 above. Moreover, in the low- ρ_t regime, the optimality region seems to be rather “insensitive” to an increase of the SNR, β and ϕ .

Observation 6. Beamforming becomes the optimum strategy as the number of receive antenna elements (M) decreases.

6.2 Simulations for different operational environments

In Chapter 5 simulations were performed for MISO 2×1 Rayleigh fading channel and different operational environments (urban micro/macroucellular, suburban macrocellular), which were produced using the channel model proposed by 3GPP. The simulated channels were tested for different channel feedback information models: perfect CSI at the transmitter (Perfect CSIT), unknown channel to the transmitter (Unknown Channel), CMI and CCI.

The results showed that the CCI model outperforms the CMI model in all environments, whereas the ergodic capacity achieved by the Perfect CSIT and the Unknown Channel models are the upper and lower information rate bounds, respectively, in all cases. The ergodic capacity of the CCI model (for all SNR) is very close to the curves for the Perfect CSIT model, for the suburban and the urban macrocellular $\mathcal{E}[\sigma_{AS}] = 8^\circ$ environments. Therefore, for these (two) environments, the solution of the computationally complex optimization problem for the calculation of the transmission strategy that achieves ergodic capacity under the long-term combined CMI-CCI model is practically meaningless and inefficient, (since the solution of the CCI model can be employed instead). On the other hand, the solution of the aforementioned optimization problem may be meaningful in urban micro and macrocellular $\mathcal{E}[\sigma_{AS}] = 15^\circ$ environments, where the ergodic capacity achieved by the CCI model shows a higher gap with respect to the ergodic capacity achieved by the Perfect CSIT model.

Moreover, simulations were performed for the probability of the optimality of beamforming, Pr_{bf} , for MISO 2×1 systems and the CMI and CCI models. This probability decreases with the SNR in all environments, for both models (CMI and CCI). In both models, the urban microcellular environment shows the lowest probability, which is logical due to the wider angular spread and the multiple multipath clusters in such environments. Higher

probability can be observed for macrocellular (suburban/urban) environments. From the curves related to the CMI model it can be observed that in the SNR range 0-18dB it is $\Pr_{\text{bf}} \geq 0.5$. For the CCI model it is:

a. The suburban environments and the urban macrocellular environments with $\mathcal{E}[\sigma_{AS}] = 8^\circ$ have $\Pr_{\text{bf}} \geq 0.6$ in the SNR range 0-20dB.

b. The urban microcellular environments and macrocellular environments with $\mathcal{E}[\sigma_{AS}] = 15^\circ$ have $\Pr_{\text{bf}} \geq 0.45$ and $\Pr_{\text{bf}} \geq 0.5$, respectively, in the SNR range 0-15dB.

Moreover, simulation were performed for MISO 4×1 Rician fading channels. Again, the 3GPP channel model was exploited in order to produce channel samples for urban microcellular operational environments with a LOS component, which simulate best MISO Rician flat fading channels and hence, the long-term combined CMI-CCI model. In the context of these simulations the ergodic beamforming capacity achieved by the optimum beamformer was compared with the average mutual information achieved by the max SNR beamformer, for the short and the long-term combined CMI-CCI feedback information model. Results, which were produced for ULA transmit antennas with $\lambda/2$ inter-element spacing, indicate that the max SNR beamformer performs very close to the optimum beamformer, for both feedback models. Comparing the two feedback models, the short-term model shows higher optimum ergodic beamforming capacity (but not exceeding 16% mean relative information rate gain), however, with increased complexity. Moreover, in both models, optimum beamforming achieves ergodic capacity in the SNR range 0-20dB. Generally, it can be concluded that the optimum beamformer used along with the short-term feedback model is the best transmission strategy for urban microcellular environments: it achieves ergodic capacity and is higher than the corresponding ergodic capacity achieved by the optimum beamformer used along with the long-term feedback model. However, if complexity issues are more important than the capacity performance of a system, then the long-term model with the max SNR beamformer is the best combination of feedback model and beamforming scheme to employ, respectively, since it almost achieves (long-term) ergodic capacity with the least computational complexity and

software/hardware cost.

6.3 Future work

Some ideas for future work are summarized below:

a. Study the ergodic capacity, the ergodic beamforming capacity and the optimality of beamforming condition, for MIMO $N \times M$ systems under different feedback information models (CMI, CCI, etc.), for different operational environments with measured data and site specific deterministic ray tracing propagation models.

b. Use of the closed-form expression of the vector set where the optimum beamformer belongs, in order to provide an alternative and less complex solution - compared to currently used interior-point and sub-optimum methods - for the calculation of the transmission strategy that achieves ergodic capacity, under the combined CMI-CCI model.

c. Study of the optimum beamforming problem and the optimality of beamforming condition in channels with complex Gaussian Channel Distribution Information (CDI) models (i.e. CCI, CMI, combined CMI-CCI) at both ends of the radio link (i.e. assumption of a CDIR-CDIT model).

d. Study the performance of the presented optimum beamformer in the context of low energy consumption Green systems.

e. Expand the analysis presented here to very large scale or massive MIMO scenarios.

LIST OF ABBREVIATIONS

CDI	Channel Distribution Information
CDIR	Channel Distribution Information at the Receiver
CDIT	Channel Distribution Information at the Transmitter
CDMA	Code Division Multiple Access
CCI	Channel Covariance Information
CMI	Channel Mean Information
CSD	Cyclic Shift Diversity
CSI	Channel State Information
CSIT	Channel State Information at the Transmitter
i.i.d	Independent identically distributed
LOS	Line Of Sight
LTE	Long Term Evolution
MBWA	Mobile Broadband Wireless Access
MIMO	Multiple Input Multiple Output
MISO	Multiple Input Single Output
MRC	Maximum Ratio Combining
OFDM	Orthogonal Frequency Division Multiplexing
OFDMA	Orthogonal Frequency Division Multiple Access
SDMA	Space Division Multiple Access
SFIR	Spatial Filtering for Interference Reduction
SINR	Signal to Interference plus Noise Ratio
SISO	Single Input Single Output
SNR	Signal to Noise Ratio
STBC	Space-Time Block Codes

STC	Space-Time Coding
STTC	Space-Time Trellis Codes
TDM	Time Division Multiplexing
TDMA	Time Division Multiple Access

BIBLIOGRAPHY

- [1] L. C. Van Atta, "Electromagnetic reflection", *U.S. Patent 2908002*, Oct. 6, 1959.
- [2] P. W. Howells, "Intermediate frequency sidelobe canceller", *U.S. Patent 3202990*, Aug. 24, 1965.
- [3] P. W. Howells, "Exploration in fixed and adaptive resolution at GE and SURC", Special Issue on Adaptive Antennas, *IEEE Trans. Antennas Propag.*, vol. AP-24, no. 5, pp. 575-584, Sept. 1976.
- [4] S. P. Applebaum, *Adaptive Arrays*, Syracuse University Research Corporation, Rep. SPL TR66-1, Aug. 1966.
- [5] B. Widrow, *Adaptive Filters I: Fundamentals*, Stanford University Electronics Laboratories, System Theory Laboratory, Center for System Research, Rep. SU-SEL-66-12, Tech. Rep. 6764-6, Dec. 1966.
- [6] B. Widrow, "Adaptive Filters", in *Aspects of Network and System Theory*, edited by R. E. Kalman and N. DeClaris, Holt, Rinehart and Winston, New York, 1971, Ch. 5.
- [7] B. Widrow, P. E. Mantley, L. J. Griffiths, and B. B. Goode, "Adaptive antenna systems", *IEEE Proc.*, vol. 55, Dec. 1967.
- [8] J. Capon, "Applications of detection and estimation theory to large array seismology", *IEEE Proc.*, vol. 58, pp. 760-770, May 1970.
- [9] Lal Chand Godara, *Smart Antennas*, CRC Press, 2004.
- [10] G. V. Tsoulos, J. P. McGeehan and M. A. Beach, "Space Division Multiple Access (SDMA) Field Trials - Part I: Tracking and BER Performance", *IEE Proc. on Radar, Sonar and Navigation*, Special Issue on Antenna Array Processing Techniques, pp. 73-78, February 1998.

- [11] M. A. Beach, J. P. McGeehan, C. M. Simmonds, P. Howard, P. Darwood, G. V. Tsoulos, A. R. Nix, P. Hafezi, and Y. Sun, "European Smart Antennas Testbeds", *Journal on Commun. Networks*, vol. 2, no. 4, pp. 317-324, Dec. 2000.
- [12] www.arraycomm.com
- [13] G.V.Tsoulos, "Smart antennas for mobile communication systems: Benefits and challenges", *IEE J. Electronics and Commun. Eng.*, vol. 11, no. 2, pp. 84-94, April 1999.
- [14] Robert A. Monzingo and Thomas W. Miller, *Introduction to Adaptive Arrays*, Wiley, 1980.
- [15] Howard Huang, Constantinos B. Papadias, and Sivarama Venkatesan, *MIMO Communications for Cellular Networks*, Springer, 2012.
- [16] N. Seshadri and J. Winters, "Two signaling schemes for improving the error performance of frequency-division-duplex (FDD) transmission systems using transmitter antenna diversity", *Int. J. Wireless Information Networks*, vol. 1, no. 1, pp. 49-60, Jan. 1994.
- [17] J. Guey, M. Fitz, M. Bell, and W. Kuo, "Signal design for transmitter diversity wireless communication systems over Rayleigh fading channels", *in Proceedings of Vehicular Technology Conference (VTC), Spring 1996*.
- [18] V. Tarokh, N. Seshadri, and A. R. Calderbank, "Space-time codes for high data rate wireless communication: Performance criterion and code construction", *IEEE Trans. Inf. Theory*, vol. 44, no. 2, pp. 744-765, Mar. 1998.
- [19] V. Tarokh, H. Jafarkhani, and A. R. Calderbank, "Space-time block codes from orthogonal designs", *IEEE Trans. Inf. Theory*, vol. 45, no. 5, pp. 1456-1467, July 1999.
- [20] S. Alamouti, "A simple transmit diversity technique for wireless communications", *IEEE J. Sel. Areas Commun.*, vol. 16, no. 8, pp. 1451-1458, Oct. 1998.

- [21] C. Papadias, "On the spectral efficiency of space-time spreading schemes for multiple antenna CDMA systems", in *Proceeding of Asilomar Conference on Signals, Systems and Computers, 1999*.
- [22] B. Hochwald, T. Marzetta, C. Papadias, "A transmitter diversity scheme for wideband CDMA systems based on space-time spreading", *IEEE J. Sel. Areas Commun.*, vol. 19, no. 1, pp. 48-60, Jan. 2001.
- [23] T. Lo, "Maximal ratio transmission", *IEEE Trans. Commun.*, pp. 1458-1461, Oct. 1999.
- [24] X. Feng and C. Leung, "A new optimal transmit and receive diversity scheme", in *Proceeding of PACRIM, 2001*.
- [25] D. Tse, P. Viswanath, *Fundamentals of Wireless Communication*, Cambridge University Press, New York, 2005.
- [26] A. Paulraj, D. Gore, R. Nabarand, and H. Bölcskei, "An overview of MIMO communications - A key to Gigabit wireless", *IEEE Proceedings*, vol. 92, no. 2, pp. 198-218, Feb. 2004.
- [27] J. Winters, "On the capacity of radio communication systems with diversity in a Rayleigh fading environment", *IEEE J. Select. Areas Commun.*, vol. 5, pp. 871-878, June 1987.
- [28] G. J. Foschini, and M. J. Gans, "On limits of wireless communications in a fading environment when using multiple antennas", *Wireless Pers. Commun.*, vol. 6, no. 3, pp. 311-335, Mar. 1998.
- [29] E. Telatar, "Capacity of multi-antenna Gaussian channels", *European Trans. Telecommun.*, vol. 10, no. 6, pp. 585-596, Nov. 1999.
- [30] A. Goldsmith, S. A. Jafar, N. Jindal, and S. Vishwanath, "Capacity limits of MIMO channels", *IEEE J. Select. Areas Commun.*, vol. 21, no. 5, pp. 687-702, Jun. 2003.

- [31] G. J. Foschini, D. Chiznik, M. Gans, C. Papadias, and R. A. Valenzuela, "Analysis and performance of some basic spacetime architectures", *IEEE J. Select. Areas Commun., Special Issue on MIMO Systems*, pt. I, vol. 21, pp. 303-320, Apr. 2003.
- [32] B. Hassibi and B. Hochwald, "Cayley differential unitary space-time codes", *IEEE Trans. Inform. Theory*, vol. 48, pp. 1485-1503, June 2002.
- [33] M. Hochwald, T. L. Marzetta, T. J. Richardson, W. Sweldens, and R. Urbanke, "Systematic design of unitary space-time constellations", *IEEE Trans. Inform. Theory*, vol. 46, pp. 1962-1973, Sept 2000.
- [34] S. Catreux, V. Erceg, D. Gesbert, and R. W. Heath, "Adaptive modulation and MIMO coding for broadband wireless data networks", *IEEE Commun. Mag.*, vol. 40, pp. 108-115, June 2002.
- [35] N. Al-Dhahir, "Overview and comparison of equalization schemes for space-time coded signals with application to EDGE", *IEEE Trans. Signal Processing*, vol. 50, pp. 2477-2488, Oct. 2002.
- [36] A. Lozano and C. Papadias, "Layered space-time receivers for frequency-selective wireless channels", *IEEE Trans. Commun.*, vol. 50, pp. 65-73, Jan. 2002.
- [37] N. Al-Dhahir, C. Fragouli, A. Stamoulis, W. Younis, and R. Calderbank, "Space-time processing for broadband wireless access", *IEEE Commun. Mag.*, vol. 40, pp. 136-142, Sept. 2002.
- [38] Chong and L. Milstein, "The performance of space-time spreading CDMA system with channel estimation errors", in *Proceedings of International Communications Conference (ICC), 2002*.
- [39] H. Huang, H. Viswanathan, and G. J. Foschini, "Multiple antennas in cellular CDMA systems: Transmission, detection and spectral efficiency", *IEEE Trans. Wireless Commun.*, vol. 1, pp. 383-392, July 2002.

- [40] Y. Li, J. Winters, and N. Sollenberger, "MIMO-OFDM for wireless communication: Signal detection with enhanced channel estimation", *IEEE Trans. Commun.*, vol. 50, pp. 1471-1477, Sept. 2002.
- [41] B. Lu, X. Wang, and Y. Li, "Iterative receivers for space-time block-coded OFDM systems in dispersive fading channels", *IEEE Trans. Wireless Commun.*, vol. 1, pp. 213-225, Apr. 2002.
- [42] Y. Xin and G. Giannakis, "High-rate space-time layered OFDM", *IEEE Commun. Lett.*, vol. 6, pp. 187-189, May 2002.
- [43] D. Gesbert, M. Shafi, D. S. Shiu, P. Smith, and A. Naguib, "From theory to practice: An overview of MIMO space-time coded wireless systems", *IEEE J. Select. Areas Commun., Special Issue on MIMO Systems*, pt. I, vol. 21, pp. 281-302, Apr. 2003.
- [44] M. Vu, and A. Paulraj, "Characterizing the capacity for MIMO wireless channels with non-zero mean and transmit covariance", *IEEE J. Select. Areas Commun.*, Special Issue on Optimization of MIMO Transceivers for Realistic Communication Networks, vol. 25, no. 7, pp. 1269-1283, Sep. 2007.
- [45] E. A. Jorswieck, A. Sezgin, H. Boche, and E. Costa, "Multiuser MIMO MAC with statistical CSI and MMSE receiver: feedback strategies and transmitter optimization", in *Proceedings of International Wireless Communications and Mobile Computing (IWCMC), 2006*.
- [46] E. Visotsky, and U. Madhow, "Space-time transmit precoding with imperfect feedback", *IEEE Trans. Inf. Theory*, vol. 47, no. 6, pp. 2632-2639, Sep. 2001.
- [47] S. A. Jafar, and A. Goldsmith, "Transmitter optimization and optimality of beamforming for multiple antenna systems with imperfect feedback", *IEEE Trans. Wireless Commun.*, vol. 3, no. 4, pp. 1165-1175, Jul. 2004.

- [48] E. A. Jorswieck, and H. Boche, "Channel capacity and capacity-range of beamforming in MIMO wireless systems under correlated fading with covariance feedback", *IEEE Trans. Wireless Commun.*, vol. 3, no. 5, pp. 1543-1553, Sep. 2004.
- [49] M. Vu, and A. Paulraj, "Capacity optimization for Rician correlated MIMO wireless channels", in *Proceeding of Asilomar Conference, 2005*.
- [50] J. Dumont, W. Hachem, S. Lasaulce, Ph. Loubaton, and J. Najim, "On the capacity achieving covariance matrix for Rician MIMO Channels: an asymptotic approach", *IEEE Trans. Inf. Theory*, vol. 56, no. 3, pp. 1048-1069, Mar. 2010.
- [51] F. Khalid and J. Speidel, "Advances in MIMO techniques for mobile communications - A survey", *Int. J. Commun., Network and System Sciences*, pp. 213-252, 2010.
- [52] M. S. Gast, *802.11 wireless networks: The definitive guide*, 2nd edition, O' Reilly, April 2005.
- [53] Wi-Fi Alliance, "WiFi CERTIFIED 802.11n draft 2.0: Longer-range, faster-throughput, multimedia grade WiFi networks", 2007.
- [54] IEEE Std 802.16-2004, "for local and metropolitan area networks Part 16: Air interface for fixed and mobile broadband wireless access systems", 1 Oct 2004.
- [55] IEEE Std 802.16e-2005 and IEEE Std 802.16-2004/Cor 1-2005 (Amendment and Corrigendum to IEEE Std 802.16-2004), "IEEE standard for local and metropolitan area networks Part 16: Air interface for fixed and mobile broadband wireless access systems amendment 2: Physical and medium access control layers for combined fixed and mobile operation in licenced bands and Corrigendum 1", 28 Feb. 2006.
- [56] J. G. Andrews, A. Ghosh, and R. Muhamed, "Fundamentals of WiMAX: Understanding broad-band wireless networking", Prentice Hall, 2007.
- [57] B. M. Bakmaz, Z. S. Bojkovic, D. A. Milovanovic, and M. R. Bakmaz, "Mobile broadband networking based on IEEE 802.20 standard", in *Proceeding of 8th International*

- Conference Telecommunications in Modern Satellite, Cable and Broadcasting Services (TELSIKS 2007), pp. 243-246, Sept. 2007.
- [58] IEEE 802.20-2008, "IEEE standard for local and metropolitan area networks Part 20: Air interface for mobile broadband wireless access systems supporting vehicular mobility - physical and media access control layer specification", Aug. 2008.
- [59] 3GPP TS 36.201 V8.1.0 (2007-11), "LTE physical layer - general description (Release 8)", 3GPP TSG RAN, 2007.
- [60] J. Zyren, "Overview of the 3GPP long term evolution physical layer", White Paper, Freescale Semiconductor, Inc., 2007.
- [61] A. Lapidoth and S. M. Moser, "Capacity bounds via duality with applications to multi-antenna systems on flat fading channels", *IEEE Trans. Inform. Theory*, vol. 49, no. 10, pp. 2426-2467, Oct. 2003.
- [62] T. Marzetta and B. Hochwald, "Capacity of a mobile multiple antenna communication link in Rayleigh flat fading", *IEEE Trans. Inform. Theory*, vol. 48, pp. 359-383, Feb. 2002.
- [63] L. Zheng and D. N. Tse, "Packing spheres in the Grassmann manifold: A geometric approach to the non-coherent multi-antenna channel", *IEEE Trans. Inform. Theory*, vol. 48, pp. 359-383, Feb. 2002.
- [64] T. Cover and J. Thomas, *Elements of Information Theory*, Wiley, New York, 1991.
- [65] C. Chuah, J. Kahn, and D. Tse, "Capacity of multi-antenna array systems in indoor wireless environments", in *Proceedings of GLOBECOM 1998*, pp. 1894-1899.
- [66] A. Paulraj, R. Nabar and D. Gore *Introduction to Space-Time Wireless Communications*, Cambridge University Press, Cambridge, 2003.
- [67] Athanasios Papoulis. *Probability, Random Variables, and Stochastic Processes*. McGraw-Hill, New York, NY, 1984.

- [68] D. Chizhik, J. Link P. Wolniasnky, R. Valenzuela, N. Costa, and K. Huber, "Multiple input multiple output measurements and modelling in Manhattan", *IEEE J. Sel. Areas Commun.*, vol. 21, no. 3, pp. 321-331, Apr. 2003.
- [69] A. M. Tulino, A. Lozano, and S. Verdu, "Capacity-achieving input covariance for single-user multi-antenna channels", *IEEE Trans. Wireless Commun.*, vol. 5, no. 3, pp. 662-671, Mar. 2006.
- [70] T. Kailath, A. Sayed, and H. Hassibi, *Linear Estimation*, Prentice Hall, 2000.
- [71] S. Simon and A. Moustakas, "Optimality of beamforming in multiple transmitter multiple receiver communication systems with partial channel knowledge", in *Proceedings of DIMACS Workshop Signal Processing Wireles Communications, DIMACS Center, Rutgers University, 2002*.
- [72] S. A. Jafar, and A. Goldsmith, "Beamforming capacity and SNR maximization for multiple antenna systems", in *Proceedings of Vehicular Technology Conference (VTC), Spring 2001*.
- [73] S. Srinivasa, and S. A. Jafar, "The optimality of transmit beamforming: a unified view", *IEEE Trans. Inf. Theory*, vol. 53, no. 4, pp. 1558-1567, Apr. 2007.
- [74] D. E. Kontaxis, G. V. Tsoulos, and S. Karaboyas, "Ergodic capacity optimization for single-stream beamforming transmission in MISO Rician fading channels", *IEEE Trans. Veh. Technol.*, vol. 62, no. 2, pp. 628-641, Feb. 2013.
- [75] G. Barriac, and U. Madhow, "Space-Time precoding for mean and covariance feedback: application to wideband OFDM", *IEEE Trans. Commun.*, vol. 54, no. 1, pp. 96-107, Jan. 2006.
- [76] Dimitri P. Bertsekas, *Nonlinear Programming*, Athena Scientific, 2nd Edition, 1999.
- [77] Stephen Boyd and Lieven Vandenberghe, *Convex Optimization*, Cambridge University Press 2004.

- [78] D. E. Kontaxis, G. V. Tsoulos, and S. Karaboyas, "Optimum beamforming for correlated Rician MISO channels", in *Proceedings of Vehicular Technology Conference (VTC), Spring 2011*.
- [79] Z. Q. Luo, W. K. Ma, A. M. Cho, Y. Ye, and S. Zhang, "Semidefinite relaxation of quadratic optimization problems", *IEEE Signal Processing Mag.*, Special Issue on Convex Optimization for Signal Processing, vol. 27, no. 3, pp. 20-34, May 2010.
- [80] R. A. Horn and C. R. Johnson, *Matrix Analysis*, Cambridge University Press, Cambridge, 1985.
- [81] Simon Haykin, *Adaptive Filter Theory*, Prentice Hall, 1996.
- [82] A. W. McDavid, and C. D. McMullen, "Generalizing cross products and Maxwell's equations to universal extra dimensions", <http://arxiv.org/abs/hep-ph/0609260v4>.
- [83] I. S. Gradshteyn and I. M. Ryzhik, *Table of Integrals, Series and Products*, 6th edition, New York: Academic, 1994.
- [84] E. D. Vagenas, P. Karadimas, and S. A. Kotsopoulos, "Ergodic capacity for the SIMO Nakagami-m channel", *EURASIP J. Wireless Commun. and Networking*, vol. 2009, Article ID 802067, 9 pages, 2009. doi:10.1155/2009/802067.
- [85] D. A. Zogas, G. K. Karagiannidis, "Infinite-series representations associated with the bivariate Rician distribution and their applications", *IEEE Trans. Commun.*, vol. 53, no. 11, pp. 1790-1794, Nov. 2005.
- [86] J. Salz, and J. Winters, "Effect of fading correlation on adaptive arrays in digital mobile radio", *IEEE Trans. Veh. Technol.*, vol. 43, no. 4, pp. 1049-1056, Nov. 1994.
- [87] 3GPP TR 25.996 V6.1.1 (2003-09).
- [88] D. Gesbert, H. Bolcskei, and D. A. Gore, et al., "Outdoor MIMO wireless channels: models and performance prediction", *IEEE Trans. Commun.*, vol. 50, no. 12, pp. 1926-1934, Dec. 2002.

- [89] T. Haustein and U. Kruger, "Smart geometrical antenna design exploiting the LOS component to enhance a MIMO system based on Rayleigh fading in indoor scenarios", in *Proceedings of Personal Indoor Mobile Radio Communications (PIMRC)*, 2003, pp. 1144-1148.
- [90] I. Sarris and A. R. Nix, "Design and performance assessment of high-capacity MIMO architectures in the presence of a line-of-sight component", *IEEE Trans. Veh. Technol.*, vol. 56, no.4, pp. 2194-2202, 2007.
- [91] F. Bohagen, P. Orten, and G. E. Oien, "Design of optimal high-rank line-of-sight MIMO channels", *IEEE Trans. Wireless Commun.*, vol. 6, no. 4, pp. 1420-1425, 2007.
- [92] L. Liu, W. Hong and H. Wang, et al., "Characterization of line of sight MIMO channel for fixed wireless communications" *IEEE Antennas Wirel. Propag. Lett.*, vol. 6, pp. 36-39, 2007.
- [93] D. E. Kontaxis, G. V. Tsoulos, and S. Karaboyas, "Beamforming capacity optimization for Rician MIMO wireless channels", *IEEE Wireless Commun. Lett.*, vol. 1, no. 3, pp. 257-260, June 2012.
- [94] D. E. Kontaxis, G. V. Tsoulos, G. E. Athanasiadou, and S. Karaboyas, "Optimality of transmit beamforming for spatially correlated MIMO Rician fading channels", *submitted*.
- [95] D. Kontaxis, G. Tsoulos, and S. Karaboyas, "Performance of multiple antenna systems in different operational environments", in *Proceedings of Personal Indoor Mobile Radio Communications (PIMRC)*, 2007.
- [96] S. A. Jafar, and A. Goldsmith, "On optimality of beamforming for multiple antenna systems with imperfect feedback", in *Proceeding of International Symposium on Information Theory*, 2001.

[97] D. E. Kontaxis, G. V. Tsoulos, and S. Karaboyas, "Optimum ergodic beamforming capacity in urban microcellular operational environments", in *Proceedings of International Wireless Communications and Mobile Computing (IWCMC)*, 2012.

[98] Theodore S. Rappaport, *Wireless Communications*, Prentice Hall.